Deriving Gas Transport Properties of Microporous Silica Membranes from First Principles and Simulating Separation of Multi-Component Systems in Different Flow Configurations

By

Sina Deyhim

Thesis submitted to the Faculty of Graduate and Postdoctoral Studies in partial fulfillment of the requirements for the degree of

Master of Applied Science

in the Department of Chemical & Biological Engineering
Faculty of Engineering
University of Ottawa
May, 2014

© Sina Deyhim, Ottawa, Canada, 2014

Abstract

Amorphous silica membranes have molecular sieving properties for the separation of hydrogen from gas mixtures at high temperature. Consequently, they are considered to be applied in separation of a shifted syngas coming out of a water-gas-shift-reactor into the syngas and hydrogen. This separation is a key to an Integrated Gasification Combined Cycle (IGCC) plant, which would allow reducing the carbon footprint in power generation industry. The main objective of this thesis was to carry out a preliminary assessment of suitability of currently available amorphous silica membranes for this separation. However, the separation properties of amorphous silica membranes reported in the open literature vary by orders of magnitude. Therefore, in the first part of this thesis the separation properties of hypothetical silica membrane with different pore size distributions were predicted from first principles.

Considering different possible gas transport mechanisms, it was concluded that gas transport in amorphous silica membranes is dominated by the activated and non-activated Knudsen diffusion. The activation energy for transport of different species was predicted using the concept of suction energy. Then, with arbitrary pore size distributions gas permeance of hypothetical silica membrane was predicted for different gas species. Since the pore size distribution of amorphous silica membrane cannot be known *a priori*, the developed model was used to determine the pore size distribution based on experimentally measured single gas permeances of three different species (kindly provided by Natural Resources Canada, CANMET Energy Technology Center (CETC) laboratory in Ottawa) by minimizing the error of the calculated permeance ratios with respect to the experimental values. The results indicate that, depending on how the objective function is defined, more than one pore size distribution can be found to satisfy the experimental permeance ratios. It is speculated that by increasing the number of experimentally determined permeances, a more unique pore size distribution for the tested silica membrane can be obtained. However, even at this early stage, the developed model provides a rational explanation for the effect of membrane densification on the properties of silica membranes. More specifically, a simultaneous decrease in membrane permeance and selectivity due to membrane densification, reported in the literature, is explained by shrinking the size of pores beyond a certain critical value, which depends on the kinetic diameter of gas molecules that are being separated.

Comparing theoretically determined permeances, which match experimentally observed permeance ratios, revealed that the experimental permeances are considerably smaller than the theoretical values. The ratio of the two provided the basis for a scaling factor, a new concept that was introduced in this thesis.

To simulate membrane module performance, a novel approach was introduced. More specifically, co- and counter-current flow configurations as well as cross-flow configuration were modelled by assuming no change in feed composition over an infinitesimally small element of membrane area. This led to a system of linear, rather than differential equations, which was readily solved numerically.

Résumé

Les membranes de silice amorphe ont des propriétés de tamisage moléculaire pour la séparation de l'hydrogène à partir de mélanges gazeux à haute température. En conséquence, leur utilisation pour la séparation du gaz de synthèse provenant du reformage par la vapeur du gaz naturel est considérée afin de séparer l'hydrogène du gaz synthétique. Cette séparation est la pierre angulaire du procédé de gazéification intégré à cycle combiné (GICC) qui permettrait de réduire l'empreinte carbonique des industries de production d'électricité. L'objectif principal de cette thèse était d'effectuer une évaluation préliminaire pour déterminer si les membranes de silice amorphe actuellement disponibles sont adéquates pour cette séparation. Cependant, les caractéristiques de séparation des membranes de silice amorphe rapportées dans la littérature varient grandement. Ainsi, dans la première partie de cette thèse les caractéristiques de séparation d'une membrane de silice hypothétique avec différentes tailles de pores ont été estimées à partir des principes fondamentaux.

En prenant en compte les phénomènes d'échange possibles, il a été déterminé que le transport de gaz dans une membrane de silice amorphe est dominé par la diffusion de Knudsen activée et non-activée. L'énergie d'activation pour le transport des différentes espèces moléculaires a été prédite en utilisant le concept d'énergie d'aspiration. Puis, la perméance des espèces gazeuses a été estimée pour des distributions arbitraires de la taille des pores de la membrane de silice hypothétique. Puisque la répartition des pores de la membrane de silice amorphe n'est pas connue *a priori*, le modèle développé a été utilisé pour déterminer la distribution de la taille des pores basée sur des mesures expérimentales de la perméance de trois gaz purs différents (données fournies par le Centre de la technologie de l'énergie CANMET-CTEC) en minimisant l'erreur entre les rapports de la perméance estimée et de la perméance mesurée expérimentalement. Les résultats indiquent que, selon la façon dont la fonction objective est définie, il existe plusieurs distributions de la taille des pores qui satisfassent les rapports expérimentaux de la perméance. Il est spéculé qu'en augmentant le nombre de perméances déterminées expérimentalement, une distribution unique de la répartition des pores pourrait être obtenue. Toutefois, même à ce stade précoce, le modèle développé fournit une explication rationnelle de l'effet de la densification de la membrane sur les propriétés des membranes de silice. Plus précisément, une diminution simultanée de la perméance et la sélectivité due à la densification de la membrane, rapportée dans la littérature, s'explique par la

réduction de la taille des pores au-delà d'une certaine valeur critique, qui dépend du diamètre cinétique des molécules de gaz qui doivent être séparées.

La comparaison des perméances déterminées théoriquement, correspondant aux rapports de perméance observés expérimentalement, a révélé que les perméances expérimentales sont beaucoup plus petites que leurs valeurs théoriques. Le rapport des deux perméances suggère un facteur d'échelle qui est un nouveau concept introduit dans cette thèse.

Pour estimer la performance d'un module de membranes, une nouvelle approche a été introduite. Plus précisément, les configurations des écoulements en co- et contre-courant ainsi que la configuration d'un écoulement transversal ont été modélisées en ne supposant aucun changement de composition de l'alimentation pour un élément de surface de membrane infiniment petit. Cela a conduit à un système linéaire d'équations, plutôt qu'un système d'équations différentielles, qui a été facilement résolu numériquement.

Statement of Collaboration

The concept of characterization of microporous membranes using multiple single gas permeation tests and solving the cross-flow model using the differential stage cut method belong to my supervisor Dr. Boguslaw Kruczek.

I acknowledge that the remainder of this work, which includes analyzing the effects of over-coating of silica layers, introduction of the concept of permeance scaling factor for permeance prediction, developing a novel method for simulating separation of multicomponent mixtures in plug flow configuration based on differential membrane area and composing this thesis were entirely done by me.

Sina Deyhim

Signature: _____ **Date: _____**

Acknowledgment

I would like to take this opportunity to thank the people that assisted me with my studies here in the University of Ottawa.

First of all I like to express my greatest gratitude to Dr. Boguslaw Kruczek for having me in his research team, and for his steady support and guidance, who his expertise and knowledge made the completion of this project possible.

Special thanks to David McCalden for his support and for providing valuable experimental data, which helped me to study the silica membrane properties. I would also like to thank Natural Resources Canada for funding my project and for kindly giving me the permission to use their experimental data on silica membranes in my research.

I would like to thank my family for their support and love, which have always encouraged me towards excellence.

List of Tables

List of Figures

CHAPTER 1

INTRODUCTION

1.1 Introduction

The Integrated Gasification Combined Cycle (IGCC) plant is a promising new technology that allows reducing the carbon footprint in power generation industry. The IGCC process requires separation of a shifted syngas (the two main component of shifted syngas are H_2 and CO_2, but it also includes N_2, CO and traces of Ar and H_2S) coming out of a water-gas-shift-reactor into the syngas and CO_2 product, which in turn requires a hydrogen selective membrane operating at high temperatures.. Since hydrogen is an important basic chemical feedstock, which has a wide range of applications ranging from the production of ammonia, and metals to petrochemical materials, the hydrogen selective membranes are among the most important gas separation membranes.

Microporous inorganic membranes are considered to be the best candidate for hydrogen selective membranes. Unlike polymer membranes, inorganic membranes can operate at high temperatures. Moreover, because of a molecular sieving capability, they offer much higher selectivities for the separation of H_2 from larger gas molecules compared to polymer membranes. Among different inorganic materials, amorphous silica is one of the most extensively studied materials for producing microporous inorganic membranes. The latter are typically synthesized by chemical vapor deposition (CVD) techniques.

The first part of this study deals with the transfer mechanisms in the microporous silica membranes with the goal to derive gas transport properties of silica membranes, such as permeance and ideal selectivity, from first principles. The second part of this study focuses on the modeling of separation of hydrogen from binary and multi-component feed systems in different flow patterns in which the effect of feed pressure drop is included.

1.2 Basic Concepts

The two most important characterises of a membrane are the productivity and selectivity. The former is assessed on the basis of a permeability coefficient (P_M), which is a pressure-gradient-membrane-thickness-normalized flux:

$$P_M = \frac{J\ t}{\Delta p} \tag{1.1}$$

where J is the steady state flux across the membrane, Δp is a pressure gradient across the membrane, which represents the driving force for gas permeation, and t is the membrane thickness. If the membrane thickness cannot be accurately determined, for example in the case of asymmetric and composite membrane, the membrane productivity is assessed on the basis of membrane permeance ($\overline{P}_M$), which is simply a ratio of the permeability coefficient and membrane thickness (P_M/t). By performing a simple, laboratory scale gas permeation test, permeability or permeance can be evaluated experimentally. In principle, the permeability coefficient is a material property, but it is well known that for a given material, the permeability coefficient strongly depends on the membrane preparation protocol. As a result, for a given gas and membrane material the permeability coefficients reported in the literature may vary by

orders of magnitude. It is therefore important to establish, for a given gas and membrane material, some kind of a reference value, or a permeability coefficient of an ideal membrane from a given material.

As a first approximation, the selective properties of a membrane for the separation of a mixture of gases *A* and *B* is evaluated on the basis of an ideal selectivity, which is simply the ratio of the permeability coefficients (or permeances) for gases *A* and *B*, determined in the respective single gas permeation tests:

$$\alpha^{*}_{A/B} = \frac{P_{M,A}}{P_{M,B}} \tag{1.2}$$

It should be noted that if the feed is a mixture of gases *A* and *B*, the permeability ratio might be lower or higher than the ideal selectivity given by Eq. (1.2) due unique interactions between *A* and *B*, as well as, because the respective interactions between *A* and *B* with the membrane.

In this thesis the focus is given to microporous silica membranes. In order to determine the reference values for the permeability coefficients and thus the ideal selectivity of microporous silica membranes, it is essential to start by identifying the dominating transfer mechanisms in these membranes.

1.3 Transfer in Microporous Membrane

The term microporous membrane implies that the pore diameter does not exceed 2 nm. In reality, defect-free microporous silica membranes have pore diameters comparable to the size of typical gaseous penetrants ranging from 3 to 5 Å. As a result, the mass transfer in these membranes cannot only be described by the well-established mechanisms for mesoporous membranes such as viscous flow, Knudsen diffusion and surface diffusion [4]. When the pore size and the molecules' size are close to each other, there is a strong overlap of the potential fields, which are described by Lennard-Jones potential, between the gas molecules and the molecules of the pore wall. The total mass transfer in this case is the sum of the mass transfer in the gas phase and that in the adsorbed phase. However, at temperatures above the iso-concentration point, the mass transfer in the gas phase is prevailing [1]. The iso-concentration point is a temperature, above which the effect of surface diffusion becomes negligible compared to the gas phase mass

transfer. Essentially, above the iso-concentration point, the gas molecules have sufficient energy to escape the surface potential of the pore molecules, and gas molecules can no longer be adsorbed on the pore walls. The transfer mechanism in this case, is referred to as an activated Knudsen diffusion or gas transitional diffusion. The activated Knudsen diffusion is hindered by the presence of small pores [5]. The expression for a trans-membrane flux at temperatures above the iso-concentration point, at which the effects of surface diffusion are negligible, can be written as [1]:

$$J = -\left(\frac{D_{gas}}{RT}\right)\frac{\Delta p}{t} \tag{1.3}$$

where, D_{gas} is the corrected diffusivity in the gas phase, which a modified Knudsen diffusion given by:

$$D_{gas} = \rho_g d_p \left(\frac{8RT}{\pi M}\right)^{0.5} \frac{\gamma}{\tau} e^{\frac{-\Delta E}{RT}} \tag{1.4}$$

where, ΔE is the activation energy, γ is the porosity and τ is the tortuosity, which accounts for the tortuous diffusion path created by the interconnected pores of silica structure, d_p is the pore diameter, M is the penetrant molecular weight, R is the universal gas constant, T is the temperature, and ρ_g is a geometrical probability factor. The latter depends on the pore size and the pore neck diameter (d_n) according to:

$$\rho_g = \frac{1}{3}\left(\frac{d_n}{d_p}\right)^2 \tag{1.5}$$

In the limiting case in which, $d_n = d_p$, i.e. for an ideal cylindrical pore, $\rho_g = 1/3$.

The expression for the modified diffusion coefficient is an Arrhenius-type correlation, which indicates that the diffusing molecules must overcome a potential barrier caused by the molecules at the wall of membrane. It is important to emphasize that as T increases, eventually TR becomes much greater than $|\Delta E|$, and Eq. (1.4) simplifies to the classical expression for Knudsen diffusion coefficient. Alternatively, as d_p increases, the activation energy decreases and the condition $TR \gg |\Delta E|$ may exist at ambient temperatures.

Substituting Eq. (1.4) into Eq. (1.3), and then the resulting expression into Eq. (1.1) leads to the following expression for the permeability coefficient:

$$P_M = \rho_g d_p \left(\frac{8}{\pi MRT} \right)^{0.5} \frac{\gamma}{\tau} e^{\frac{-\Delta E}{RT}} \tag{1.6}$$

Eq. (1.6) can be used for predicting the permeability coefficient of gases in microporous silica membranes. However, this requires the knowledge of the pore size and the pore size distribution of the membrane as well as the relationship between ΔE and d_p. It is also required to assume some values for the porosity, tortuosity and the geometrical probability factor.

Several approaches have been used for determining the activation energy in microporous membranes. Some researchers attempted to use molecular dynamic modeling techniques, which require complex and tedious computations. The advantage of the molecular dynamic modeling is that it allows to build a hypothetical structure for the microporous silica membrane and thus to obtain all the geometrical and morphological parameters required by Eq. (1.6). However, because of the complex structure of silica networks and its pores, and an amorphous nature of microporous silica membrane, molecular dynamic simulations may lead to ambiguous results.

A much simpler alternative to the molecular dynamic simulation is an approach proposed by Thornton et al. [6], which introduces a concept of a suction energy. More specifically, the activation energy is quantified by integrating the repulsive and attractive forces along the travelling distance of the molecules at the pore neck. This has been demonstrated for carbon tubes and silica membranes. In the case of a small pore, the attractive Van der Waals forces are not strong enough to suck the molecules inside the pore, and so the molecules need a certain amount of kinetic energy to pass through the energy barrier created by the pore neck. The total work done by the forces acting between the gas molecule and the pore wall is calculated and then integrated over the penetrant traveling distance to determine the suction energy. The transfer mechanism of the diffusants can also be determined by looking at the suction energy, as activated diffusion would be dominant when suction energy becomes negative, and Knudsen diffusion can be seen when the kinetic energy of the gas is higher than the calculated suction energy.

The concepts introduced here will be further discussed in a greater detail in Chapter 2 and are going to be used for estimating the permeance and ideal selectivity for silica membranes. It shall also be demonstrated how the knowledge of the gas transport mechanism along with single gas permeation data can be used for the characterization of the pore size distribution of microporous silica membranes.

1.4 Simulating Silica Membrane's Performance

The objective of the second part this thesis is to develop tools that would allow deciding whether the selective properties of the available amorphous silica membranes are sufficient to meet the separation objectives of the IGCC process. Subsequently, these tools can be used to design a suitable membrane separation unit. In simulations of the separation of binary and multicomponent gas mixtures, it is commonly assumed that the permeability coefficient of a given gas in a given membrane is not affected by the presence of other gases in the feed mixtures. In others words, it is assumed that the permeability coefficients or permeances determined in the respective single gas permeation experiments can used be in simulation of multicomponent gas separations.

For a binary gas mixture consisting of *A* and *B*, the separation factor is defined as:

$$\alpha_{A/B} = \frac{y_A / y_B}{x_A / x_B} \tag{1.7}$$

where *x* and *y* indicate mole fractions in the feed and permeate, respectively. The separation factor is related to the ideal selectivity through:

$$\alpha_{A/B} = \alpha^{*}_{A/B} \left(\frac{x_A \left(\alpha_{A/B} - 1 \right) + 1 - r\alpha_{A/B}}{x_A \left(\alpha_{A/B} - 1 \right) + 1 - r} \right) \tag{1.8}$$

in which, $r = p_l/p_h$, and p_l and p_h refer to permeate and feed pressures, respectively. It follows from Eq. (1.8) that in the limiting case when $r \rightarrow 0$, which can be achieved when the permeate side of membrane is under vacuum, the separation factor approaches the ideal selectivity. Otherwise, with $r > 0$, the separation actor is lower than the ideal selectivity.

It is important to emphasize that Eqs. (1.7) and (1.8) are applicable only at so called "zero stage cut" condition, and the stage cut (θ) is defined as:

$$\theta = \frac{V_p}{L_f} \tag{1.9}$$

where L_f and V_p are feed the permeate rate flow rates, respectively. When $\theta \approx 0$, the composition of the feed is approximately constant. However, when θ becomes greater than zero, the feed composition changes along the membrane. More specifically, the feed is depleted from a more permeable component whereas the mole fraction of a less permeable component increases. Therefore, the composition of the feed is no longer a unique value. The greater the stage cut, the greater the variation in the composition of the feed along the membrane. However, the magnitude of this variation also depends on the membrane selectivity, the flow configuration, and the pressure drop at the feed side of the membrane.

There are four basic types of flow configurations at which membrane gas separation can be carried out: complete mixing, cross-flow, parallel flow, and counter current flow. The simplest of these is the complete mixing configuration, which, for a binary gas separation, is shown schematically in Fig. 1.1. The mole fractions x_f, x_o, and y_p are those of the more permeable component. The complete mixing gas separator is similar to a continuous stirred tank, which implies that the compositions of feed and permeate are uniform along the membrane. Moreover, the composition of the gas at the high pressure side of the membrane is represented by the composition of the retentate (x_o). The retentate stream is a part of the feed stream that did not permeate through the membrane. In addition, as a first approximation, similarly to other flow configurations, the complete mixing model assume that the process is isothermal, and the pressure drops at the feed and permeate sides are negligible.

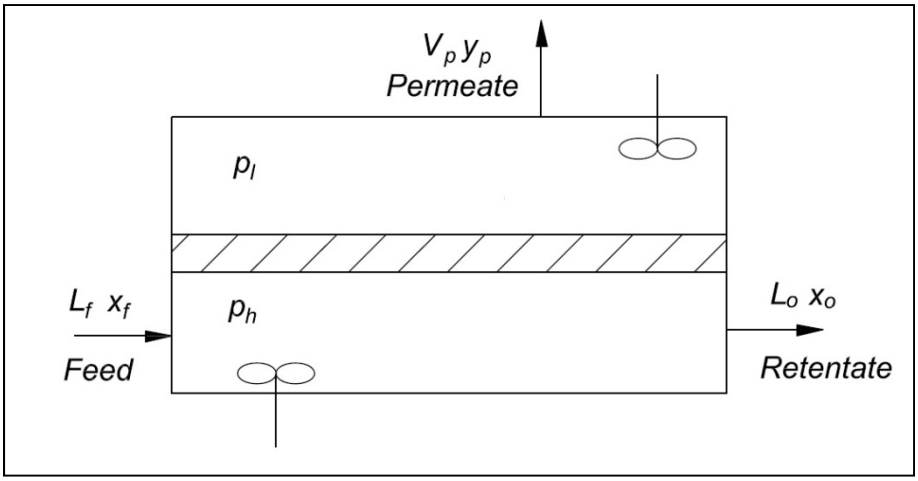

Figure 1-1 Schematic diagram of complete mixing model separation.

Referring to Fig. 1.1, the overall mass balance and component balance on the more permeable component are given by:

$$L_f = L_o + V_p \tag{1.10}$$

$$L_f x_f = L_o x_o + V_p y_p \tag{1.11}$$

Unlike single gas permeation, the driving force is the partial pressure difference across the membrane. Since the composition at the permeate side is represented by the composition of the retentate, the flow rate of the more permeable component across the membrane is described by:

$$y_p V_p = \frac{P_{MA} A_m}{t}(p_h x_o - p_l y_p) \tag{1.12}$$

where, P_{MA} is the permeability coefficient of the more permeable component, and A_m is the area of membrane. The same equation can be written for the less permeable component B, and by dividing the two rate equations, the following expression is obtained:

$$\frac{y_p}{1-y_p} = \frac{\alpha^*[x_o - (p_l/p_h)y_p]}{(1-x_o) - (p_l/p_h)(1-y_p)} \tag{1.13}$$

Eq. (1.13) is a quadratic equation that can be used to determine the permeate composition y_p. Alternatively, y_p can be expressed in terms of the stage cut using the total and component mass balances:

$$y_p = \frac{x_f - x_o(1-\theta)}{\theta} \tag{1.14}$$

Knowing the composition of the permeate and the stage cut, the required membrane area can be determined by rearranging Eq. (1.12):

$$A_m = \frac{\theta y_p L_f}{(P_{MA}/t)(p_h x_o - p_l y_p)} \tag{1.15}$$

Modelling binary gas separation in complete mixing model is straight forward, but in reality membrane separation processes is not operated in the complete mixing pattern. Nevertheless, the complete mixing model represents the important reference for the more realistic flow configurations.

In a cross-flow pattern the feed is plug flow and parallel to the membrane due to its longitudinal velocity, while the permeate is pulled out on the other side perpendicular to the membrane surface. The cross-flow model was solved analytically by Weller et al. [9], but the effect of pressure drop cannot be considered in the analytical solution. Alternatively, the cross-flow model can be solved by dividing the membrane into small differential elements, which then can be analyzed using the equations for complete mixing model. A differential element can be expressed in terms of a differential change in feed composition, a differential stage cut, or a differential membrane area. Different approaches for numerical solution of the cross-flow model will be discussed in Chapter 3.

In co-current and counter-current flow configurations, the feed and permeate are both in a plug flow. Solving these flow patterns require solving the governing differential equations numerically, which for the counter-current flow configuration may require an iterative procedure. The analysis is further complicated when instead of binary, multicomponent systems are considered. In addition, for more realistic models, the effect of pressure drop due to plug flow at the high pressure side should also be considered. The latter, affects the variation in the

driving force along the membrane. In this thesis, we propose a new approach for solving modelling co- and counter-current flow configurations, which is based on using a differential area and solving all the rate equations simultaneously in each element. The details of this new approach along some illustrative examples are presented and discussed in Chapter 3.

1.5 Thesis Objectives

There are two main objectives of this thesis. The first objective is to estimate, from the first principles, the permeability coefficients of different gases in an ideal silica membrane. This requires defining the term ideal silica membranes. Subsequently, by comparing the properties of the actual microporous silica membranes with those of the ideal silica membrane, and using the governing transport mechanisms in microporous silica membranes, it is intended to develop a tool for the characterization of the pore size and the pore size distribution of the actual silica membranes. This tool may eventually be used for the optimization of the synthesis protocol of the actual microporous silica membranes.

The second objective of this work is to develop a computer program that can be used for simulating the performance silica membranes based on the known single gas permeances at different operating conditions. The simulator is to be capable of solving binary and multi-component systems for different flow patterns including cross-flow, co-current, and counter-current flow. In order to get more accurate results, the effects of the pressure drop are to be incorporated into the simulator. While the main goal is to simulate the performance of the microporous silica membranes, the intended simulator will be applicable for any membrane gas separation process, in which the permeability coefficients of the gases of interest are known and can be assumed to be independent on the operating conditions. Alternatively, the simulator is to have a capability of recovering the intrinsic properties of the microporous silica membranes based on the their gas separation performance at a non-zero stage cut operation in a known flow configuration and the known operating conditions.

1.6 Thesis Outline

This thesis is divided into two parts according to the two main objectives of this work. The first part, which is presented in Chapter 2, discusses the methods for deriving the properties of the silica membranes from the first principles. After reviewing the literature, and considering the applications of the silica membranes, the most suitable and practical method is chosen. The procedure for determining the permeances of different gases in the ideal silica membrane is discussed in this chapter. The concept of the permeance scaling factor is also introduced and its potential application is described, Finally a new characterization method for the silica membranes or in general for any type of molecular sieve membranes is proposed. The application of proposed method for the characterization of the pore size and the pore size distribution of the microporous silica membranes using the available experimental data is then demonstrated.

The second part of this work, which focuses on the simulation of the silica membrane performance in gas separations involving binary and multi-component gas mixtures in different flow configurations, is presented and discussed in Chapter 3. Two new approaches for simulations are presented in this work. The cross-flow configuration is modelled using the concept of a constant differential stage cut, and the advantages of this approach are discussed. On the other hand, the co- and counter-current flow configurations are modelled using the approach of a constant differential membrane area, which allows limiting the modelling activities in these to flow configurations to exclusively linear set of equations. Moreover, the effects of the pressure drop at the high pressure side of membrane in all flow configurations are investigated and discussed. The simulated results are validated using the available experimental data.

Finally, Chapter 4 summarizes the findings from both parts of this thesis and provides the conclusions from each section. This last Chapter also includes the recommendations for the future research, and lists the contributions arising from this work to the general fields of science and engineering.

References

[1] Shelekhin, B. Dixon, G. Ma, Y. Theory of gas diffusion and permeation in inorganic molecular-sieve membranes, AIChE Journal, 41.(1) (1995) 58-67.

[2] Lamprecht, D. (2010), Advanced gasification technology study, Canadian Clean Power Coalition.

[3] Nagasawa, H. Shigemoto, H. Kanezashi, M. Characterization and gas permeation properties of amorphous silica membranes prepared via plasma enhanced chemical vapor deposition, Journal of Membrane Science, 441 (2013) 45–53.

[4] Markovic, A. Stoltenberg, D. Gas permeation through porous glass membranes: Part I. Mesoporous glasses—Effect of pore diameter and surface properties, Journal of Membrane Science 336 (2009) 32–41.

[5] Oyama, S. Yamada, M. Review on mechanisms of gas permeation through inorganic Membranes Journal of the Japan Petroleum Institute, 54 (5) (2011) 298-309.

[6] Thornton, A. Hilder, T. Hill, A. Predicting gas diffusion regime within pores of different size, shape and composition J. Journal of Membrane Science 336 (2009) 101‑108.

[7] Geankoplis, C. 2003. Transport Processes and Separation Process Principles. 4th ed. Prentice Hall.

[8] Walawender, W. Stern, S. Analysis of Membrane Separation Parameters. II. Counter-current and Co-current Flow in a Single Permeation Stage, Separation Science, 7:5, (1972) 553 584.

[9] Weller, S. Steiner, A. Separation of Gases by Fractional Permeation through Membranes, Journal of Applied Physics 21, (1950), 279 .

[10] Khatib, S. Oyama, S. Silica membranes for hydrogen separation prepared by chemical vapor deposition (CVD), Separation and Purification Technology, 111 (2013) 20–42.

[11] Dong, J. Lin ,Y. Kanezashi, M. Microporus inorganic membranes for high temperature hydrogen purification, Journal Of Applied Physics 104, (2008) 121301.

PART ONE

Deriving Gas Transport Properties of Microporous Silica Membranes From First Principles

CHAPTER 2

DERIVING GAS TRANSPORT PROPERTIES OF MICROPOROUS SILICA MEMBRANES FROM FIRST PRINCIPLES

2.1 Introduction

The Integrated Gasification Combined Cycle (IGCC) plant with carbon capture is a promising new technology that may allow reducing the carbon footprint in power generation industry. The IGCC process with carbon capture requires separation of a shifted syngas coming out of a water-gas-shift-reactor into the syngas and CO_2 product, which in turn requires a hydrogen selective membrane operating at high temperatures to avoid cooling the syngas and reducing the thermal efficiency of the process. Since hydrogen is an important basic chemical feedstock, which has a wide range of applications ranging from the production of ammonia, and metals to petrochemical materials, the hydrogen selective membranes are among the most important gas separation membranes.

Microporous inorganic membranes are considered to be the best candidate for hydrogen-selective membranes. Unlike polymer membranes, inorganic membranes can operate at high temperatures. Moreover, because of a molecular sieving capability, they offer much higher

selectivities for the separation of H_2 from larger gas molecules compared to polymer membranes. Among different inorganic materials, amorphous silica is one of the most extensively studied materials for producing microporous inorganic membranes. The latter are typically synthesized by chemical vapor deposition (CVD) techniques. The hydrogen permeance of microporous silica membranes reported in the literature vary by orders of magnitude, which is not surprising considering the complexity of the membrane synthesis protocol and virtually an infinite number of possible arrangements of amorphous silica network.

The objective of this chapter is to systemize the literature-reported performance of silica membranes by comparing them with the properties of a hypothetical, ideal silica membrane. This requires defining the structure of the ideal silica membrane, and then derivation of the properties of the ideal membrane from first principles. Comparing the properties of the ideal silica membrane with the performance of the actual amorphous silica membranes has led to introducing a novel concept of a scaling factor, which is then used as a basis for the determination of the pore size and pore size distribution of microporous silica membranes based on experimentally observed single gas permeances. The proposed new method is not limited to microporous silica membranes; it is applicable for any membrane in which the gas transport is governed by an activated Knudsen diffusion.

2.2 Background

2.2.1 Silica Membranes

The amorphous silica membrane is a network of interconnecting micropores, which allows permeation of smaller while restricting the transport of larger molecule. As a result, the amorphous silica network allows gas separation by molecular sieving. The amorphous silica membranes can be produced by sol-gel or chemical vapor deposition (CVD) techniques. Typically, the membranes prepared by the sol-gel method have higher permeances but lower gas selectivities compared to the membranes prepared by the CVD method [1]. The sol-gel method is based on dip-coating a mesoporous substrate with a silica polymeric or particulates suspension, and then drying and firing the product at high temperatures [2]. In general, the silica membranes prepared by the sol-gel methods cannot separate hydrogen from other small molecules such as

carbon dioxide or nitrogen, and therefore, we shell focus here only on the silica membranes prepared by the CVD method.

In the CVD method silica membranes can be fabricated using different silica precursors, reaction geometries, and support types. The selective silica layer is produced by the reaction between gaseous silica precursors such as SiH_4, $SiCl_4$, tetraethyl orthosilicate (TEOS), or dimethoxydiphenylsilane (DMDPS) and the reactive agents (oxygen, air, water, ozone, etc.). It should be noted that the pore size of the final silica membrane is enlarged when the side chain groups in the silica precursor become larger [2].

In the CVD process the gaseous silica precursor is applied on a support layer with relatively large pores, which has little resistance to mass transfer. Vycor glass and alumina are the two common supports that are used for preparing silica membranes. In general, the of silica membranes prepared using the Vycor glass support is lower compared to α-alumina support. Often, instead of a direct application of the silica precursor on to porous α-alumina support, the latter is first coated with a denser γ-alumina layer. Using the intermediate γ-alumina layer between the selective silica layer and porous α-alumina support, results in improved the selectivity because by limiting the pinhole defects in the selective layer [3]. A schematic of the structure of a microporous of silica membrane with an intermediate layer is illustrated in Fig. 2.1.

The other important factor in fabrication of amorphous silica membranes is the reaction geometry, which is either one-sided or counter-current. In the one-sided geometry the precursors and the reactive agents (in inert gas) are introduced to one side of the support. On the other hand, in counter-current approach the two streams are fed to the opposite sides of the support, and then the silica film is formed inside the support where the precursor and the reactive agents meet. The later method results in more homogeneous pore size distribution, which consequently leads to better selectivities [3]. Deposition of silica results in two types of pores: intraparticle pores, which are created as the silica network grows, and interaparticle pores, which are formed as result of spacing between particles [4]. As for any other type of membranes, the performance of the silica membranes is evaluated on the basis of their productivity and selectivity, which are discussed next.

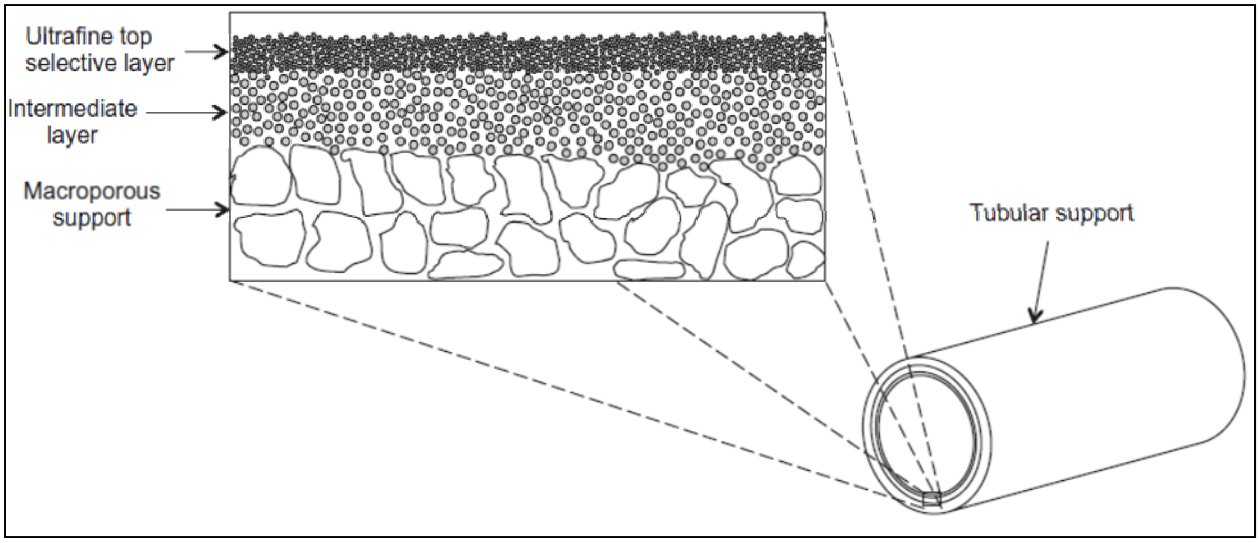

Figure 2-1 Schematic of an asymmetric composite silica membrane for gas separation (Adapted from Khatib et al. [3]).

2.2.2 Gas Transport in Porous Membrane

Gas transport mechanism in porous membranes depends on the pore size and temperature at which the transport takes place. When the pore size is comparable to the size of the molecules that pass through the membrane, the transport requires some activation energy, and depending on the temperature at which the transport occurs, it may occur by surface diffusion or activated Knudsen diffusion. When the pore size is much greater than then size of the molecules that pass through the membrane, the transport may occur by a viscous or Knudsen flow.

Regardless of the actual transport mechanism, the productivity of any membrane, including a silica membrane, is assessed on the basis of a permeability coefficient (P_M), which is a pressure-gradient-membrane-thickness-normalized flux:

$$P_M = \frac{J\ t}{\Delta p} \tag{2.1}$$

where J is the steady state flux across the membrane, Δp is a pressure gradient across the membrane, which represents the driving force for gas permeation, and t is the membrane thickness. If the membrane thickness cannot be accurately determined, for example in the case of asymmetric membranes, the membrane productivity is assessed on the basis of permeance ($\overline{P}_M$), which is simply the ratio of the permeability coefficient and the membrane thickness (P_M/t).

By performing a simple laboratory-scale gas permeation test, the permeability coefficient or permeance can be evaluated. Knowing the experimental permeability coefficients (permeances) of gases *A* and *B*, the membrane selectivity is assessed on the basis of the ideal selectivity as follow:

$$\alpha^{*}_{A/B} = \frac{P_{M,A}}{P_{M,B}} \tag{2.2}$$

It should be noted that if the feed is a mixture of gases *A* and *B*, the permeability ratio might be lower or higher than the ideal selectivity given by Eq. (2.2) due to unique interactions between *A* and *B*, as well as, because the respective interactions between *A* and *B* with the membrane might be modified in the presence of the other component.

In principle, the permeability coefficient is a material property, but it is well known that for a given material, the permeability coefficient strongly depends on the membrane preparation protocol. As a result, for a given gas and membrane material the permeability coefficients reported in the literature may vary by orders of magnitude. Therefore, it is important to establish a reference for a given gas and membrane material, to which the experimentally determined permeability may be compared to.

In the case of a porous membrane, the gas flux can be written as a sum of the fluxes in the gas phase and the adsorbed phase [5-8]:

$$J = -\left(D_{ads} \frac{d\ln(p)}{d\ln(C_{ads})} \frac{dC_{ads}}{dp} + \frac{D_{gas}}{RT} \right) \frac{\Delta p}{t} \tag{2.3}$$

where D_{ads} is the diffusivity in the adsorbed phase, C_{ads} is the concentration of the gas in adsorbed phase, D_{gas} is the diffusivity in the gas phase, R is the gas constant, and T is the temperature. The first term in parentheses in the Eq. (2.3) corresponds to the transport of the adsorbed phase while the second one to the transport in the gas phase. Depending on the pore size and temperature, there are several limiting cases for the gas transport in porous membranes, which are discussed next.

2.2.3 Pore Sizes Much Larger than Gas Molecular Size

When the pore size is much larger than the size of gas molecules, the first term in Eq. (2.3) becomes negligible and the gas-phase transport dominates. The latter may occur by viscous and/or Knudsen flow, depending on the mean free path of gas molecules. The mean free path indicates the average distance traveled by molecules between collisions, which may be evaluated from the kinetic theory of gases [9]:

$$\lambda = \frac{1}{\sqrt{2}\pi d^2 n} \tag{2.4}$$

where d is the molecular size and n is the number of molecules per unit volume, which is directly proportional to pressure. Knowing the mean free path and the pore diameter (d_p), the actual transport mechanism depends on Knudsen number (K_n):

$$K_n = \frac{\lambda}{d_p} \tag{2.5}$$

Knudsen flow is dominant when $K_n >> 1$, i.e., the collision with the pore walls are more frequent than the collisions between molecules, which occurs when the mean free path of the molecules is much larger than the pore size. In the other limit, when $K_n << 1$, the transport occurs by viscous flow. When K_n is order of unity, both Knudsen and viscous flow occur simultaneously.

The gas transport in viscous flow is governed by the Hagen-Poiseuille equation, and the corresponding permeability coefficient is given by [10]:

$$P_M = \frac{\rho\gamma^3}{2(1-\gamma)^2 \tau a_v^2 \mu'} \tag{2.6}$$

$$a_v = \frac{a'}{1-\gamma} \tag{2.7}$$

where ρ and μ' are fluids the density and viscosity, a_v is the specific surface area and a' is the total pore surface area over membrane volume. Viscous flow provides no selectivity, and should be avoided by preparing a good support and intermediate layer.

The Knudsen diffusion coefficient of gas in a perfect cylindrical pore of diameter d_p is derived from the kinetic theory of gases [10]:

$$D_K = \frac{d_p \bar{v}}{3} \tag{2.8}$$

in which $\bar{v}_A$, the velocity of gas molecule of gas A is given by:

$$\bar{v} = \left(\frac{8RT}{\pi M} \right)^{1/2} \tag{2.9}$$

where, M is the molecular weight of the gas. Combining Eq. (2.8) with Eq. (2.9), and considering geometric parameters of the membrane, porosity (γ) and tortuosity (τ), the expression for the Knudsen diffusivity in the membrane become:

$$D_K = \frac{\gamma d_p}{\tau} \left(\frac{8RT}{9\pi M} \right)^{1/2} \tag{2.10}$$

Consequently, in Knudsen diffusion is dominant; the corresponding expression for the permeability coefficient is obtained by dividing Eq. (2.10) by RT, which leads to:

$$P_M = \frac{\gamma d_p}{\tau} \left(\frac{8}{9\pi RTM} \right)^{1/2} \tag{2.11}$$

Unlike viscous flow, Knudsen diffusion offers a limited selectivity, with the ideal selectivity for the separation of gases A and B inversly proportional to the square root of the ratio of the molecular weights of the two gases:

$$\alpha_{A/B} = \frac{P_{M,A}}{P_{M,B}} = \left(\frac{M_B}{M_A} \right)^{1/2} \tag{2.12}$$

According to Eq. (2.12) the ideal selectivity for the separation of CO_2 from H_2 would be just 4.7, which is insufficient for practical separation of these two gases.

2.2.4 Pores Comparable to Gas Molecular Size and Effect of Temperature

As the membrane pore size becomes close to the molecular size, strong overlap of potential fields begins to develop between molecules of the pore wall and gas molecules because of the Van der Waals interactions. In this case the total concentration of diffusants inside the membrane is the sum of gas phase and adsorbed phase concentrations. The temperature at which the amounts of the diffusant in the adsorbed phase and the gas phase are the same is referred to as an iso-concentration point. Above the iso-concentration point, the transport is dominated by the activated Knudsen diffusion whereas below the iso-concentration point the transport is dominated by surface diffusion. The iso-concentration point depends on the nature of the diffusant and the membrane material.

Shelekhin et al. [7] studied the transport of He, H_2, N_2, O_2, CH_4 and CO_2 in molecular sieve silica membranes at different temperature. Fig. 2.2 presents the effect of temperature on the concentration in the adsorbed phases of He, H_2, N_2, O_2, CH_4 and CO_2 at 5 atm. in the molecular sieve silica membrane. It is evident that the iso-concentration points in Fig. 2.2 increase in the following order: He < H_2 < N_2 < O_2 < CH_4 < CO_2. For He the iso-concentration point is approximately -250^{o}C while for CO_2 it is approximately 160^{o}C.

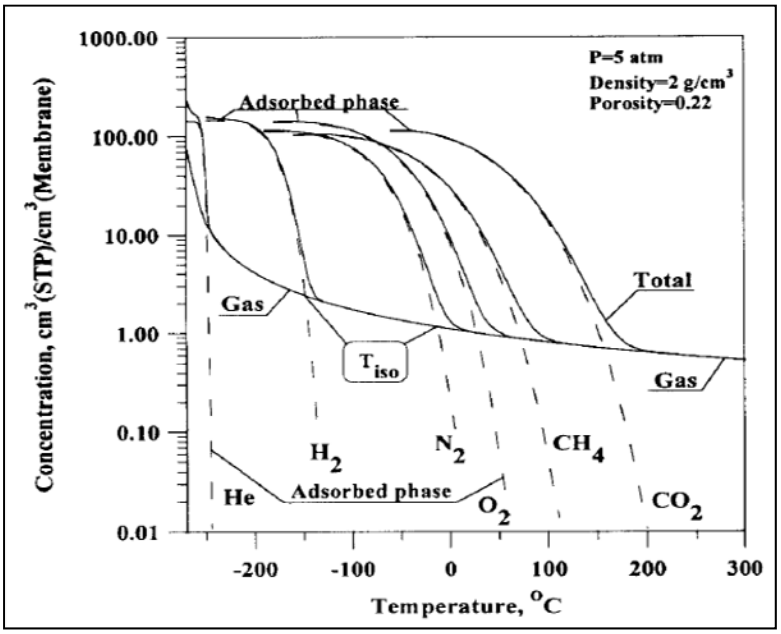

Figure 2-2 Total gas phase and adsorbed phase in molecular sieve silica membrane vs. temperature (Adopted from Shelekhin e. al. [7]).

2.2.4.1 Surface Diffusion

When the pore size becomes comparable to the diffusant size and the process occurs below the iso-concentration point, the second term in Eq. (2.3) becomes negligible and the transport occurs by surface diffusion. For mixtures containing absorbable and non-absorbable gases competitive adsorption-diffusion mechanisms will be observed [5]. In this case adsorbing gases will be adsorbed into the pores and block the passage of other components, which might result in inverse selectivity. Maxwell–Stefan model [12,13] is commonly used to described the multi-component gas diffusion in micropores at temperatures below the iso-concentration point. The Maxwell-Stephan model uses the information of single gas permeation data to predict the diffusion behaviour of multi-component mixtures based on dusty gas model approach [14].

Adsorption in gas separation by microporous membranes is described by Langmuir adsorption model [15,16], the pores are too small to allow multilayer adsorption. Consequently,

$$\bar{\theta} = \frac{q}{q_s} = \frac{bp}{1+bp} \tag{2.13}$$

where $\bar{\theta}$ is the fractional occupancy of adsorption sites, q is the amount of gas molecules adsorbed per unit mass of adsorbent, q_s is the saturation amount of adsorbed molecules, and b is adsorption equilibrium constant, which depends on temperature according to:

$$b = b_o e^{\frac{-\Delta H_a}{RT}} \tag{2.14}$$

where ΔH_a is heat of adsorption. If bp is much smaller than unity then the gas concentration can be expressed by:

$$C \approx \rho q_s bp = \rho b_o e^{\frac{-\Delta H_a}{RT}} p \tag{2.15}$$

The movement of molecules in this mechanism is described by the gas molecules jumping between the adsorption sites along the membrane pore wall by overcoming the energy barriers [6]:

$$D_{ads} = D_o \, e^{\frac{-\Delta E_{ads}}{RT}} \tag{2.16}$$

where D_o is a pre-exponential factor and ΔH_{ads} is the activation energy required for moving from one adsorption site to another. Substituting Eqs. (2.15) and (2.16) into Fick's first law, the following expression is obtained:

$$J_{ads} = -\rho b_o D_o \, e^{\frac{-\Delta H_a - \Delta E_{ads}}{RT}} \frac{dp}{dx} \tag{2.17}$$

Consequently, the permeability coefficient is surface diffusion is given by:

$$P_M = P_o e^{\frac{-\Delta H_a - \Delta E_{SD}}{RT}} \qquad \text{where} \qquad P_o = \rho b_o D_o \tag{2.18}$$

As shown by Eq. (2.18), the difference between the heat of adsorption and the activation energy for surface diffusion and represents the effective barrier for diffusing molecules to permeate through membrane. As the heat of adsorption is normally higher than the activation energy, then the surface diffusion permeability decreases as the temperature increases. In this transfer mechanism membrane becomes selective to more condensable gases, and for instance for the mixture of H_2 and CO_2 membrane would be selective to CO_2 rather than to H_2. Since H_2 is a smaller molecule than CO_2, this type of selectivity is often referred to as an inverse selectivity. According to Fig. 2.2 inverse selectivity in the molecular sieve silica membranes would be observed at ambient temperatures.

2.2.4.2 Activated Knudsen Diffusion

Above the iso-concentration point the first term in Eq. (2.3) becomes negligible, and the transfer mechanism, when the pore size is similar to the molecular size, is referred to as an activated Knudsen diffusion, or gas transitional. Gas molecules have enough energy to escape the surface potential, but the process in hindered because of the presence of small pores [6]. The diffusion coefficient in a medium with spatial restrictions is given by:

$$D_{gas} = \bar{\rho} \omega \bar{v} \tag{2.19}$$

where, ω is a jump length and $\bar{\rho}$ is the probability of the diffusant making a jump, which is the function of geometrical and energetical factors [7]:

$$\overline{\rho} = \rho_g \rho_E = \rho_g e^{\frac{-\Delta E_{gas}}{RT}} \tag{2.20}$$

where ΔE_{gas} is the diffusion energy barrier, which represent the activation energy for diffusion, ρ_g is the geometrical probability factor, which indicates the probability of gas jumping in the desired direction and ρ_E is the probability that the molecule has sufficient kinetic energy. For spherical molecules ρ_g is determined using the following equation:

$$\rho_g = \frac{1}{3}\left(\frac{d_n}{d_p}\right)^2 \tag{2.21}$$

where d_n is the pore neck diameter. The value of ρ_g is 1/3 for a 3-D space without obstruction. For non-spherical molecules, the probability of molecules being oriented in right way before entering the pore should also be taken into consideration. The expression for the diffusivity can be obtained by substituting the expression for probability factor from Eqs. (2.20) and (2.21) in diffusivity equation, and by setting $\omega = d_p$. Furthermore, expressing the mean velocity by using Eq. (2.9) and correcting for the amorphous structure of silica network, the expression for diffusivity given by Eq. (2.19) becomes:

$$D_{gas} = \rho_g d_p \left(\frac{8RT}{\pi M}\right)^{0.5} \frac{\gamma}{\tau} e^{\frac{-\Delta E_{gas}}{RT}} \tag{2.22}$$

As can be seen from the above equation the diffusion coefficient not only depends on the size of the molecule, but it is also affected by the geometrical probability and the activation energy, which are determined by pore characteristics. In the actual silica membranes there would be a pore size distribution, so diffusivity would depend on the location within the membrane as well.

Ignoring the first term in Eq. (2.3) and substituting the resulting expression into Eq. (2.1) the permeability of the membrane in the activated Knudsen diffusion becomes:

$$P_M = \rho_g d_p \left(\frac{8}{\pi MRT}\right)^{0.5} \frac{\gamma}{\tau} e^{\frac{-\Delta E_{gas}}{RT}} \tag{2.23}$$

Eq. (2.23) will be used for determining the permeability in this study, but in order to do so it is necessary to find the relationship between the ΔE_{gas} and the membrane pore size. It is also required to assume some values for the porosity, tortuosity and geometrical probability factor.

2.2.4.3 Solid State Diffusion

It should be mentioned that Lee et al. [16] modeled the diffusion of the small gases such as He, Ne and H_2 in silica membrane by solid state diffusion mechanism, and justified the abnormal order of the permeances of Ne and H_2 by assuming that the solid state diffusion is dominant for small gases such as these two, but the diffusion mechanism of the larger gases is a combination of activated and non-activated Knudsen diffusion. This theory will be investigated later in this chapter by analyzing the experimental results, and commenting on the behaviour of the test membranes as their pore sizes decrease.

2.2.5 Methods for Determining Activation Energy

Several approaches have been used for determining the activation energy in microporous membranes. Some researchers attempted to use molecular dynamic modeling techniques, which require complex and tedious computations. The advantage of the molecular dynamic modeling is that it allows to build a hypothetical structure for the microporous silica membrane and thus to obtain all the geometrical and morphological parameters required by Eq. (2.23). However, because of the complex structure of silica networks and its pores, and an amorphous nature of microporous silica membrane, molecular dynamic simulations may lead ambiguous results.

McElfresh et al. [17] estimated the diffusion activation energy by calculating the strain energy needed for dilation of a straight pore in an elastic medium from the radius r_p to r_{pd} using bulk shear modulus:

$$E_s = lG\pi(r_p - r_{pd})^2 \tag{2.24}$$

where, l is the pore length, G is the shear modulus, r_p is the pore radius, and r_{pd} is the dilated pore radius. Their study showed that there is a linear relation between size of the molecules and the square root of the activation energy in silica glass.

Roberts et al. [18] investigated the effect of solid-gas potential, which leads to a potential barrier that has to be overcome by the activation energy. It was pointed out that in the real microporous membrane the diffusing molecule may be forced to pass through more than one constriction, but the rate of transport is determined by the one with the highest activation energy. Diffusing through small pores (with dimensions close to that of the diffusant) is governed by the molecular interactions of the gas and the pore surface atoms. The potential energy of diffusant is considered to be affected by a number of factors including dispersion forces, close range repulsion, polarization, field dipole interactions, and field gradient quadrupole interactions. The potential energy is the sum of all these terms. The attractive dispersion forces (Φ_D) and the close-range repulsive forces (Φ_R), which are the most contributors to the potential energy, are represented by Lennard-Jones potential [18]:

$$\Phi_D + \Phi_R = 4\varepsilon\left[\left(\frac{\sigma}{r^*}\right)^{12} - \left(\frac{\sigma}{r^*}\right)^{6}\right] \tag{2.25}$$

where σ is the collision diameter of the molecule, which is the distance at which the interactions between two molecules become zero, ε is a characteristic energy, i.e. the maximum attractive energy between a pair of molecules, and r^* is the distance between the center of two molecules. Eq. (2.25) is applicable for identical molecules (single gas transport), and the pair-wise interactions. In the case of non-identical molecules A and B the characteristic energy and the collision diameter are determined based on the respective individual values using:

$$\varepsilon_{AB} = (\varepsilon_A \varepsilon_B)^{0.5} \tag{2.26}$$

$$\sigma_{AB} = \frac{(\sigma_A + \sigma_B)}{2} \tag{2.27}$$

Roberts et al. [18] approximated the activation energy and the ideal selectivity of a silica membrane for H_2 over N_2 by assuming that the potential energy of a gas at the pore neck is a sum of the potentials for each surface-bound hydrogen atom. They considered a pore neck with a diameter of 5.6 Å consisting of 8 hydrogen atoms in the length of the neck, and two on the perimeter, so the total potential was determined by assuming the interactions of hydrogen molecule with 2 hydrogen atoms on surface:

$$\Phi = 8\varepsilon\left[\left(\frac{\sigma}{r^*}\right)^{12} - \left(\frac{\sigma}{r^*}\right)^{6}\right] \tag{2.28}$$

A positive potential indicates repulsion of the molecule from the pore, and the greater the potential, the greater the repulsive force. In their work [18], the calculated activation energies for the membrane with the above pore size of 5.6 Å were 1 and 18 kJ/mol for H_2 and N_2, respectively. This indicates a little resistance for the transport of H_2 molecules and a high resistance for the transport of N_2 molecules. In general, the ideal selectivity of a microporous membrane for the separation of gasses *A* and *B* is then evaluated from:

$$\alpha^*_{A/B} = \frac{\exp\left\{\frac{-8\varepsilon_{As}}{kT}\left[\left(\frac{\sigma_{As}}{r^*}\right)^{12} - \left(\frac{\sigma_{As}}{r^*}\right)^{6}\right]\right\}}{\exp\left\{\frac{-8\varepsilon_{Bs}}{kT}\left[\left(\frac{\sigma_{Bs}}{r^*}\right)^{12} - \left(\frac{\sigma_{Bs}}{r^*}\right)^{6}\right]\right\}} \tag{2.29}$$

where ε_{As} and σ_{As} are the Lennar-Jones parameters for species *A* interacting with pore surface atoms. Using Eq. (2.29) Roberts et al. [18] estimated the ideal selectivity of the silica membrane for H_2 over N_2 at 343 K to be equal to 1060. Shelekhin et al. [7] used the same method for determining the activation energies, but assuming that the perimeter of the pore neck consisted of 8 oxygen atoms. However, the authors did not report the corresponding the ideal selectivity for H_2/N_2

Hacarlioglu et al. [19] determined the activation energies for the transport in amorphous silica membranes based on the interaction energy between a diffusant and the saddle point of siloxane rings. The geometries of the ring cluster were obtained by minimizing the energy of the structures using the density functional calculations method in *Gaussian 98* program. The $H_{2n}Si_nO_n$ (n = 4 – 8) silica n-membered rings were considered to determine the activation energies for the transport H_2 and He. It was then seen that the oxygen atoms in the 5-membered rings were located in the exterior of the ring while in the 6-, 7- and 8- membered rings were located in the interior of the ring. This indicates that oxygen atoms tend to move to the center of the ring as the ring size increases. It is therefore essential to determine the activation energy based on interactions between diffusant and oxygen atom as opposed to hydrogen, which was

done by the other authors [7,18]. After calculating the activation energies for H_2 and He for the 4-8 membered rings pores and considering the literature activation energies for permeation of H_2 and He ranging from 10-20 kJ/, it was concluded that the actual silica membranes must consist mostly of 6- and 7-membered silica rings. Consequently, the latter should be used for estimating the activation energies of other diffusants in amorphous silica membranes.

Another approach for the determination of the activation energy is based on the concept of suction energy, which was introduced by Thornton et al. [20]. Suction energy is a result of interactions between the gas molecules and the pore neck; it can be positive or negative. To determine the suction energy the Van der Waals forces are integrated along the path of the gas molecule passing through the pore neck, and if the value is positive the molecules will be sucked to the pore. If the suction energy is negative, then there is an energy barrier which has to be overcome, and the absolute of suction energy becomes the activation energy. To overcome this energy barrier in the case of the negative suction energy, the kinetic energy of the molecule must be increased by increasing the temperature of the gas. The kinetic energy of the gas molecules is given by [9]:

$$E_k = \frac{3}{2} kT \tag{2.30}$$

where k is the Boltzmann constant.

Assuming that the molecules of which the membrane is made are evenly distributed in the pore wall, the total interaction potential energy can be calculated by using a hybrid discrete-continuum formulation [20]:

$$PE = \sum_i \eta \int \nu(\beta_i) dS \tag{2.31}$$

where, η is the mean atomic surface density, and $\nu(\beta_i)$ is the potential function of an atom i of the gas molecule that interacts with the surface element dS; the distance between the atom and the surface element is β_i. This is shown schematically in Fig. 2.3 for the case of a molecule whose center is at a distance Z from the entrance of an ideal cylindrical pore with an effective pore radius of $d_p/2$. The latter is smaller than the actual pore radius, because the atoms in the pore

wall have an electron cloud of thickess δd, which must be substracted from the actual pore radius. The molecule consists of N atoms and the z-component of the distance between the center of the molecule and the center of atom i is z_i.

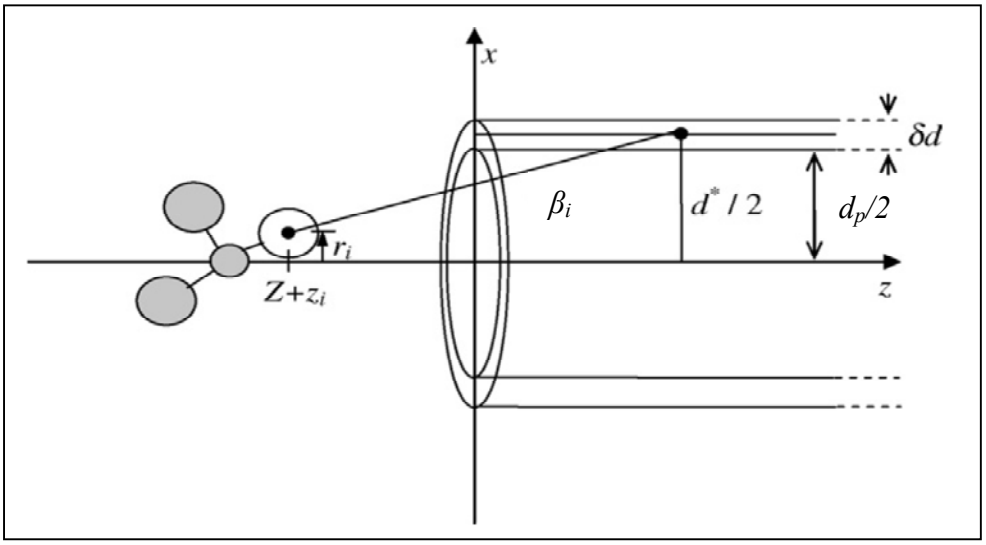

Figure 2-3 Schematic of molecule reaching the pore entrance (adapted from Thornton et al. [20]).

The total force along the pore axis (z-axis) can be obtained by the following double integration:

$$F_z^{tot}(Z) = -\pi(d_p + \delta d)\eta \sum_{i=1}^{N} \int_0^{2\pi} \int_0^{\infty} \frac{d\nu(\beta_i)}{d(\beta_i)} \frac{(Z + z_i - z)}{\beta_i} dz d\theta \tag{2.32}$$

The potential function in Eq. (2.31) can be expressed in terms of the Lennard-Jones potential given in Eq. (2.25):

$$\nu(\beta_i) = 4\varepsilon\left[\left(\frac{\sigma}{\beta_i}\right)^{12} - \left(\frac{\sigma}{\beta_i}\right)^{6}\right] \tag{2.33}$$

or

$$\nu(\beta_i) = -A\beta_i^{-6} + B\beta_i^{-12} \tag{2.34}$$

where, $A = 4\varepsilon\sigma^6$ and $B = 4\varepsilon\sigma^{12}$.

For light gases such as He, H_2, CO_2 and N_2, the center of mass may be is assumed to be on the z axis, and consequently Eq. (2.32) becomes:

$$F_z^{tot}(z) = \sum_{i=1}^{N} \pi (d_p + \delta d)\eta \left[\left(\frac{A_i}{(((d_p + \delta d)/2)^2 + (Z + z_i)^2)^3} \right) \left(\frac{B_i}{(((d_p + \delta d)/2)^2 + (Z + z_i)^2)^6} \right) \right] \quad (2.35)$$

The suction energy (W) is then determined by integrating the total force acting on the molecule as it travels along the pore axis:

$$W = \int_{-\infty}^{\infty} F_z^{tot}(z) dz \quad (2.36)$$

In reality it is sufficient to integrate Eq. (2.36) from -10Å to 10Å, because the interactions become negligible beyond 10Å form pore entrance.

2.3 Results and Discussion

The concept of suction energy, described in the previous section, was used for the estimation of the activation energy required by Eq. (2.23). Moreover, by treating gas molecules as spherical entities with an interaction point at its center, the expression for suction energy obtained by substituting Eq. (2.35) into Eq. (2.36) simplifies to:

$$W = \frac{12\pi^2 \eta}{(d_p + \delta d)^4} \left(A - \frac{42B}{(d_p + \delta d)^6} \right) \quad (2.37)$$

The numerical values of the Lennard-Jones parameters for atoms of which silica membranes are made of, and molecules of light gases that are of interest in this study are presented in Table 2.1.

Table 2-1 Lennard-Jones constants used in this study [20].

Pore atoms	**σ (Å)**	**ε/k (K)**
C	3.85	53
H	2.89	22
O	3.50	30
Si	4.30	202
Gas atoms	-	-
He	2.60	10
H_2	2.89	60
CO_2	3.30	195
N_2	3.64	71

In addition to evaluation of the activation energy required by Eq. (2.23), Eq. (2.37) may also be used for the determination of the mass transfer mechanism as a function of the effective pore diameter for different gas molecules in silica membranes. Setting $W = 0$ in Eq. (2.37) and solving for d_p allows estimation of the maximum effective pore diameter (d_a) for which the Knudsen activated diffusion is a dominant mechanism of gas transport [20]. When the pore size is greater than d_a the mechanism of gas transport depends on the temperature at which the transport takes place, which can be either surface diffusion (which also requires activation energy) or a non-activated Knudsen diffusion. The latter occurs when the kinetic energy of gas molecules is greater than the suction energy. Consequently, knowing the kinetic energy of gas molecules given by Eq. (2.30), one can calculate the pore diameter (d_k) above which non-activated Knudsen diffusion becomes dominant mechanism. In general, $d_k > d_a$, but as temperature increases d_k and the difference between d_k and d_a decreases.

2.3.1 Permeability and Selectivity of Ideal Silica Membrane

Knowing how, for a given type of gas molecules, the mechanism of gas transport depends on the effective pore diameter and temperature one can attempt to predict the permeability coefficient using Eq. (2.23). In turn, this requires the information on the effective pore size (d_p), the geometrical probability factor (ρ_g), as well as the membrane porosity (γ) and tortuosity (τ). These are generally not available. Nevertheless one can define a hypothetical membrane with an ideal morphology for which the calculated permeability coefficients will serve as reference values. In this work the hypothetical (ideal) silica membrane is defined as follow: ρ_g =1/3, $\gamma = 0.25$ and $\tau = 1$. In addition, the atomic surface density of a 7-membered silica ring with oxygen atoms in the ring area was used, and the resulting value of 0.1815 was obtained. It should be emphasized that the latter value may slightly change with the effective diameter of the pore, but it was assumed to be constant in all calculations.

Considering microporous silica membranes reported in the literature, they are most commonly tested with single H_2 and N_2 gases, and thus the respective permeances and the corresponding ideal selectivity are widely available. Consequently, we shell focus now on prediction of the permeability coefficients of H_2 and N_2 in the hypothetical silica membrane defined above.

Using Eq. (2.37) along with Eqs. (2.26) and (2.27), and the Lennard-Jones parameters from Table 2.1 the suction energy of a single molecule was calculated for H_2 and N_2 for different pore sizes, and the results are plotted in Fig. 2.4. As can be seen suction energy is a strong function of pore size and it is negative at first, but as the pore size increases the suction energy increases and it eventually becomes positive. The pore size at which the suction energy is equal to zero corresponds to the maximum pore size at which the activated Knudsen diffusion is expected to occur. It can be noticed that the values of d_a for H_2 and N_2 are different; more specifically for H_2 d_a = 2.63 Å while N_2 d_a = 3.33 Å. This difference arises from the fact that the kinetic diameter of H_2 is smaller than that of N_2.

After becoming positive, the suction energy quickly increases with the pore size reaching a maximum value. It is evident from Fig. 2.4 that for H_2 the maximum suction energy is achieved at smaller pore size than for nitrogen, and the value of the maximum suction energy for H_2 is smaller than that for N_2. After reaching the maximum value, the suction energy decreases as the pore size increases. Eventually, for very large pores it asymptotically approaches zero. When the suction energy becomes smaller than the kinetic energy of gas molecules the non-activated transport in gaseous phase (Knudsen diffusion) becomes dominant.

The maximum suction energy of H_2 in the studied pore size range is 0.86 *eV*, and the temperature at which the kinetic energy of gas molecule reaches that value is 680 K. This is much greater than the iso-concentration point of H_2 of approximately 120 K (Fig. 2.2). In principle, between 120 K and 680 K surface diffusion of H_2 is still possible, but it should be safe to neglect any effects of surface diffusion even at ambient temperatures. For N_2 on the other hand, as expected the suction energy is higher since the molecule has a larger kinetic diameter. The corresponding maximum value of the suction energy for the hypothetical membrane considered in this project is 0.115 *eV*, and the kinetic energy of gas molecules matches this value at 890 K. According to Fig. 2.2 the iso-concentration point for N_2 is approximately 273 K. It is well known that unlike H_2 adsorption of N_2 at ambient temperatures is still significant, but the effects of surface should become negligible well below 890 K. Neglecting the effects of surface and considering only activated and non-activated surface diffusion greatly facilitates the prediction of the permeability coefficients in the hypothetical silica membrane defined above, as a function of the pore size and the pore size distribution.

The thickness of the selective layer in microporous silica membrane is generally unknown, thus the performance of these membranes in the literature is reported in terms of permeance, which the ratio of the permeability and the membrane thickness. Consequently, the permeability of the hypothetical microporous silica membrane defined in this work will be converted into permeance by assuming the thickness of the selective layer to be 30 nm.

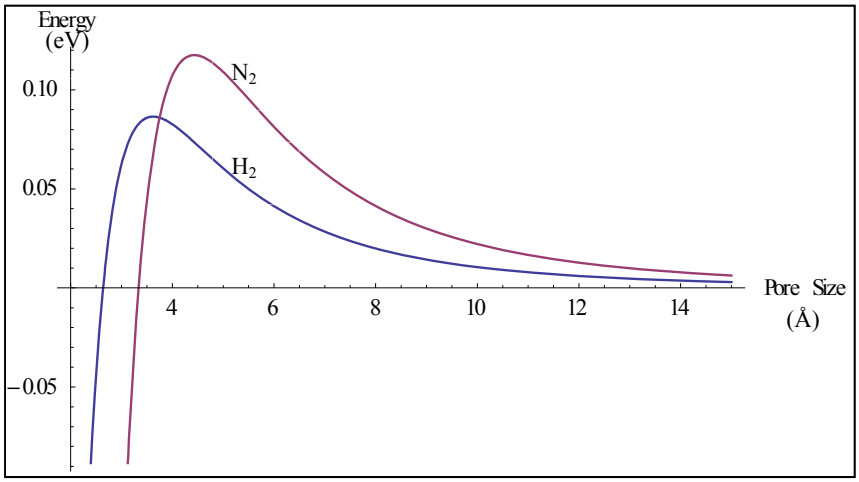

Figure 2-4 Calculated suction energies for different pore sizes for H_2 and N_2.

In this study the permeance of the proposed ideal membrane is going to be determined by defining discrete pore size ranges and determining the permeance of each considering the dominating transfer mechanism in them. The overall permeance is then calculated by considering the calculated permeances of each pore size range, and its weight in membrane's pore size distribution. Before analyzing the experimental data it was decided to demonstrate the application of the proposed permeance calculation method by considering a number of hypothetical pore size distributions for our ideal membrane for H_2, CO, N_2 and CO_2 at 773 K. It should be mentioned that the pore size distribution is the only piece of information required for carrying out the calculations as the structural properties of the membrane are assumed to be constant and were provided earlier in this section. Five different hypothetical pore size distributions are assumed for performing the calculations and they are presented in Fig. 2.5. It should be noted that although the pore size distribution was defined in discrete format, but here they are presented in continuous format in order to make the analysis more convenient. As can be observed from the figure the membranes' average pore size decreases from membrane A to

membrane E, which means that they become more selective to smaller gases. The average pore sizes, the calculated permeances and the ideal selectivities for each membrane are determined and presented in Table 2.2.

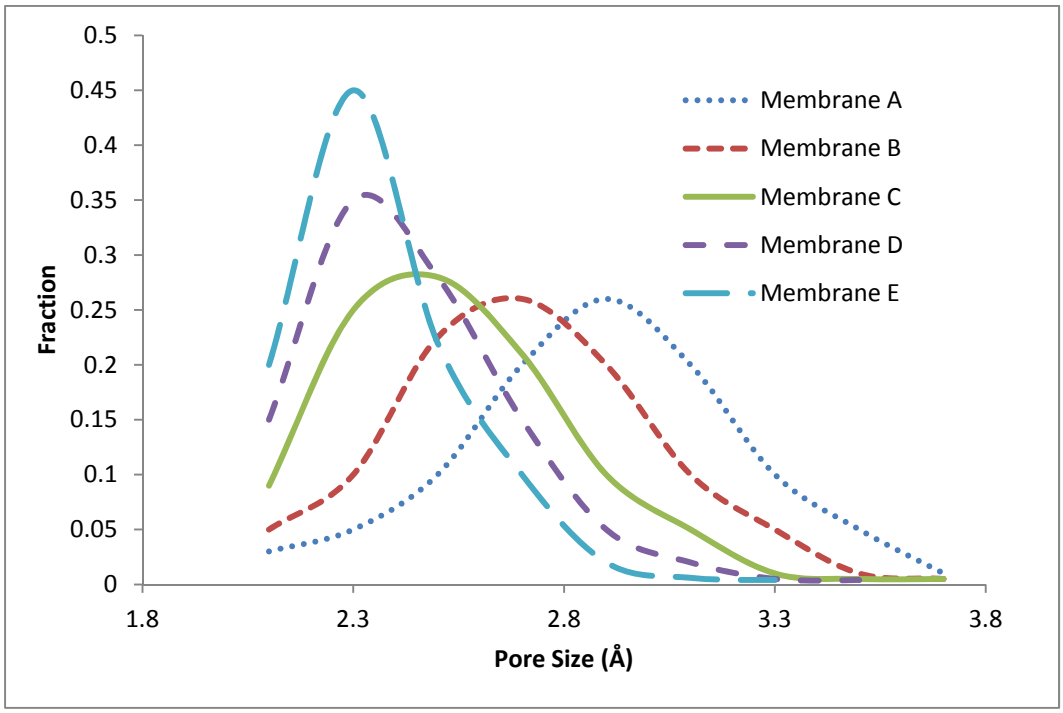

Figure 2-5 Five membranes with different pore size distributions used in permeance calculations for demonstrating the proposed method (discrete results presented in continuous format).

Table 2-2 The calculated permeances, ideal selectivities and average pore sizes for membranes with different pore size distributions.

Membrane	H_2 permeance (mol/Pa s m^2)	CO permeance (mol/Pa s m^2)	N_2 permeance (mol/Pa s m^2)	CO_2 permeance (mol/Pa s m^2)	$\alpha^*_{H_2/N_2}$	Average Pore size (Å)
A	1.21×10^{-5}	7.28×10^{-7}	3.14×10^{-7}	4.13×10^{-8}	19.5	2.88
B	9.01×10^{-6}	2.95×10^{-7}	8.84×10^{-8}	2.00×10^{-8}	38.15	2.71
C	5.45×10^{-6}	9.46×10^{-8}	5.32×10^{-8}	1.94×10^{-8}	60.60	2.58
D	3.30×10^{-6}	4.17×10^{-8}	2.10×10^{-8}	1.74×10^{-10}	98.65	2.46
E	1.90×10^{-6}	1.79×10^{-8}	1.35×10^{-9}	8.15×10^{-12}	212.30	2.36

By looking at the results it can be seen that the permeance decreases from H_2 to CO_2 which is the expected trend as the kinetic diameter of the gases increase. Also as the average pore size decreases permeances of all gases drop but the changes in gases with greater kinetic diameter are more dramatic, because of their higher activation energies.

2.4 Experimental Results

The results of single gas permeation tests with N_2, H_2 and He on four microporous silica membranes were kindly provided by Natural Resources Canada, CANMET Energy Technology Center (CETC) laboratory in Ottawa. All membranes were also prepared in the same laboratory using commercial α-alumina tubes as a support. Prior to deposition of SiO_2, a layer of γ-alumina was coated on the alumina support. The process of coating with γ-alumina was repeated several times to provide uniform and defect-free surface of the supports, which is critical for the placement of a thin and selective top-layer. The selective SiO_2 layer was synthesized using a chemical vapour deposition (CVD) process with tetraethyl orthosilicate (TEOS, $Si(OC_2H_5)_4$) as the silica precursor and oxygen. After each SiO_2 deposition, single gas permeation tests with N_2, H_2 and He were carried out. All gas permeation tests were performed at 773 K (500^oC). The purpose of this was to determine the optimum number of the SiO_2 layers. In general, the selectivity of the membranes was increasing with the number of the SiO_2 layers up to the point at which a subsequent SiO_2 layer did not bring any improvement in membrane selectivity. The details of the membrane synthesis protocol and the gas permeation protocol were not subject of investigation in this project. Table 2.3 summarizes the performance of four microporous after the last SiO_2 deposition.

Table 2-3 Single gas permeation tests results for four different membranes at 773 K.

Membrane	He permeance (mol/Pa s m^2)	H_2 permeance (mol/Pa s m^2)	N_2 permeance (mol/Pa s m^2)	α^*_{He/H_2}	α^*_{He/N_2}	$\alpha^*_{H_2/N_2}$
1	1.74×10^{-7}	8.02×10^{-8}	7.44×10^{-9}	2.16	23.33	10.78
2	5.98×10^{-8}	2.00×10^{-8}	5.19×10^{-10}	2.99	115.30	38.50
3	1.82×10^{-8}	3.53×10^{-9}	6.22×10^{-11}	5.15	291.67	56.67
4	2.34×10^{-8}	1.01×10^{-8}	1.77×10^{-9}	2.33	13.26	5.69

It is evident that the performance of the membranes in Table 2.3 varies quite significantly. For example, helium permeance ranges by an order of magnitude from 1.82×10^{-8} to 1.74×10^{-7} mol/Pa s m^2. Similarly, the ideal selectivity for He/N_2 also varies by an order of magnitude from 13.26 to 291.67. Interestingly, the least permeable membrane is not the most selective membrane in Table 2.2. In other words, the commonly expected trade-off behavior (permeance increases – selectivity decreases and vice versa) is not evident in the data shown in Table 2.2.

Figure 2.6 summarizes the performance of membranes shown in Table 2.3 in terms of H_2 permeance and H_2/N_2 ideal selectivity. In addition, Fig. 2.6 also includes the literature data from Khatib et al. [3] for the microporous silica membranes tested at 773 K with these two gases and the results of the calculations for the five ideal membranes which were carried out in previous section. In general, the literature microporous silica membranes outperform the NRCan membranes. However, the literature data shows even a greater scatter than the NRCan data, with the respective permeances and ideal selectivities stretching over three orders of magnitude. As for the ideal membranes it can be said that the obtained results with hypothetical pore size distributions are comparable with the literature data, but as it can be seen the obtained selectivity increases dramatically as average pore size slightly decrease. In terms of ideal selectivity the hypothetical ideal membranes can be considered to be in the middle of the available range, but in terms of permeance they are located in the highest end of the range. In the following analysis we will focus only on the membranes synthesized in the NRCan laboratory. Despite a significant variation in their performance, there are several important observation which should be emphasized now.

Among the tested gases N_2 has the largest kinetic diameter and molecular weight so it will have the lowest permeance in both activated and Knudsen diffusion. For H_2 and He pair, the selectivity can be quite different depending on the transfer mechanism as in activated diffusion the gas with larger kinetic diameter (H_2) will face a higher energy barrier for diffusion so its permeance will be lower than He, and the membrane will be He selective. At pore sizes above d_k (or d_a as they are equal in our case) both of them will diffuse by Knudsen mechanism, and the membrane will be H_2 selective as it has a smaller molecular weight comparing to the He.

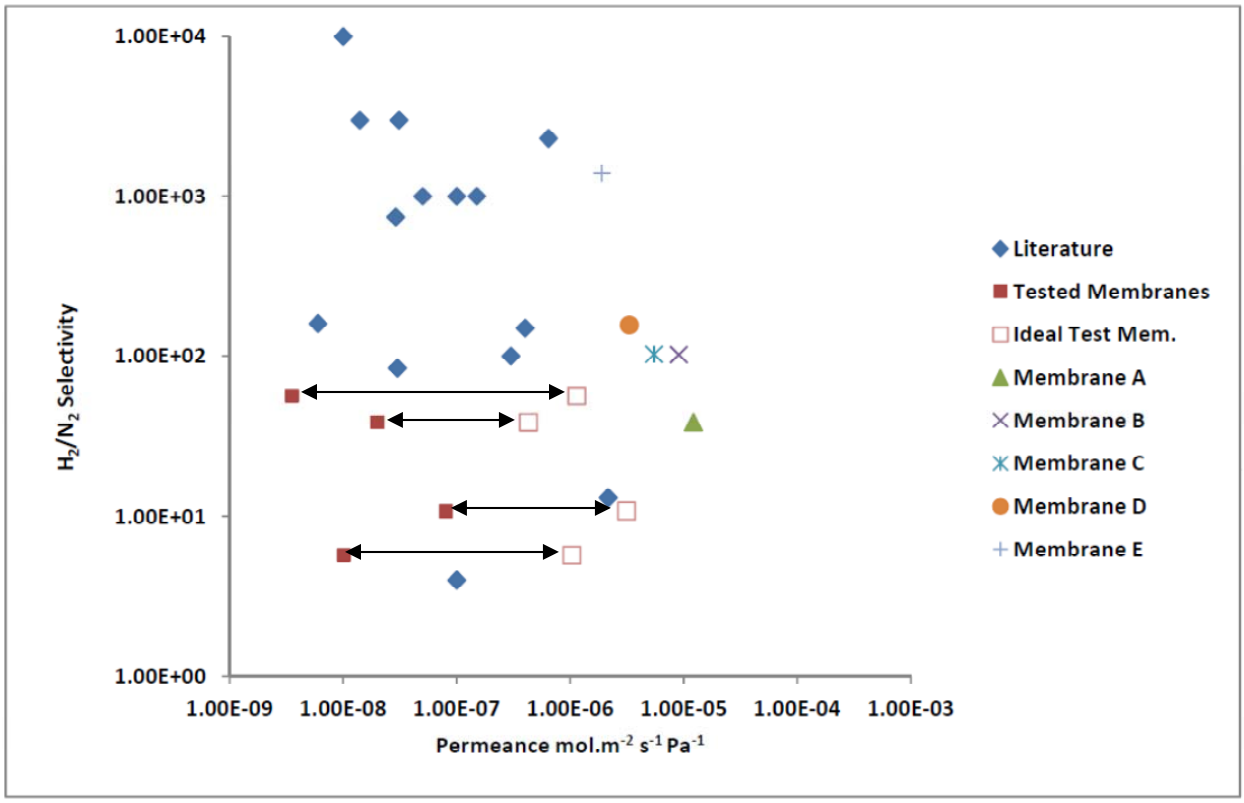

Figure 2-6 Comparing the performance of the available silica membranes with some reported silica membranes in the literature gathered by Khatib et al. [3] and also the calculated properties of some ideal membranes with hypothetical pore size distributions.

It should be noted that in previous section the iso-concentration for He was not determined but as it has a smaller kinetic diameter comparing to H_2 it can be assured that it is below 680 K. As for N_2 although the temperature that surface diffusion can be neglected is 890 K and our test were carried out at 773 K, but here it is going to be assumed that there is no surface diffusion and $d_k = d_a$ for N_2 as well other tow gases.

As can be seen the activated diffusion is the dominating transfer mechanism as the values of ideal selectivities are well above the Knudsen selectivities (2.64 for He/N_2 and 3.73 for H_2/N_2). Even for the smallest pair the diffusion is activated because if it was Knudsen diffusion the membranes should have been H_2 selective instead of He.

2.4.1 Membrane Characterization and Pore Size Distribution

In next step it is tried to determine the permeance of the ideal membrane capable of delivering the observed selectivity for each of the four test membranes theoretically. In order to do this it is required to estimate the pore size distribution of the membranes using the provided selectivities. This can be done by minimizing the error of the calculated selectivity with respect to experimental selectivity by defining some discrete pore size ranges and setting their weights as the variables:

$$f(x)=\left|\frac{\sum_{i=1}^{m}x_i\overline{P}_{MHe,i}}{\sum_{i=1}^{m}x_i\overline{P}_{MH_2,i}}-\alpha^*_{He/H_2}\right|+\left|\frac{\sum_{i=1}^{m}x_i\overline{P}_{MHe,i}}{\sum_{i=1}^{m}x_i\overline{P}_{MN_2,i}}-\alpha^*_{He/N_2}\right|+\left|\frac{\sum_{i=1}^{m}x_i\overline{P}_{MH_2,i}}{\sum_{i=1}^{m}x_i\overline{P}_{MN_2,i}}-\alpha^*_{H_2/N_2}\right| \tag{2.38}$$

$$\sum_{i=1}^{m}x_i=1 \tag{2.39}$$

$$0<x_i<1 \tag{2.40}$$

where m is the number of pore size ranges, and $\overline{P}_{MHe}$ is the permeance of He in pore size i. It should be noted the ideal permeance of each gas is determined by calculating the permeance of each pore size range and multiplying it by its weight, and consequently theoretical ideal selectivity is the ratio of two calculated ideal permeances. The objective function also can be defined alternatively if non-linear optimization employed:

$$f(x)=\left(\frac{\sum_{i=1}^{m}x_i\overline{P}_{MHe,i}}{\sum_{i=1}^{m}x_i\overline{P}_{MH_2,i}}-\alpha^*_{He/H_2}\right)^2+\left(\frac{\sum_{i=1}^{m}x_i\overline{P}_{MHe,i}}{\sum_{i=1}^{m}x_i\overline{P}_{MN_2,i}}-\alpha^*_{He/N_2}\right)^2+\left(\frac{\sum_{i=1}^{m}x_i\overline{P}_{MH_2,i}}{\sum_{i=1}^{m}x_i\overline{P}_{MN_2,i}}-\alpha^*_{H_2/N_2}\right)^2 \tag{2.41}$$

$$f(x)=\left(\frac{\sum_{i=1}^{m}x_i\overline{P}_{MHe,i}}{\sum_{i=1}^{m}x_i\overline{P}_{MH_2,i}}-\alpha^*_{He/H_2}\right)^4+\left(\frac{\sum_{i=1}^{m}x_i\overline{P}_{MHe,i}}{\sum_{i=1}^{m}x_i\overline{P}_{MN_2,i}}-\alpha^*_{He/N_2}\right)^4+\left(\frac{\sum_{i=1}^{m}x_i\overline{P}_{MH_2,i}}{\sum_{i=1}^{m}x_i\overline{P}_{MN_2,i}}-\alpha^*_{H_2/N_2}\right)^4 \tag{2.42}$$

Eqs. (2.42) and (2.43) are two alternative forms of the objective function, and they are presented here to see if these changes can affect the calculated pore size or not. These objective functions were used to estimate the pore size distribution of the Membrane 2 from Table 2.3 and the determined pore size distributions are presented in Table 2.4 and Fig. 2.7. It should be noted that PSD1 is obtained using the liner objective function presented in Eq. (2.38) and PSD2 and PSD3 and determined using the non-linear objective functions shown in Eqs. (2.42) and (2.43) respectively.

Table 2-4 Different pore size distributions (PSD) and ideal permeances for membrane 2 using different forms of objective functions.

d_p (Å)	PSD1	PSD2	PSD3
2.1	7.24×10^{-4}	7.29×10^{-2}	7.68×10^{-1}
2.3	9.01×10^{-1}	1.89×10^{-1}	9.89×10^{-2}
2.5	7.50×10^{-2}	6.05×10^{-1}	1.06×10^{-1}
2.7	2.10×10^{-2}	2.37×10^{-2}	3.50×10^{-5}
2.9	2.04×10^{-5}	1.62×10^{-2}	2.88×10^{-5}
3.1	5.55×10^{-5}	2.15×10^{-2}	1.82×10^{-4}
3.3	1.72×10^{-4}	6.19×10^{-2}	2.50×10^{-2}
3.5	8.25×10^{-4}	4.73×10^{-3}	1.20×10^{-3}
3.7	1.47×10^{-3}	4.61×10^{-3}	3.41×10^{-4}
f(x)*	5.56×10^{-3}	5.47×10^{-3}	5.42×10^{-3}

* The presented value of f(x) for PSD2 and PSD3 are the 4th and 6th root of the calculated f(x) in non-linear optimizations.

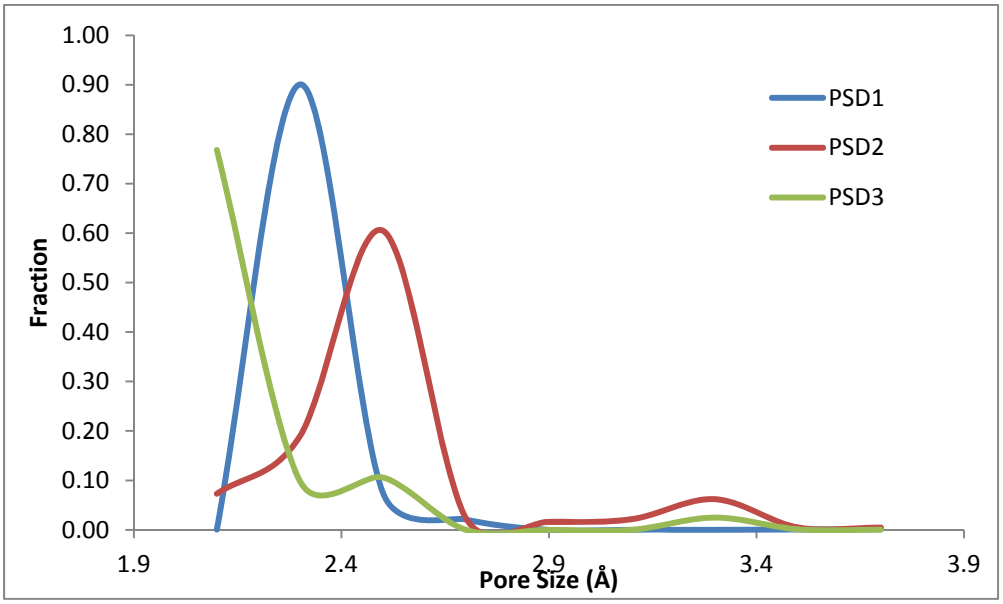

Figure 2-7 Pore size distributions determiend using different objective functions.

As can be seen the determined pore size distributions by different forms of objective functions are not identical and there are considerable differences between them, but they all provide the same ideal selectivity. Also if the numerical value of the objective is taken into account it can be seen that they are more or less the same, and it is hard to choose one of the three pore size distributions just based on the values of their objective functions. Furthermore smaller objective function might not necessarily mean more accurate results as the terms used in the objective function (experimental ideal selectivities) are not in the same order. For instance $\alpha^*_{He/H_2} = 2.99$, but $\alpha^*_{He/H_2} = 115.30$ so changes in the value of the objective will not cause identical deviations in both selectivities.

Based on the above discussion it was decided to use all the three objective functions for determining the pore size distributions as they all can satisfy the ideal selectivity conditions, but it is recommended to test this method for membranes with more number of test gases which supposedly can eliminate the multiple answers. The three different pore size distributions calculated for each of the four test membranes are presented in Tables 2.3 and 2.4. The weight of each pore size is presented in the corresponding rows and those can be used to determine the ideal permeances, which are also presented in the same tables.

Table 2-5 Different pore size distributions (PSD) and ideal permeances for membrane 1 and 2.

d_p (Å)	PSD1	PSD2	PSD3	PSD1	PSD2	PSD3
	Membrane 1			Membrane 2		
2.1	1.49×10^{-1}	5.69×10^{-1}	3.15×10^{-1}	7.24×10^{-4}	7.29×10^{-2}	7.68×10^{-1}
2.3	1.49×10^{-1}	2.41×10^{-2}	1.52×10^{-2}	9.01×10^{-1}	1.89×10^{-1}	9.89×10^{-2}
2.5	5.18×10^{-1}	2.97×10^{-1}	4.94×10^{-1}	7.50×10^{-2}	6.05×10^{-1}	1.06×10^{-1}
2.7	2.02×10^{-2}	1.03×10^{-4}	1.69×10^{-2}	2.10×10^{-2}	2.37×10^{-2}	3.50×10^{-5}
2.9	1.83×10^{-2}	6.51×10^{-3}	2.48×10^{-3}	2.04×10^{-5}	1.62×10^{-2}	2.88×10^{-5}
3.1	7.06×10^{-2}	6.60×10^{-2}	7.61×10^{-2}	5.55×10^{-5}	2.15×10^{-2}	1.82×10^{-4}
3.3	1.65×10^{-2}	8.43×10^{-5}	2.33×10^{-2}	1.72×10^{-4}	6.19×10^{-2}	2.50×10^{-2}
3.5	3.19×10^{-2}	3.52×10^{-2}	5.44×10^{-2}	8.25×10^{-4}	4.73×10^{-3}	1.20×10^{-3}
3.7	2.69×10^{-2}	7.86×10^{-4}	2.42×10^{-3}	1.47×10^{-3}	4.61×10^{-3}	3.41×10^{-4}
$\overline{P}_M$ (mol/pa.sm^2)						
$\overline{P}_{MHe}$	6.68×10^{-6}	3.97×10^{-6}	6.36×10^{-6}	1.27×10^{-6}	6.83×10^{-6}	1.46×10^{-6}
$\overline{P}_{MH_2}$	3.13×10^{-6}	1.86×10^{-6}	2.98×10^{-6}	4.27×10^{-7}	2.30×10^{-6}	4.91×10^{-7}
$\overline{P}_{MN_2}$	2.86×10^{-7}	1.70×10^{-7}	2.73×10^{-7}	1.10×10^{-8}	5.92×10^{-8}	1.27×10^{-8}

Table 2-6 Different pore size distributions (PSD) and ideal permeances for membrane 3 and 4.

d_p (Å)	PSD1	PSD2	PSD3	PSD1	PSD2	PSD3
	Membrane 3			Membrane 4		
2.1	1.79×10^{-1}	4.76×10^{-1}	1.49×10^{-2}	2.59×10^{-1}	1.93×10^{-1}	6.07×10^{-1}
2.3	1.87×10^{-1}	4.33×10^{-2}	3.06×10^{-3}	5.20×10^{-1}	3.68×10^{-1}	1.86×10^{-1}
2.5	5.73×10^{-1}	4.36×10^{-1}	8.87×10^{-1}	1.66×10^{-1}	3.37×10^{-1}	1.55×10^{-1}
2.7	1.35×10^{-2}	9.42×10^{-6}	6.48×10^{-4}	4.52×10^{-3}	2.58×10^{-3}	2.52×10^{-5}
2.9	1.68×10^{-2}	1.26×10^{-2}	8.82×10^{-2}	5.07×10^{-3}	1.12×10^{-2}	3.19×10^{-4}
3.1	1.54×10^{-2}	1.40×10^{-2}	2.84×10^{-4}	4.07×10^{-3}	8.96×10^{-4}	1.63×10^{-2}
3.3	1.14×10^{-2}	1.64×10^{-2}	1.06×10^{-4}	3.67×10^{-3}	1.88×10^{-2}	1.52×10^{-5}
3.5	1.40×10^{-3}	2.08×10^{-3}	2.58×10^{-3}	2.25×10^{-2}	3.43×10^{-2}	3.09×10^{-2}
3.7	2.01×10^{-3}	2.42×10^{-4}	3.54×10^{-3}	1.53×10^{-2}	3.40×10^{-2}	4.38×10^{-3}
$\overline{P}_M$ (mol/pa.sm^2)						
$\overline{P}_{MHe}$	5.76×10^{-6}	4.43×10^{-6}	8.72×10^{-6}	2.38×10^{-6}	4.36×10^{-6}	2.19×10^{-6}
$\overline{P}_{MH_2}$	1.14×10^{-6}	8.74×10^{-7}	1.72×10^{-6}	1.03×10^{-6}	1.89×10^{-6}	9.45×10^{-7}
$\overline{P}_{MN_2}$	1.97×10^{-8}	1.52×10^{-8}	2.99×10^{-8}	1.80×10^{-7}	3.29×10^{-7}	1.65×10^{-7}

By comparing the calculated permeances for each membrane with different pore size distributions it can be seen that they are not identical as expected because they are calculated using different pore size distributions, which consequently leads to different permeance values. Another issue to be considered is that the calculated values for either pore size distribution is greater than the experimental permeance for all of the gases that are presented in Table 2.2. For instance for the membrane 1, the average calculated permeance considering three different pore size distributions is 5.67×10^{-6} compared to the experimental value of 1.74×10^{-7}. The calculated values were also plotted in Fig. 2.6 in order to compare them with the actual values, and the corresponding calculated values to the experimental values are connected with arrows.

Pore size distribution and silica network's properties can be considered as uncertainties in determining the membrane's permeance theoretically. Currently there is no method available for estimating the pore size distribution of microporous materials, and the current methods such as nitrogen adsorption/desorption and boiling point depression only work for mesoporous material. Knowing that the amorphous silica networks has a random and complex structure, which is built of silica molecules connecting together with no particular order makes estimating the permeance of silica membranes challenging. These facts suggest that characterization of silica membrane cannot simply be done by relying on theoretical methods.

This method can also be used the other way around to estimate the pore size distribution but as it was shown there are number of pore size distribution combinations that can provide a certain selectivity for a membrane, and the calculated ideal permeance for each of them are different. It is true that using this method for estimating the pore size distribution results in more than one pore size combination, but as the number of gases used in the characterization process increases the probability of getting multiple answers decreases as the terms in objective function will increase significantly. If the experimental results of n gases are used for characterization, then the objective function will have N terms which it can be determined by Eq. (2.43). For instance if instead of three gas four gases are used the number of terms in objective function will get doubled.

$$N = \frac{n(n-1)}{2} \tag{2.43}$$

One of the estimated possible pore size distributions (PSD1) for the four test membranes are presented in Fig. (2.8) based on the ideal selectivities. It should be noted that PSD1 is chosen randomly as all the presented pore size distribution combinations will provide same selectivities.

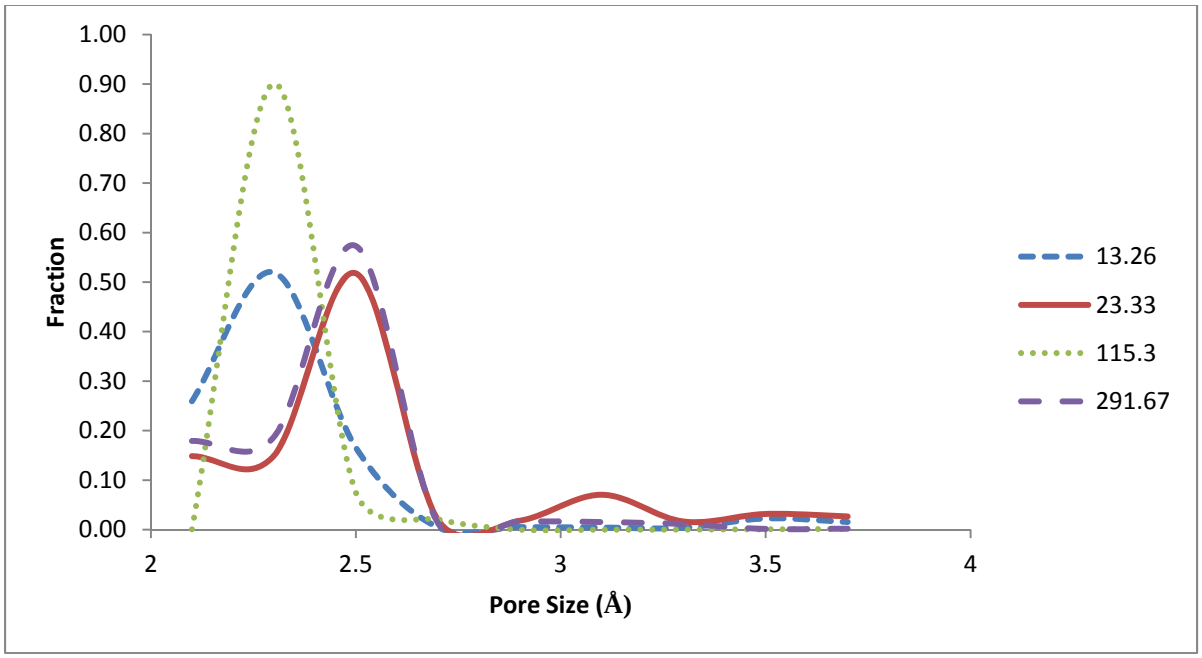

Figure 2-8 Pore size distribution of the four different test membranes presented based on low to high hydrogen selectivity

As can be understood from the calculated pore sizes, in all the membranes activated diffusion is the dominant mechanism of mass transfer, which is in agreement with what is anticipated. High selective membranes (ideal selectivity of 115.3 and 291.67 for He/N_2 which are membranes 2 and 3 respectively) do not have significant fraction of pore sizes greater 2.7 Å, and they almost have no pores greater than 3.3 Å where pure Knudsen diffusion happens.

Another remarkable fact is revealed by comparing the pore size distribution of the two most selective membranes (2 and 3), and that is although membrane 2 ($\alpha^*_{H_2/N_2} = 115.3$) is less selective comparing to the membrane 3 ($\alpha^*_{H_2/N_2} = 291.67$), but it has a smaller effective pore size as about 90% percent of its pore are in 2.3 Å range. This can be justified by considering the transition from activated to Knudsen diffusion, which means although the pores of the membrane 3 are bigger in overall, but it has more pores in 2.5 Å range, which is where He transfers by Knudsen diffusion with no energy barrier, but N_2 still permeates by activated diffusion, so the selectivity in this pore size range is greater than the previous smaller range.

This is a very important point as it implies that at some point making the pores smaller does not necessarily result in higher selectivities in all cases, and it just affects the permeance of the membrane negatively. This issue was further investigated by monitoring the effect of number of silica coats on the membranes selectivity for He/N_2 system for four more membranes, and the results are presented in Figs. (2.7) to (2.9). As can be seen the selectivity has increased as the number of silica layers increased, but it has stopped at some point and started to decline instead of going up. This confirms that over-depositing the silica after a certain point may result in loss of both selectivity and permeance. These observation can be used to justify the simultaneous decrease in selectivity and permeance as the result of densification of silica membrane in presence of water .

These results are not in agreement with the proposed theory by Lee et al. [16] as they mentioned that small gases diffuse by solid state diffusion mechanism while the larger gases permeate by a combination of activated and Knudsen diffusion. As can be seen here by coating more silica the permeance of the smaller gas has decreased as opposed to increasing, which contradicts the claim made by Lee et al. This matter can be further investigated by performing permeation tests for Ne, and also repapering the single gas permeation tests in different

temperature to study the effect of temperature on mass transfer. These tests will eventually help us to obtain a better understanding about silica membranes, as solid state diffusion and activated diffusion respond differently to temperature increase.

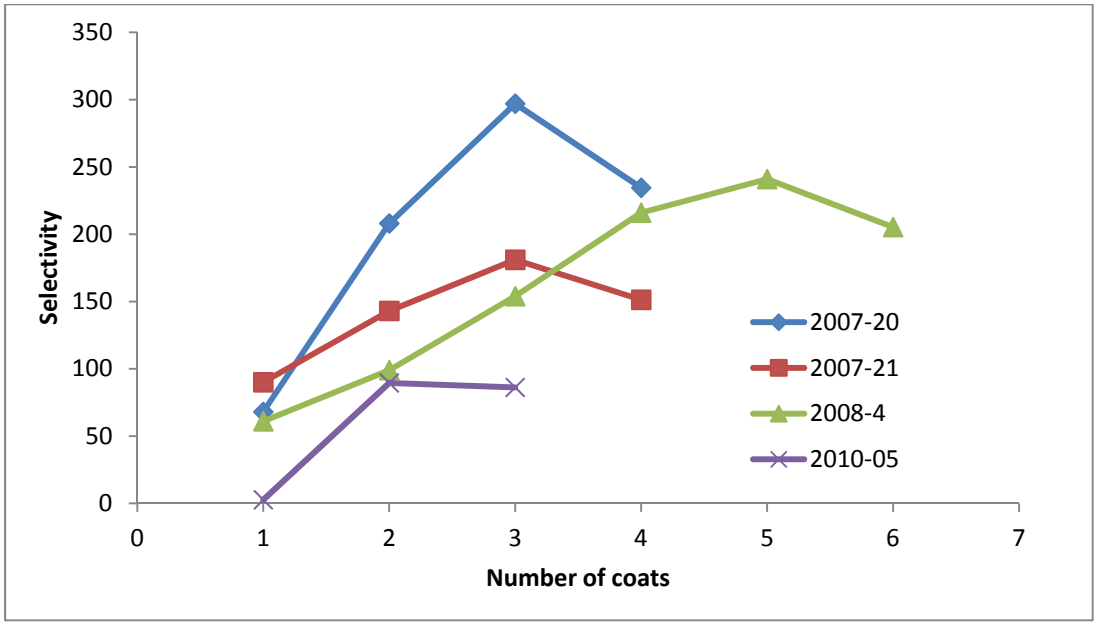

Figure2-9 Selectivity of He over N_2 vs. number of silica coats for four different membranes.

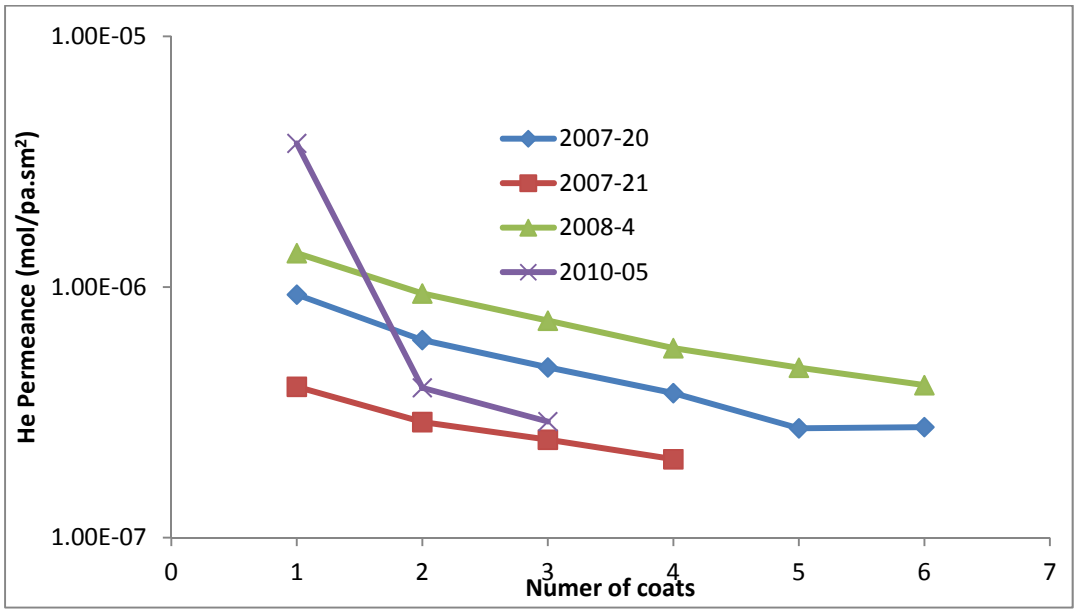

Figure 2-10 Permeance of He vs. number of silica coats for four different membranes.

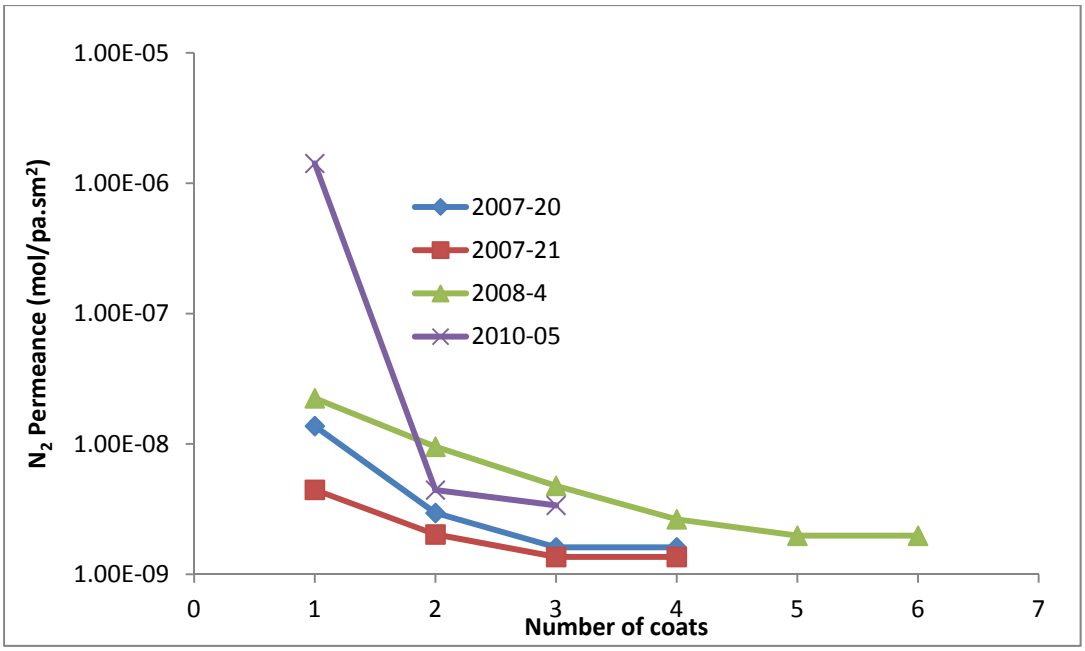

Figure 2-11 Permeance of N2 vs. number of silica coats for four different membranes.

It should be noted that in the proposed characterization method (depending on the size of the diffusant) the permeance in pores below a certain size can be neglected as it would be insignificant and practically zero, so a lower limit can be defined for the pore size distribution. This method can be used to determine the pore size distribution up to the pore size that the larger molecules starts to diffuse by Knudsen mechanism, but that it cannot be used to predict the pore size distribution for pores greater than that, because beyond that point there is no tool to track the membranes behaviour as the transfer happens due to pure Knudsen diffusion. This problem can be overcome by using relatively large molecules such as SF_6, which can extend the range of applicability of this method or even limit the upper pore size value if it fails to permeate through the membrane. By considering the fact that the membranes with pore sizes greater than the kinetic diameter of SF_6 (5.5 Å) are not suitable for hydrogen separation, this gas can be used to set the upper limit of the pore sizes in the characterization calculations of hydrogen selective membranes.

2.4.2 Scaling Factor

As the calculated ideal permeances were not close to the actual values it was decided to improve the accuracy of the proposed method with help of experimental data. The idea is to predict the permeance of a gas for which there is no experimental permeation data available using permeation results of other gases. In order to do this the term scaling factor is introduced which is the ratio of the experimental permeance to ideal calculated permeance for a hypothetical membrane:

$$\zeta_A = \frac{\overline{P}_{M,A}}{\overline{P}_{MI,A}} \tag{2.44}$$

where ζ_A is the scaling factor, $\overline{P}_{M,A}$ and $\overline{P}_{MI,A}$ are the actual and the ideal permeances of component A respectively. Scaling factor can be determined by carrying out permeation tests and comparing the experimental permeances with the ideal calculated permeances. The pore size distribution can be estimated using the permeation tests and it can be used along with the assumed structural properties of the hypothetical membrane to calculate the ideal permeances. The calculated scaling factor then can be used to estimate the permeances of other gases based on their ideal permeances without requiring any further permeation tests.

The proposed concept of the scaling factor can be easily verified experimentally. It would simply require testing newly synthesized amorphous silica membranes with as many single gases as possible. For example, by testing membrane with four gases, the permeance of any three of them can be used to determine the pore size distribution and the scaling factor. Then the theoretically predicted permeance of the fourth gas could be compared with the experimental data. It is anticipated that by increasing the number of single gases used for the determination of the pore size and the scaling factor would improve the prediction of permeances of other gases in a given membrane.

2.5 Conclusion

The objectives of the current Chapter was to derive the properties of the amorphous silica membrane, such as permeability and ideal selectivity, from first principles. Such fundamentally-derived properties are to serve as a bench mark when evaluating experimentally determined properties of amorphous silica membranes. Moreover, ultimately they are to be used as a tool for the optimization of the fabrication protocol of amorphous silica membranes.

This part of the study started with reviewing the mass transfer mechanisms in hydrogen selective silica membranes. Knudsen diffusion, surface diffusion and activated diffusion were identified as the main transfer mechanisms that might occur simultaneously, with the respective contributions depending on the membrane pore size distribution and the temperature of the process. The permeability in Knudsen diffusion can be determined theoretically provided that the properties of the silica network such as porosity and tortuosity are known. For surface diffusion, in addition to the silica network properties, estimating the permeability coefficient also requires adsorption isotherms of every gas from the feed mixture on amorphous microporous silica. However, in the case of hydrogen selective membranes, which must be operated at elevated temperatures that are normally considerably above the iso-concentration point of every gas from the feed mixture, surface diffusion can be neglected. In order to be able to estimate the permeance of gases in activated diffusion region it is essential to determine the activation energy of diffusion. Here the activation energy was determined based on the concept of suction energy which is quantified by integration of Van der Waals forces at the membrane pore entrance. The concept of suction energy can also be used to identify the transfer mechanisms based on the membrane pore size and the gas iso-concentration points. Negative suction energy indicates that the transfer mechanism is activated and on the other hand Knudsen diffusion is dominant if the kinetic energy of gas is greater than the suction energy. Surface diffusion happens in pore sizes between activated and Knudsen diffusion, but if the gas temperature is higher than the iso-concentration point then surface diffusion cannot take place as the interactions between gas and membrane's wall are less than the kinetic energy of the gas. In this case the transfer mechanism will shift directly from activated to Knudsen diffusion.

In the next step the properties of a hypothetical ideal silica membrane were determined for H_2, CO, N_2 and CO_2 gases by assuming five different hypothetical pore size distributions. In order to determine the permeance first the transfer mechanisms were identified and it was seen that the effect of surface diffusion is negligible so it was concluded that activated and Knudsen diffusion can happen. The overall permeances were determined based on the permeances in each pore size range and the weight of the each them. The calculated permeances were comparable to those of that are available in the literature, and it was observed that the calculated values are in the operating range of available silica membranes.

The method then was used to estimate the permeances of the four test membranes to compare them with the available experimental data which were kindly provided by Natural Resources Canada, CANMET Energy Technology Center (CETC) laboratory in Ottawa. First it was necessary to estimate the pore size distribution of the membranes, which was estimated based on the experimental selectivities for the available three gases, and it was observed that there is more than one pore size distribution that is capable of satisfying the ideal selectivity criteria and they vary depending on the type of the objective function (linear or non-linear). As the numerical values of the objective functions were close to each other it was not clear which method of presenting the objective function is better so it was decided to determine the pore size distributions with all of the presented objective functions for the four test membranes. This was also done because the numerical value of the objective function is not a proper measure for determining the most accurate method because the terms in the objective function (selectivities) are not in the same order so the deviations in selectivities will not be the same.

The ideal permeances were determined for three different pore size distribution combinations for each membrane and the results were compared with the experimental data. The calculated values in all cases were much greater than the actual permeances, which was not surprising considering that the hypothetical membrane was assumed to be very thin (20 nm) with straight cylindrical channels and thus the tortuosity and the probability factor equal to unity and 1/3 (the highest possible values), and a porosity of 25%. By reviewing the results it can be concluded that relying on pure theoretical methods for determining the permeance of amorphous silica membranes is not going to be successful as silica membrane has a complex and amorphous structure. It should be noted that this method can be used for estimating the pore size distribution

of the silica membranes based on multiple gas permeations tests with different gases. By increasing the number of the test gases the number of the terms in the objective function will increase significantly and supposedly the probability of getting multiple answers will reduce. Application of the method is not limited to this specific type of membranes; it can be used for any type of membrane with pore sizes in the order of few Angstroms.

By looking at determined pore size distribution for the four available test membranes it was evident that smaller pore size does not necessarily mean higher ideal selectivity as for microporous membranes there is a an optimum pore size range where the smaller gas permeates by Knudsen diffusion but the larger gas is passing through by activated diffusion. This combination of the transfer mechanisms results in higher selectivity comparing to its adjacent smaller pore size range as the both gases permeate by activated diffusion. This can be considered as a very important point, as unlike what is normally believed that more silica coats would result in higher selectivity and lower permeance, overdoing the coating procedure may actually result in both lower selectivity and lower permeance. This was investigated further on four more membranes and it was observed that for all of them the selectivity dropped after a certain point while adding more silica layers. This finding can be used to justify the ideal selectivity drop caused by silica membrane's densification, which happens in presence of water and degrades both permeance and selectivity of membrane. From membrane making point of view having a tool for estimating pore size distribution of fabricated membranes would be beneficial, as makes it possible to track the effects of fabrication processes on the pore size distribution in order to aim for the optimum pore size.

Considering that regardless of the objective function and the resulting pore size distribution, the permeances of the hypothetical membrane matching the experimental ideal selectivities, were much higher than the experimental permeances, the concept of a scaling factor was introduced. The scaling factor, which is simply the ratio of the experimental permeance to the permeance of the hypothetical membrane that matches the experimental selectivities, provides a cumulative correction factor for the assumed morphology of the hypothetical membrane. The proposed concept of the scaling factor can be easily verified experimentally. It would simply require testing newly synthesized amorphous silica membranes with as many single gases as possible. For example, by testing membrane with four gases, the permeance of

any three of them can be used to determine the pore size distribution and the scaling factor. Then the theoretically predicted permeance of the fourth gas could be compared with the experimental data. It is anticipated that by increasing the number of single gases used for the determination of the pore size and the scaling factor would improve the prediction of permeances of other gases in a given membrane.

For future studies it is recommended to investigate the transfer mechanisms in the silica membranes further by performing single gas permeation tests for Ne gas, and also to repeat the permeation tests for He, H_2, N_2 and some larger gases such as CO_2, and CH_4 at few temperature point above the iso-concentration point of the most condensable gas. The results of these tests would help us solidify our knowledge about the transfer mechanisms in silica membranes and especially study the possibility of presence of solid state diffusion in silica membranes as activated diffusion and solid state diffusion would behave differently as temperature increases.

Nomenclature

a_v : Specific surface area (m^2/kg)

A: Membrane area (m^2)

C: Concentration (mol/m^3)

d: Diameter (m)

D: Diffusivity (m^2/s)

E: Activation energy (kJ/mol)

G: Shear modulus (Pa)

t: Membrane thickness (m)

M: Molecular weight (gr/mol)

n: Molar flow rate (mol/s)

p: Pressure (Pa)

P_M: Permeability ($mol.m.Pa^{-1}.s^{-1}.m^{-2}$)

$\overline{P}_M$: Permeance ($mol.Pa^{-1}.s^{-1}.m^{-2}$)

R: Gas constant ($J/mol.K$)

T: Temperature (K)

W: Suction energy (J)

Greek letters

α^*: Ideal selectivity

α: Actual selectivity

τ: Tortuosity

γ : Porosity

μ: Viscosity (*Pa.s*)

ρ: Density (kg/m^3)

Φ : Potential energy (*J*)

σ : Characteristic diameter of the molecules (*m*)

ε : Characteristic energy (*J*)

ζ : Scaling factor

References

[1] Nagasawa, H. Shigemoto, H. Kanezashi, M. Characterization and gas permeation properties of amorphous silica membranes prepared via plasma enhanced chemical vapor deposition, Journal of Membrane Science, 441 (2013) 45–53.

[2] Ohta, T. Akamatsua, K. Sugawara, T. Nakao, A. Development of pore size-controlled silica membranes for gas separation by chemical vapor deposition, Journal of Membrane Science 315 (2008) 93‑99.

[3] Khatib, S. Oyama, S. Silica membranes for hydrogen separation prepared by chemical vapor deposition (CVD), Separation and Purification Technology, 111 (2013) 20–42.

[4] Tsuru, T, Nano/subnano-tuning of porous ceramic membranes for molecular separation, Nano/subnano-tuning of porous ceramic membranes for molecular separation, 46, (2008), 349-361.

[5] Dong, J. Lin ,Y. Kanezashi, M. Microporus inorganic membranes for high temperature hydrogen purification, Journal Of Applied Physics 104, (2008) 121301.

[6] Oyama, S. Yamada, M. Review on Mechanisms of Gas Permeation through Inorganic Membranes, Journal of the Japan Petroleum Institute, 54, (5), (2011), 298-309.

[7] Shelekhin, B. Dixon, G. Ma, Y. Theory of gas diffusion and permeation in inorganic molecular-sieve membranes, AIChE Journal, 41.(1) (1995) 58-67.

[8] Markovic, A. Stoltenberg, A. Enke, D. Schlünder, E. Gas permeation through porous glass membranes Part II: Transition regime between Knudsen and configurational diffusion. Journal of Membrane Science 336 (2009) 32‑41

[9] Bird, B. Stewart, W. Lightfoot, E. Transport Phenomena, 2nd, 2002, Wiley.

[10] Seader, J. Henley, E. (Author), Roper, D. Separation Process Principles, 3rd, 2010 Wiley.

[11] Shelekhin, B. Dixon, G. Ma, Y. Adsorption, diffusion and permeation of gases in microporous membranes. III. Application of percolation theory to interpretation of porosity,

tortuosity, and surface area in microporous glass membranes, Journal of Membrane Science, 83 (1993) 181-198.

[12] Van Den Broeke, L. Krishna R. Experimental verification of the Maxwell-Stephan theory for micropore diffusion. Chemical engineering science, 50, (1995), 2507-2522-911.

[13] Krishna, R. Wesselingh A. Maxwell-Stephan approach to mass transfer, Chemical engineering science, 52, (1997), 861-911.

[14] Mason, E. Malinauskas, A , Gas Transport in Porous Media: The Dusty Gas Model, 1983, Elsevier.

[15] Langmuir, I. Journal of American Chemical Society. 37, (1915) 1139.

[16] Lee, D. Oyama, S. Gas permeation characteristics of a hydrogen selective supported silica membrane, Journal of Membrane Science,210 ,(2002) , 291-306.

[17] Mcelfresh, D. Howitt, Activation Enthalpy for Diffusion in Glass, *D. J. Am. Ceram. SOC.*, 69, (1986), C-237-C-238.

[18] Roberts, D. L., I. C. Abraham, Y. Blum, and J. D. Way, "Gas Separation with Glass Membranes," Final Report, DOE Contract No. DE-AC21-88MC25204 (May 8, 1992).

[19] Hacarlioglu, P. Lee, D. Gibbs, G. Oyama, S. Activation energies for permeation of He and H_2 through silica membranes: An ab initio calculation study Journal of Membrane Science 313 (2008) 277–283.

[20] Thornton, A. Hilder, T. Hill, A. Predicting gas diffusion regime within pores of different size, shape and composition J. Journal of Membrane Science 336 (2009) 101‑108.

[21] Takaba, H. Matsuda, E. Nair, B. Nakao, I. Molecular Modeling of Gas Permeation through an Amorphous Microporous Silica Membrane Journal of Chemical Engineering of Japan, 35, (2002), 1312–1321.

PART TWO

Simulating of Gas Separation in Membranes

CHAPTER 3

SIMULATING SEPARATION OF MULTI-COMPONENT SYSTEMS IN DIFFERENT FLOW CONFIGURATIONS

3.1 Introduction

The objective of the second part this thesis is to develop tools that would allow deciding whether the selective properties of the available amorphous silica membranes are sufficient to meet the separation objectives of the IGCC process. Subsequently, these tools can be used to design a suitable membrane separation unit. In simulating the separation of binary and multicomponent gas mixtures, it is commonly assumed that the permeability coefficient of a given gas in a given membrane is not affected by the presence of other gases in the feed mixtures. In others words, it is assumed that the permeability coefficients or permeances determined in the respective single gas permeation experiments can used be in simulation of multicomponent gas separations.

For a binary gas mixture consisting of *A* and *B*, the separation factor is defined as:

$$\alpha_{A/B} = \frac{y_A / y_B}{x_A / x_B} \tag{3.1}$$

where x and y indicate the mole fractions in the feed and permeate, respectively. The separation factor is related to the ideal selectivity through:

$$\alpha_{A/B} = \alpha^{*}_{A/B}\left(\frac{x_A\left(\alpha_{A/B}-1\right)+1-r\alpha_{A/B}}{x_A\left(\alpha_{A/B}-1\right)+1-r}\right) \tag{3.2}$$

in which, $r = p_l/p_h$, and p_l and p_h refer to permeate and feed pressures, respectively. It follows from Eq. (3.2) that in the limiting case when $r \rightarrow 0$, which can be achieved when the permeate side of membrane is under vacuum, the separation factor approaches the ideal selectivity. Otherwise, with $r > 0$, the separation actor is lower than the ideal selectivity.

It is important to emphasize that Eqs. (3.1) and (3.2) are applicable only at so called "zero stage cut" condition, and the stage cut (θ) is defined as:

$$\theta = \frac{V_p}{L_f} \tag{3.3}$$

where L_f and V_p are feed the permeate rate flow rates, respectively. When $\theta \approx 0$, the composition of the feed is approximately constant. However, when θ is greater than zero, the feed composition changes along the membrane. More specifically, the feed is depleted from a more permeable component whereas the mole fraction of a less permeable component increases. Therefore, the composition of the feed is no longer a unique value. The greater the stage cut, the greater the variation in the composition of the feed along the membrane. However, the magnitude of this variation also depends on the membrane selectivity, the flow configuration, and the pressure drop at the feed side of the membrane.

There are four basic types of flow configurations at which membrane gas separations can be carried out: complete mixing, cross-flow, parallel flow, and counter current flow. The simplest of these is the complete mixing configuration, which, for a binary gas separation, is shown schematically in Fig. 3.1. The mole fractions x_f, x_o, and y_p are those of the more permeable component. The complete mixing gas separator is similar to a continuous stirred tank, which implies that the compositions of feed and permeate are uniform along the membrane. Moreover, the composition of the gas at the high pressure side of the membrane is represented by

the composition of the retentate (x_o). The retentate stream is a part of the feed stream that did not permeate through the membrane. In addition, as a first approximation, similarly to other flow configurations, the complete mixing model assume that the process is isothermal, and the pressure drops at the feed and permeate sides are negligible.

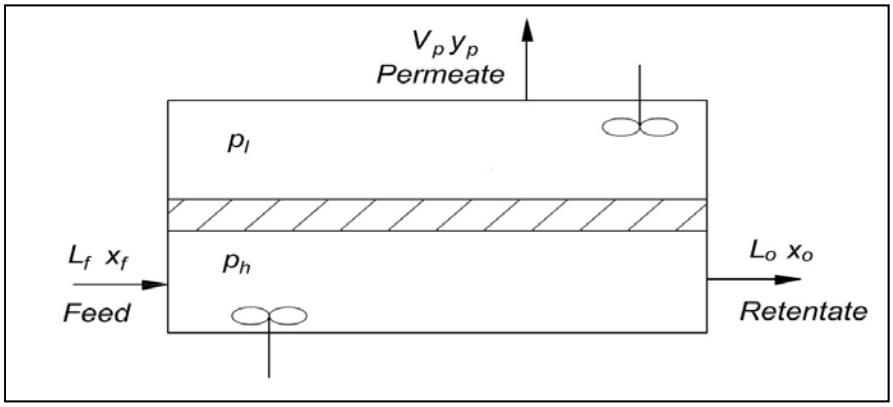

Figure 3-1 Schematic representation of a complete mixing model membrane separator.

Solving binary systems using the complete mixing model is straight forward, but this configuration is not of practical importance, because of the approximation of a constant driving force for permeation along the membrane. A better representation of flow configuration in the actual membrane modules is provided by the cross-flow model. In this model it is assumed that there is no mixing at the permeate nor the feed-side of the membrane. Feed flow is parallel to the membrane, while the permeate is pulled out perpendicularly from the membrane. As a result, and permeate flow is considered unhindered locally, which means a local permeation is a function of a local driving force only [3]. The membrane module is divided into differential elements, and the complete mixing model is assumed to apply in a differential element. The cross-flow configuration is shown schematically in Fig. 3.2.

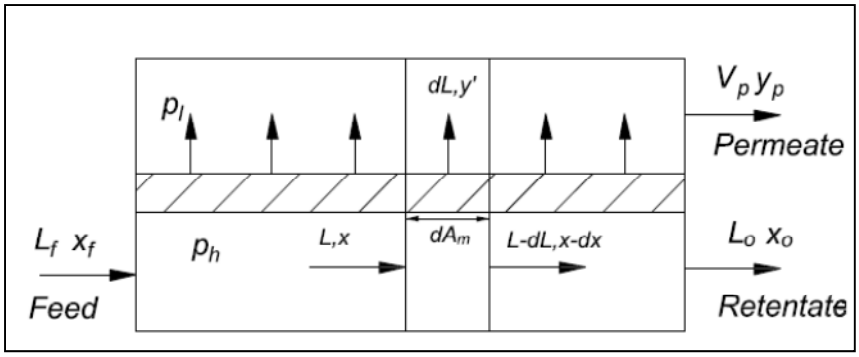

Figure 3-2 Schematic representation of a of cross-flow model membrane separator.

In co-current and counter current flow configurations the feed and permeate are parallel to the membrane surface. Similarly to the cross-flow configuration, the membrane module is divided into differential elements. However, unlike the cross-flow configuration, the local driving force is affected by the concentrations of the penetrant in the preceding differential element. As the names suggests, feed and permeate travel in the same direction in the co-current flow configuration, while in counter current flow configuration they flow in opposite directions. The co-current and counter current flow configurations are show schematically in Figs. 3.3 and 3.4, respectively.

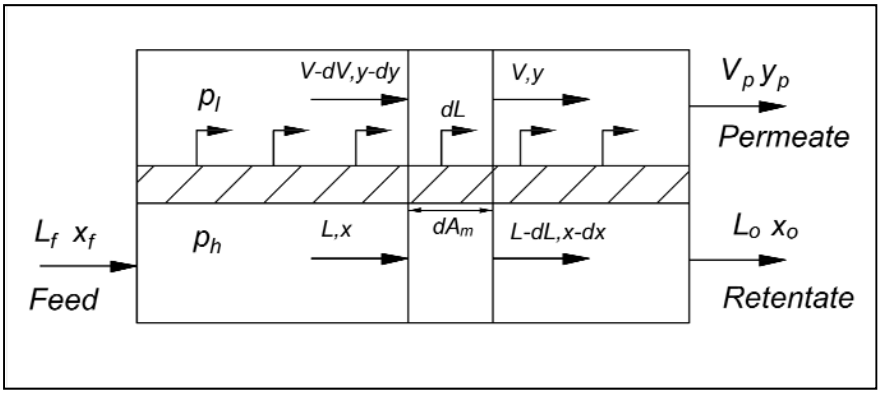

Figure 3-3 Schematic representation of a co-current model membrane separator.

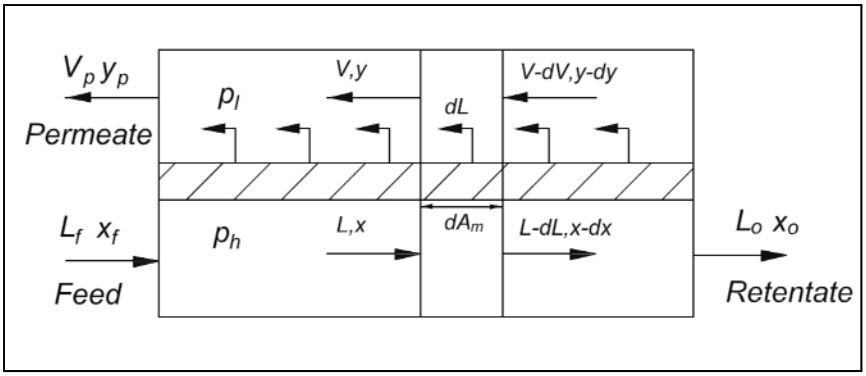

Figure 3-4 Schematic representation of a counter-current model membrane separator.

Modelling activities in the literature can be divided into two categories, (i) binary and (ii) multicomponent systems. Binary systems are much easier to solve compared to multicomponent systems. The latter require trial and error iterative procedure, which demand considerable amount of computations. The gas pressure drop is also a factor to be considered in modelling of membranes, which itself introduces further complications to system. In the next section, the calculation methods available in the literature are introduced.

3.2 Theoretical Background

3.2.1 Complete Mixing

The review of binary systems is started with the complete mixing model. Referring to Fig. 3.1, the overall mass balance and component balance on the more permeable component are given by:

$$L_f = L_o + V_p \tag{3.4}$$

$$L_f x_f = L_o x_o + V_p y_p \tag{3.5}$$

Unlike the single gas permeation, the driving force is the partial pressure difference across the membrane. Since the composition at the high-pressure side is represented by the composition of the retentate, the flow rate of the more permeable component across the membrane is given by:

$$y_p V_p = \frac{P_{MA} A_m}{t}(p_h x_o - p_l y_p) \tag{3.6}$$

where, P_{MA} is the permeability coefficient of the more permeable component, and A_m is the area of membrane. A similar rate equation can be written for the less permeable component *B*, and by dividing the two rate equations, the following expression is obtained:

$$\frac{y_p}{1-y_p} = \frac{\alpha^*[x_o - (p_l / p_h) y_p]}{(1-x_o) - (p_l / p_h)(1-y_p)} \tag{3.7}$$

Eq. (3.7) is a quadratic equation that can be used to determine the permeate composition y_p. Alternatively, y_p can be expressed in terms of the stage cut using the total and component mass balances:

$$y_p = \frac{x_f - x_o(1-\theta)}{\theta} \tag{3.8}$$

Knowing the composition of the permeate and the stage cut, the required membrane area can be determined by rearranging Eq. (3.6):

$$A_m = \frac{\theta y_p L_f}{(P_{MA} / t)(p_h x_o - p_l y_p)} \tag{3.9}$$

Solving the systems involving multicomponent feed streams requires a trial and error procedure. The rate equations for each component are similar to Eq. (3.6). The trial and error procedure starts by guessing the concentration of the most permeable component in the permeate stream, and determining the required membrane area. In turn, knowing the membrane area it is possible to determine the composition of the other components in the permeate stream. If the sum of the calculated values of mole fractions in the permeate stream is not equal to unity, then the new concentration of the most permeable component is guessed and procedure is repeated until the sum of the mole fractions at the permeate side is equal to unity. Once the actual

composition of the permeate stream is obtained, the corresponding composition of the retentate can be determined from equation similar to Eq. (3.8), which is essentially as simple mass balance.

3.2.2 Cross-Flow

In the cross-flow model, the longitudinal velocity of the feed stream is high enough for the gas stream to be in a plug flow (Fig. 3.2). On the permeate side, the permeate stream is essentially perpendicular to the membrane surface [1]. The cross-flow configuration was solved analytically by Welver et al. [4], but the down side of the analytical solution is that the pressure drop calculations cannot be incorporated into the analytical model. Moreover, the analytical solution is limited to binary systems.

Shindo et. al [5] proposed a solution for solving cross-flow which is based on dividing the membrane into differential elements (based on membrane area), and solving the governing differential equations numerically in each element. First the mole fraction of one of the components in permeate side is determined with iteration and then that is used for finding the mole fractions of the rest of the components. In this method for an *n* component system, one differential equation is solved to determine the change in the feed flow rate and *n-1* equations are solved to determine the changes in the composition in each step. The effect of pressure drop in this method is neglected, but this method can be used for all systems regardless of the number of components.

3.2.3 Co-Current Flow

In co-current model the feed and the permeate stream are parallel to the membrane surface, and the local driving force is affected by the concentrations of the diffusant in both feed and permeate side. Several methods have been proposed in the literature for solving these flow configurations, and they all tackle the problem by dividing the membrane into the small differential elements, and then track the composition changes in the elements to evaluate the overall performance of the membrane by manipulating the rate equations [5-10].

To solve binary co-current problems, Walawender and Stern [9] divided the membrane into differential elements, and developed the following approach, which starts from differential rate equations for both components:

$$dL_A = y_A dL = \frac{P_{MA} dA_m}{t}(p_h x_A - p_l y_A) \tag{3.10}$$

$$dL_B = (1 - y_A)dL = \frac{P_{MB} dA_m}{t}\left[p_h(1 - x_A) - p_l(1 - y_A)\right] \tag{3.11}$$

Then the total change in the feed flow as a result of permeation in a differential element is simply:

$$dL = dL_A + dL_B \tag{3.12}$$

The material balance on the component *A* in the differential is given by:

$$Lx_A = (L - dL)(x_A - dx_A) + dL_A \tag{3.13}$$

By rearranging Eq. (3.13) and neglecting the product of differential terms, $dLdx_A$, Eq. (3.13) becomes:

$$dL_A = Ldx_A + x_A dL \tag{3.14}$$

Substituting Eq. (3.14) into Eq.(3.12) leads to:

$$Ldx_A = (1 - x_A)dL_A + x_A dL_B \tag{3.15}$$

Similar analysis can be carried out at the permeate side, which lead to:

$$Vdy_A = (1 - y_A)dL_A + y_A dL_B \tag{3.16}$$

The overall and the material balances can then be written as:

$$L_f = L + V \tag{3.17}$$

$$L_f x_{Af} = Lx_A + Vy_A \tag{3.18}$$

V and L in Eq. (3.18) can be eliminated by recognizing that:

$$L = L_f \frac{(x_{Af} - y_A)}{(x_A - y_A)} \tag{3.19}$$

$$V = L_f \frac{(x_{Af} - x_A)}{(x_A - y_A)} \tag{3.20}$$

Substituting Eq. (3.19) into Eq. (3.15) leads to:

$$L_f \frac{(x_{Af} - y_A)}{(x_A - y_A)} dx_A = (1 - x_A) dL_A + x_A dL_B \tag{3.21}$$

Then, substituting Eq. (3.6) and the rate equation for component B into Eq. (3.21) leads to:

$$L_f \frac{(x_{Af} - y_A)}{(x_A - y_A)} dx_A = (1 - x_A) \frac{P_{MA} dA_m}{t} (p_h x_A - p_l y_A) + x_A \frac{P_{MB} dA_m}{t} \left[p_h (1 - x_A) - p_l (1 - y_A) \right] \tag{3.22}$$

rearranging:

$$\frac{L_f}{p_h (P_{MB} / t) dA_m} dx_A = -\left(\frac{x_A - y_A}{x_{Af} - y_A} \right) \left\{ (1 - x_A) \alpha^*_{A/B} (x_A - r y_A) - x_A \left[(1 - x_A) - r (1 - y_A) \right] \right\} \tag{3.23}$$

where r, as already defined is simply, $r=p_l/p_h$. Similarly, substituting Eq. (3.20) into Eq. (3.16), the equation analogous to Eq. (3.21) is obtained, which then after application of the rate equation and rearrangements leads to:

$$\frac{L_f}{p_h (P_{MB} / t) dA_m} dy_A = -\left(\frac{x_A - y_A}{x_{Af} - x_A} \right) \left\{ (1 - y_A) \alpha^*_{A/B} (x_A - r y_A) - y_A \left[(1 - x_A) - r (1 - y_A) \right] \right\} \tag{3.24}$$

Dividing Eq. (3.24) by Eq.(3.23) gives:

$$\frac{dy_A}{dx_A}=\frac{(y_A-x_{Af})\left\{(1-y_A)\alpha^*_{A/B}(x_A-ry_A)-y_A\left[(1-x_A)-r(1-y_A)\right]\right\}}{(x_A-x_{Af})\left\{(1-x_A)\alpha^*_{A/B}(x_A-ry_A)-x_A\left[(1-x_A)-r(1-y_A)\right]\right\}} \tag{3.25}$$

In first element from the feed-end, where $x_A = x_{Af}$, Eq. (3.25) cannot be used, since the denominator becomes zero. However, applying the L' Hospital rule, Eq. (3.25) for the first element becomes:

$$\left.\frac{dy_A}{dx_A}\right|_{x_{Af}}=\frac{(y_A-x_{Af})[\alpha^*_{A/B}-y_A(\alpha^*_{A/B}-1)]}{\alpha^*_{A/B}(1-x_{Af})(x_{Af}-ry_A)-x_{Af}[(1-x_{Af})-r(1-y_A)]-(y_A-x_{Af})[(\alpha^*_{A/B}-1)(2ry_A-x_{Af}-r)-1]} \tag{3.26}$$

Finally, the membrane area can be determined by isolating dA_m in Eq. (3.23):

$$dA_m=\frac{-dx_A L_f t(y_A-x_{Af})/(x_A-y_A)}{P_{MB}p_h\left\{(1-x_A)\alpha^*_{A/B}(x_A-ry_A)+x_A[(1-x_A)-r(1-y_A)]\right\}} \tag{3.27}$$

The differential element in the above procedure for the co-current configuration must be based on differential change in composition at the high pressure side of the more permeable component, dx_A. The protocol for solving the design and rating problems in the co-current configuration can be summarized as follow:

1. Start from x_f, and set dx_A.
2. The concentration of component A in the permeate at "zero stage cut", y_A', is determined from Eq. (3.7) in which x_o is replaced by x_f.
3. Knowing dx_A and y_A', the composition of permeate leaving the first element is:

   $y_{A1}=y_A'-dx_A\left.\frac{dy_A}{dx_A}\right|_{x_{Af}}$ in which $\left.\frac{dy_A}{dx_A}\right|_{x_{Af}}$ is calculated from Eq. (3.26).

4. The composition of the feed leaving the first element and thus entering the second element is simply $x_{A1} = x_f - dx_A$. Knowing y_{A1} and x_{A1}, the differential stage cut and the differential permeation rate in the first element are calculated from:

   $d\theta_1=\frac{dx_A}{y_{A1}-x_{A1}}$ and $dV_1=L_f d\theta_1$

5. The area of the first and consecutive elements is calculated from Eq.(3.27).

6. The steps 3-5 are continued until the specified composition of the retentate, or the specified composition of the permeate, or the specified membrane area are obtained. In step 3 the change in composition of the permeate is calculated using Eq. (3.25) instead of Eq. (3.26).

Pan et. al [10-12] extended the analysis of binary systems into multicomponent systems by introducing a mathematical formulation that assumes that the driving force in the element having plug flow at both sides of a membrane is the same as to that in a cross-flow.

Shindo et al. [5] proposed an alternative approach for binary systems based on dimensionless area, permeability and the flow rate. Then using the overall and component mass balances they derived a set of dimensionless equations. The complete analysis of the system requires simultaneous solving of two dimensionless differential equations. Li et al. [13] t solved the multicomponent problem very similar to the approach used by Shindo et al. but with slight modifications of the differential equations.

Pettersen and Lien [14] presented a model for solving multicomponent systems using the analogy with shell-and-tube heat exchangers, with the driving force for permeation over the entire membrane area expressed in terms of a log-mean-partial pressure difference. Consequently, the rate equation for the transport of component *A* is given by:

$$y_{Ap}V_p = \overline{P}_{MA}A_m\Delta p_{A,lm} \tag{3.28}$$

Assuming a negligible pressure drop, the driving force for the transport of component *A* in a co-current flow is given by:

$$\Delta p_{A,lm} = \frac{(p_h x_{Af} - p_l y_{Af}) - (p_h x_{Ao} - p_l y_{AP})}{\ln\left(\dfrac{p_h x_{Af} - p_l y_{Af}}{p_h x_{Ao} - p_l y_{AP}}\right)} \tag{3.29}$$

where y_{Af} is the mole fraction of component *A* at zero stage cut, which can be determined from Eq. (3.7) in which x_o is replaced by x_{Af}. This method works well for design problems, but in case of rating problems involving *n* components, it requires simultaneous solving of a system of *3n* non-linear equations with *3n* unknowns. The solution requires iterative procedures using optimizations algorithms, which leads to computational difficulties, in particular when the

number of the components increases. Also, this approach does not allow to incorporate pressure drop due to plug flow over the membrane surface.

3.2.4 Counter Current Flow

Counter current flow is similar to the co-current flow, but this time the feed and permeate move in opposite directions as shown in Fig. 3.4. Basically all the methods for solving co-current configuration can be used, with slight modifications, for solving the counter-current configuration. The main difference is the fact that in the latter case the analysis should start from the retentate-end rather than feed-end. However, unless the desired composition of the retentate is specified, it is an unknown parameter. Consequently, the analysis of the counter-current configuration requires an iterative procedure, which starts from guessing the composition of the retentate, and then following a procedure described above for the co-current configuration.

Walawender and Stern [9] derived a set of differential equations that are analogous to Eqs. (3.25-3.27). The first equation relates the changes in the composition at the permeate side corresponding the set change in the composition at the feed side (dx_A).

$$\frac{dy_A}{dx_A} = \frac{(y_A - x_{Ao})\left\{(1-y_A)\alpha^*_{A/B}(x_A - ry_A) - y_A[(1-x_A) - r(1-y_A)]\right\}}{(x_A - x_{Ao})\left\{(1-x_A)\alpha^*_{A/B}(x_A - ry_A) - x_A[(1-x_A) - r(1-y_A)]\right\}} \tag{3.30}$$

Starting from the retentate-end, in the first element $x_{Ao} = x_A$ and Eq. (3.30) cannot be used, but application of the L'Hospital rule allows rewriting Eq. (3.30) in the following form:

$$\left.\frac{dy_A}{dx_A}\right|_{x_{Ao}} = \frac{(y_A - x_{Ao})[\alpha^*_{A/B} - y_A(\alpha^*_{A/B} - 1)]}{\alpha^*_{A/B}(1-x_{Ao})(x_{Ao} - ry_A) - x_{Ao}[(1-x_{Ao}) - r(1-y_A)] - (y_A - x_{Ao})[(\alpha^*_{A/B} - 1)(2ry_A - x_{Ao} - r) - 1]} \tag{3.31}$$

Then, membrane area can be determined using Eq. (3.32):

$$dA_m = \frac{-dx_A L_o t(y_A - x_{Ao})/(x_A - y_A)}{P_{MB} p_h \left\{(1-x_A)\alpha^*_{A/B}(x_A - ry_A) + x_A[(1-x_A) - r(1-y_A)]\right\}} \tag{3.32}$$

The procedure for solving the design and rating problems are the same as for the co-current flow, but starting from retentate end the procedure continues until the feed composition is

reached. If at x_f the corresponding A_m, or y_{Ap}, θ are different from the actual values, a new value for the composition of the retentate is chosen. The procedure continues until specified A_m, or y_{Ap}, or θ are obtained at x_f.

3.2.5 Effect of Pressure Drop

The effect of pressure drop is neglected in most of the studies done so far, and as the gas flow in membranes is usually laminar this does not introduce considerable error to the system. Pan [12] included the pressure drop calculations in their study, which made their solution a trial and error method.

Pan and Habgood [11] investigated the effect of pressure drop by assuming that the feed always flows inside the tubes. They also assumed a constant viscosity along the membrane module to avoid difficulties of calculating new viscosities due to composition changes along the membrane. The procedure starts from determination of the number of tubes in membrane module to ensure laminar flow in tubes. By having the required area of each element it is possible to determine the length of the differential element, *dz,* which is used in pressure drop calculations. The element length is calculated form Eq. (3.33):

$$dz = \frac{dA_m}{\pi N_t d_t} \tag{3.33}$$

where N_t is the number of tubes and d_t is the tube inside diameter. Since the flow in tubes is laminar, the pressure drop is determined using the Hagen-Poiseuille equation [11]:

$$\frac{dp_h}{dz} = \frac{-32\mu v}{d_t^{\,2}} \tag{3.34}$$

where dp_h is the pressure drop, μ is the viscosity and v is the mean velocity. By converting the velocity to the flow rate at T_s and p_s, the above equation becomes:

$$dp_h = \frac{-128 dz \mu}{\pi N_t d_t^{\,4}} \left(L_{av} \frac{T}{T_s} \frac{p_s}{p_{hav}} \right) \tag{3.35}$$

where p_s and T_s are the standard pressure and temperature respectively. It should be noted that determining the pressure drop along each differential element is an iterative procedure. At first iteration $p_{hav} = p_h$, and L_{av} are the average flow rate in the element considering the inlet and outlet flows. After determining dp_h, the average pressure can be calculated:

$$p_{hav} = p_h + \frac{dp_h}{2} \tag{3.36}$$

In the next iteration pressure drop is recalculated using the new value of p_{hav} and the procedure continues until the two p_{hav} are the same. Once this is achieved, the calculations are carried out in the second and then in the subsequent differential elements. This approach leads to accurate predictions of the pressure drop, but it considerably increases the computation time. Alternatively, using inlet pressure instead of the average pressure to estimate the pressure drop would allow avoiding the iterative approach in cross-flow and co-current flow configurations. In this case, the size of the differential element (*dz*) should be minimized.

It should be noted that for determining pressure drop in the counter-current flow configuration it is necessary to assume a value for the pressure drop and solve the system by adding the calculated pressure drops for each element to obtain the pressure at the feed-end of the membrane. If such determined feed pressure is different from the actual feed pressure, it is necessary to estimate a new value for pressure drop and continue until the actual feed pressure is recovered. Consequently, the prediction of the pressure drop in counter-current flow configuration is inherently an iterative process. It is important to note that the pressure drop is coupled with the design calculations. In design problems, including the effects of pressure drop increases the required surface area of the membrane for a given separation.

3.3 Modifications of the Available Approaches

The ultimate objective of this work is to develop modeling tools that would allow assessing suitability of the membranes being synthesized by Natural Resources Canada, CANMET Energy Technology Center (CETC) laboratory in Ottawa, for the IGCC process. Details of the membrane synthesis were provided in Chapter 2. The final product of synthesis is a tubular membrane with a selective silica layer deposited on surface of a 7.0 *mm* OD-tube. Considering

that the thickness of the selective layer is much smaller than the diameter of the tube, it is possible to neglect the effect of tube's curvature, and to treat the membrane as a slab. The validity of this assumption is verified by carrying out a case study for the determination of the required membrane area for O_2/N_2 separation. More specifically, the area obtained by using Eq. (3.6), Cartesian coordinates, is compared with the area obtained by using the rate equation in the cylindrical coordinates, which is given by:

$$y_p V_p = \frac{2\pi l P_{MA}(p_h x_o - p_l y_p)}{\ln(r_o/r_i)} \tag{3.37}$$

where r_o and r_i are the outside in inside radius of the tube and l is the tube length. The parameters for this case study are presented in Table 3.1.

Table 3-1 Parameters used in investigating the effect of slab membrane's simplifying assumption.

Feed	Tube-Side
Flow rate *(cm^3 STP/s)*	10000
Feed pressure *(cmHg)*	190
Permeate pressure *(cmHg)*	19
Temperature *(K)*	300
Stage cut	0.75
O_2 permeability *(Barrer)*	500
Ideal selectivity (O_2/ N_2)	15
Thickness of membrane's selective layer (*cm)*	2.5×10^{-3}
Tube inside diameter *(cm)*	0.7

The calculated area by treating the membrane as a slab is 2.47×10^7 cm^2 compared to 2.48×10^7 cm^2 when using the cylindrical coordinates. The latter is just 0.36% greater than the value for the slab membrane. It should emphasized this deviation would disappear with a more realistic thickness of the selective layer which in the actual silica membranes should be in order of nanometers [1] rather than microns.

As already mentioned, there are two categories of problems, the design and the rating problems. In the design problems the feed composition, flow rate, retentate composition, high and low side pressures are specified and the composition of the permeate, stage cut and membrane area should be determined. Another type of the design problem is the case when the

feed composition, feed flow rate, stage cut, high and low side pressures are specified and the composition of the permeate, composition of retentate and membrane area are to be determined. In this study the former case is of interest. In the rating problems, feed composition, feed flow rate, membrane area, high and low side pressures are specified, and the composition and flow rates of the permeate and retentate should be calculated.

To carry out the required analysis, several modifications to currently available methods have been made. The details of these modifications are summarized next.

3.3.1 Cross-Flow

To carry out the analysis in cross-flow configuration the membrane was divided into differential elements based on the membrane area and each differential element is treated as a complete mixing configuration, and the analysis is started at the feed-end.

Knowing the feed flow rate and $d\theta$ the differential permeation rate in the first element is calculated from Eq. (3.3), which for a general case of *i*-th element is written as:

$$dV_i = L_{i-1} d\theta \tag{3.38}$$

The composition of the permeate leaving the *i*-th element is determined using Eq. (3.7) in the following form:

$$\frac{y_i^{'}}{1-y_i^{'}} = \frac{\alpha^* [x_i - (p_l / p_h) y_i^{'}]}{(1-x_i) - (p_l / p_h)(1-y_i^{'})} \quad \text{where } x_i = \frac{x_{i-1} - y_i^{'}}{1-d\theta};\ \text{for } i = 1,\ x_{i-1} = x_f \tag{3.39}$$

However, x_i is unknown, but it can be expressed in terms of $d\theta$ using a component mass balance:

$$x_i = \frac{x_{i-1} - y_i^{'}}{1-d\theta};\ \text{for } i = 1,\ x_{i-1} = x_f \tag{3.40}$$

Substituting Eq. (3.40) into Eq. (3.39), the only unknown is $y_i^{'}$, and the resulting quadratic equation can be solved to determine $y_i^{'}$. Then, knowing $y_i^{'}$ and $d\theta$ the composition of the retentate leaving the *i*-th element (x_i) is calculated from Eq. (3.40). Finally, the differential membrane area corresponding to $d\theta$ is calculated from Eq. (3.9): while total membrane

$$dA_{mi} = \frac{dV_i y_i^{'}}{\left(P'_A / t\right)\left(p_h x_i - p_l y_i^{'}\right)} \tag{3.41}$$

The cumulative composition of the permeate after the *i*-th element (y_i) and the corresponding total membrane area are:

$$y_i = \frac{\sum_i y_i^{'} dV_i}{\sum_i dV_i} \text{ and } A_{mi} = \sum_i dA_{mi} \tag{3.42}$$

To extend the above analysis for a binary system into a multicomponent system requires application of an iterative approach normally used for complete mixing model that was already discussed. Essentially, the steps are identical to what was described for binary systems but this time the composition of the permeate is determined by iteration as described in Section 1.2.1 instead of using Eq. (3.39).

The differential elements also can be defined based on a differential composition (dx) in each element, and a similar approach can be taken for solving the system, but this approach has some drawbacks comparing to the differential stage cut method. The main advantage of using $d\theta$ over dx as a differential step is better stability of the system in modelling very demanding separations. More specifically, if the retentate is to be depleted from the more permeable component, i.e. $x_o \to 0$, even very small dx at the retentate end may result in very high $d\theta$. It is important to note that the assumption of complete mixing model is valid only when $d\theta$ is very small. This problem is avoided altogether by controlling $d\theta$ while letting dx to vary from element to element. In general, with a constant $d\theta$, dx decreases as the feed is depleted from the more permeable component. In addition, pressure drop calculations can be easily integrated into this approach, which will be discussed in a subsequent section.

3.3.2 Co-Current and Counter Current

The analysis of co-and counter-current configurations discussed in Sections 3.2.3 and 3.2.4 rely on controlling the change in feed composition dx. In this work, the alternative approach is proposed based on differential membrane area dA_m. It is important to note assuming the complete

mixing in such-defined control element would lead to implicit equations for $d\theta$ and dx, which would complicate, rather than simplify the analysis. However, by keeping dA_m very small, i.e. when $dA_m \to 0$, one can assume that a change in the composition of the feed becomes negligible, and the analysis in each element can be carried out assuming a zero stage cut. In other words, it is not necessary to assume the complete mixing model, and the analysis is carried out based on the composition of the feed entering the differential element rather than that leaving element. As a result, Eq. (3.6) simplifies to:

$$y_i = \frac{p_h x_i}{p_l + Vt/(dA_m P_{MA})} \qquad (i = 1,..,N) \tag{3.43}$$

$$\sum_{i=1}^{N} y_i = 1 \tag{3.44}$$

where N is the number of components. The protocol for solving the design and rating problems in the co-current configuration can be summarized as follow:

1. Start from x_f, and set dA_m.
2. Knowing dA_m and x_f, the composition of permeate leaving the first element is calculated by solving Eqs. (3.43) and (3.44) simultaneously.
3. The flow rate leaving the element is determined by overall mass balance using Eq. (3.4).
4. The composition of the feed entering the next element can simply determined with a component mass balance using Eq. (3.5).
5. The steps 2-4 are continued until the specified composition of the retentate, or the specified composition of the permeate, or the specified membrane area are obtained.

By solving the above system of equations in each element it is possible to determine the local composition and flow rate of permeate, and by integrating it over the entire module the overall compositions and flow rates can be determined for the permeate and retentate streams. It should be noted that the composition of the feed entering the next step can simply be calculated by setting up the component mass balance for each gas. The counter current flow configuration can be solved similarly to co-current flow configuration, but in this flow pattern the calculations

should be started from the retentate side and continue backward to the membrane's inlet. Solving the counter current flow requires a trial an error procedure as the composition and flow rate of the retentate are unknown and must be guessed. As the performance of cross-flow configuration is close to counter current flow, it is possible to obtain reasonable initial guesses for retentate composition in counter current problem using cross-flow mode's solution. In this work retentate's composition is estimated for multicomponent counter current rating problems by solving the same problem for the cross-flow configuration. As counter current flow has a better performance comparing to cross-flow, the cross-flow problem is solved a few times by increasing the total area in small increments and a table is generated which can be used for providing reasonable estimates for retentate composition in counter current flow.

Comparing to the available methods for solving plug flow systems, the proposed approach does not require solving of any differential equation. In addition, all equations that must be solved are linear, which simplifies the analysis and decreases the required computation time. Pressure drop calculations can also be easily integrated to this approach without requiring any iterative procedure, which is going to be presented next.

3.3.3 Pressure Drop Calculation

In this study the pressure drop calculations in cross-flow configuration are carried with equations developed by Pan [12], however using a different approach. First the system of the governing equations is solved neglecting the pressure drop, and then the solution is used as initial values in the pressure drop calculations. More specifically, the area of each element without a pressure drop is calculated and used to determine the element's length. Then, knowing the length of the element, the pressure drop in the element is calculated using Eq. (3.35). Inclusion of the pressure drop changes the driving force in each element, and thus it is necessary to determine the new area for each element. This procedure continues until the calculated area remains constant. Despite the iterations, this approach allows a rapid conversion of the pertinent calculations.

In case of co-current and counter current flows, it is possible to avoid the iterative pressure drop calculations as the area of each element is known prior to solving the problem. By knowing the differential area the length of the element is calculated, and then used to determine the pressure drop. If the chosen elements are small enough, it is possible to use the inlet pressure

instead of the average pressure for each element in Eq. (3.35). Pressure drop calculations can be carried out between steps 4 and 5 in the presented protocol for solving co-current problems using differential membrane area. This makes it possible to solve the problem and to determine the pressure drop all in one step without any iteration.

It should be mentioned that the approach based on the differential membrane area can also be used for solving cross-flow problems. Both differential stage cut and differential membrane area approaches are easy to implement, but if the differential area method is used then it is not necessary to determine pressure drop using an iterative procedure and the described method for plug flow can be used to calculate the pressure drop directly.

3.4 Results and Discussion

In this section first the proposed approaches are validated with help of the available experimental results from literature. Then the proposed approaches are used to design a template separation unit in IGCC process using the actual operating conditions.

3.4.1 Model Validation

The membrane performance for the separation of binary feed in different flow configurations, but without pressure drop were compared with results of Walawender et al. [9]. Their results indicate that the counter-current configuration has the best performance followed by the cross-flow, the co-current, and complete mixing configurations. To verify the proposed new approach for the cross-flow, as well as the new approach for the co- and counter-current flows, it was first attempted to generate the graphs similar to those presented by Walawender et al. [9]. The data required for these simulations is provided in Table 3.2.

Table 3-2 Input data for validation of models.

Feed	Tube-Side
Flow rate (cm^3 STP/s)	10000
Feed pressure (cmHg)	190
Permeate pressure (cmHg)	38
Temperature (^oC)	27
Membrane thickness (cm)	2.54×10^{-3}
O_2 permeability (barrer)	500
Ideal selectivity (O_2/ N_2)	2
O_2 mole fraction in feed	0.209

The feed flow rate was not provided by Walawender et al. in their work but as here the goal is to assess the performance of models in different stage cuts this would not affect the results. This is because the composition of the permeate and retentate are presented as a function of stage cut so they would be independent of flow rate, and changes in flow rate would just change the required area. The simulation results are presented in Figs. 3.5 and 3.6.

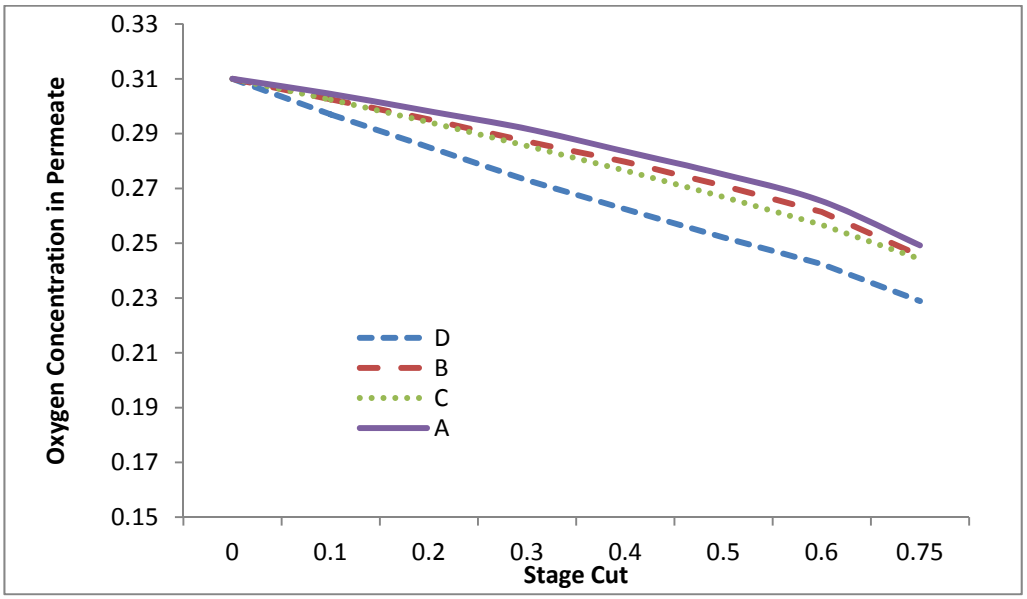

Figure 3-5 Results of solving the problem using different flow modes, permeate composition for A: Counter-Current, B: Cross-flow, C: Co-Current and D: Complete mixing.

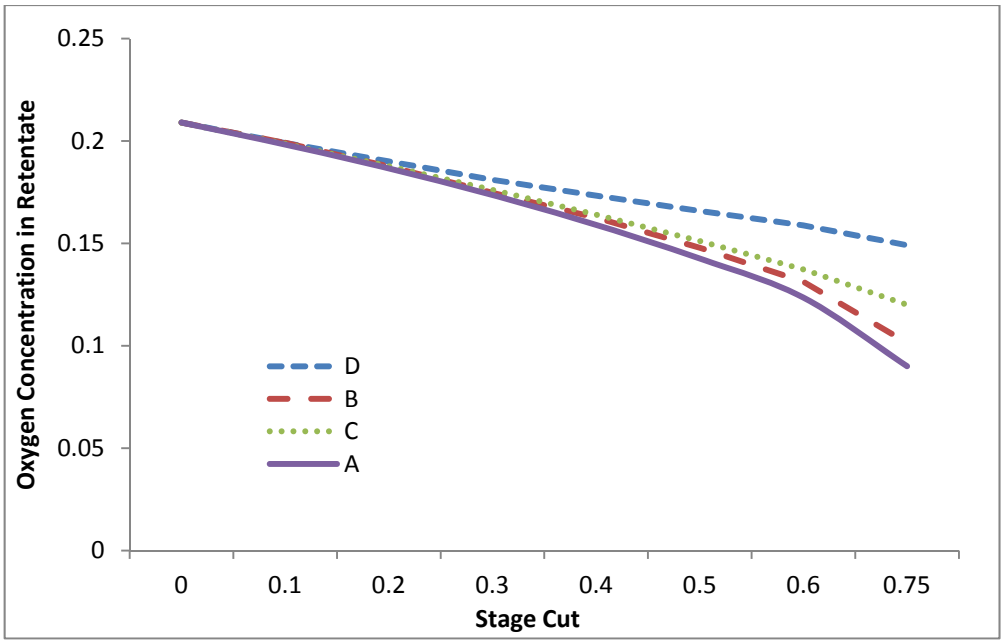

Figure 3-6 Results of solving the problem using different flow modes, retentate composition for A: Counter-Current, B: Cross-flow, C: Co-Current and D: Complete mixing.

The simulation results are in agreement with what is presented by Walawender et al., and as expected counter current flow has the best performance followed by cross-flow, co-current flow and complete mixing mode. The results show that the difference in performance of different flow patterns becomes more significant as the stage cut is increased.

The proposed pressure drop calculation methods could not be validated using the available experimental data because some key information such as flow rates and tube dimensions were not provided in the reviewed studies. In order to investigate the effect of pressure drop it was decided to perform as series of case studies, and analyse the outcome to see how pressure drop affects the gas separation. Cross-flow model was chosen as the flow pattern in this section and the effect of pressure drop was investigated for four cases by changing the tube diameter while keeping the stage cut constant. The same input data from previous section which was shown in Table 3.2 is used in the simulations and the membrane area was assumed to be 2.52×10^{7} for the first case, but this value had to be adjusted for the other cases to keep the stage cut constant. The description of each case and the simulation results are shown in Table 3.3.

Table 3-3 Different configurations used in pressure drop case studies and the simulation results with 0.75 stage cut.

	Case 1	Case 2	Case 3	Case 4
Tube ID (cm)	0.7	0.5	0.3	0.1
Number of tubes	106	208	579	5210
Membrane area (cm^2)	2.52×10^{7}	2.54×10^{7}	2.60×10^{7}	2.90×10^{7}
Pressure drop (cmHg)	5.9	8.3	13.7	45.7
O_2 mole fraction in permeate	0.2087	0.2088	0.2087	0.2088
O_2 mole fraction in retentate	3.36×10^{-4}	3.38×10^{-4}	3.54×10^{-4}	3.38×10^{-4}

It should be noted that if the provided total area is divided by the number of tubes the tube length will appear to be very long, which may seem unreasonable. In fact the tubes can be put in series to obtain the desired length and they do not have to be put in a straight line as they can be stacked on top of each other. Another point to consider is that these results are just presented for the purpose of demonstrating the application of the developed methods, and the selectivity and permeance of the available membranes are not in the acceptable range to be used in a industrial application, which itself makes the justification of the numerical results more challenging.

As can be seen by decreasing the tube diameter the pressure drop increases, which is what is expected to happen. The mole fraction of the more permeable component in permeate remains constant in all the cases, which indicates that if the stage cut is kept constant the purification is not going to be affected by the pressure drop. Furthermore as it is shown a module with greater pressure drop will require more area to achieve the same degree of purification, so it can be concluded the pressure drop negatively affects the driving force and the membrane's performance.

In next step, it was attempted to simulate separation of a binary O_2/N_2 system and compare the results with the experimental data provided by Blaisdell et al. [6]. The experimental data was obtained for a membrane having the ideal O_2/N_2 selectivity of 2.05 tested at the pressure ratio, p_l/p_h = 0.359, using a feed containing 20.9 mol% of O_2. The membrane was tested in both co- and counter-current flow configurations at different stage cuts. The simulated results are compared with the experimental data in Figs. 3.7 and 3.8. It should be mentioned that the method used for changing the stage cut is unknown here as Blaisdell et al. did not mention that in their work.

As it was expected the counter current flow mode demonstrated a better performance compared to the co-current flow in terms of enriching the permeate with the more permeable O_2 and depleting the retentate from O_2. By comparing the experimental results with the results obtained by simulation of the both flow modes it can be seen that the predicted values follow the experimental data very closely. However, small deviations can be observed in high stage cuts, where counter current simulation, underpredicts the amount of oxygen in the retentate. This might be a result of ignoring the effect of pressure drop as the required information was not provided by Blaisdell et al. in order to carry out the pressure drop calculations. Here the performance of the membrane is overestimated, and that can be justified by overestimation of the driving force caused by neglecting the pressure drop.

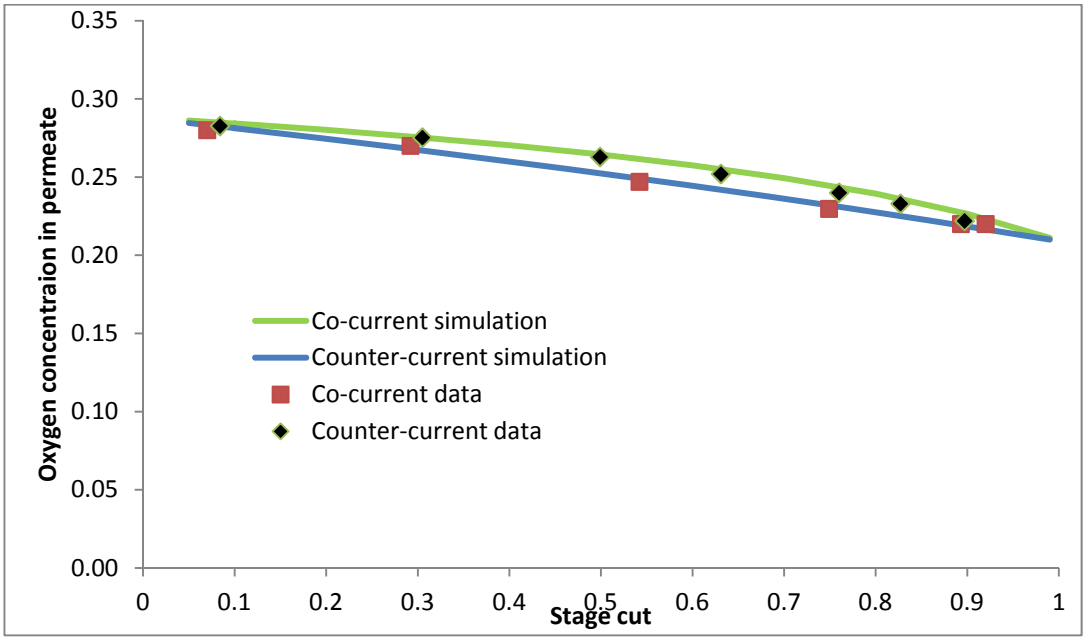

Figure 3-7 Comparing the results of the simulation with experimental data provided by Blaisdell et al. (permeate composition).

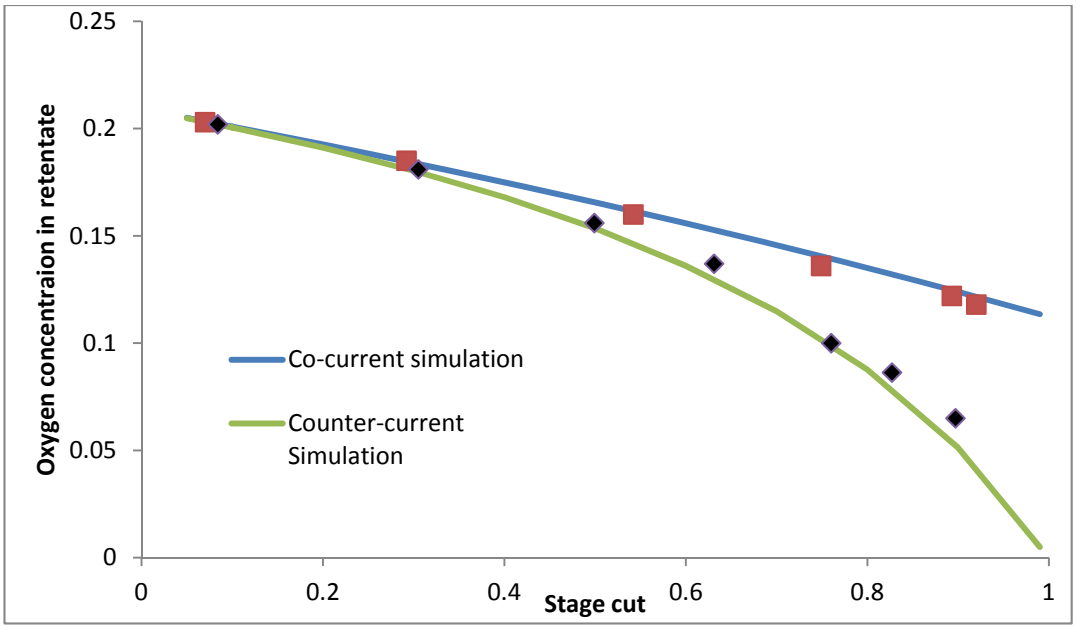

Figure 3-8 Comparing the results of the simulation with experimental data provided by Blaisdell et al. (retentate composition).

In next step the performance of the proposed approach based on a differential membrane area was evaluated for multicomponent separation using experimental data reported by Pan [12]. The mixture separated by Pan et al. [12] consisted of hydrogen, nitrogen, argon and methane, and the tests were carried out at different stage cuts in both co-current and counter-current configurations. Again it is not mentioned that how the stage cut was varied throughout the experiment, but changing the flow rate or the module area the possible options as the pressure was kept constant. The problem input data are presented in Table 3.2, and the simulation results are shown in Figs. 3.9-3.12.

As can be seen the proposed method can successfully predict the membrane's performance for both co-current and counter current configurations. The presented solution is a simple yet robust method for solving plug flow problems, which can predict the outcome of the separation with a very good precision.

Table 3-4 Input data from Pan et al. [12] used in the multicomponent simulation.

Feed	Tube-Side
Flow rate (cm^3 STP/s)	10000
Feed pressure (cmHg)	5223
Permeate pressure (cmHg)	842
Temperature (^oC)	25
Membrane thickness (cm)	2.54×10^{-3}
H_2 permeability (barrer)	2154
Ideal selectivity	
H_2/ N_2	96.15
H_2/ CH_4	100
H_2/ Ar	36.9
Feed component mole fraction	
H_2	0.5178
N_2	0.2469
CH_4	0.1957
Ar	0.0396

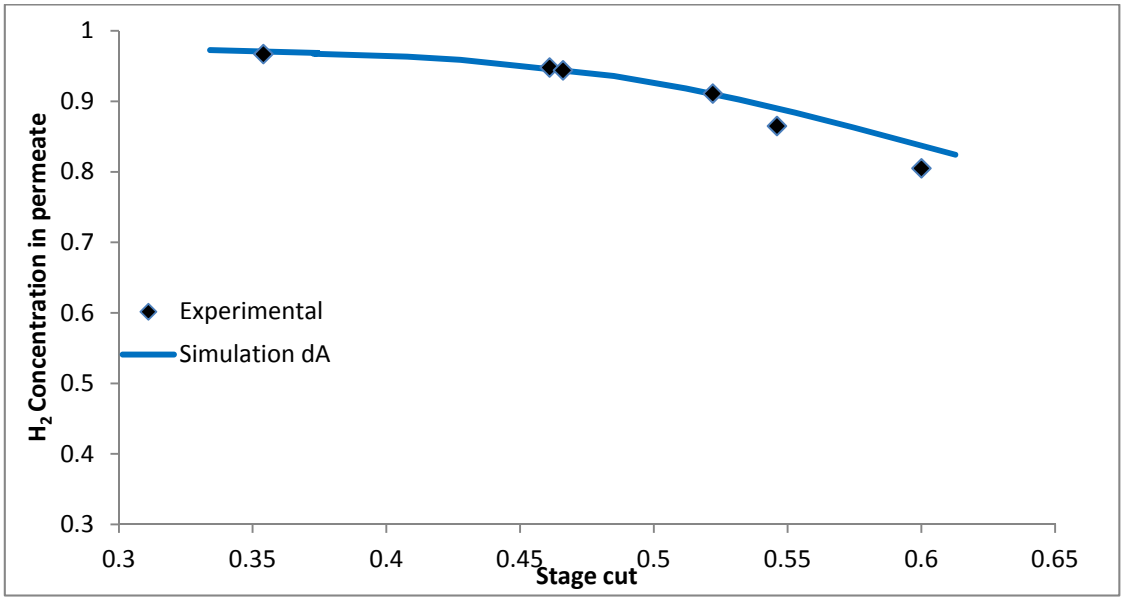

Figure 3-9 Simulation results of concentration of hydrogen in the permeate comparing to the experimental data for co-current mode.

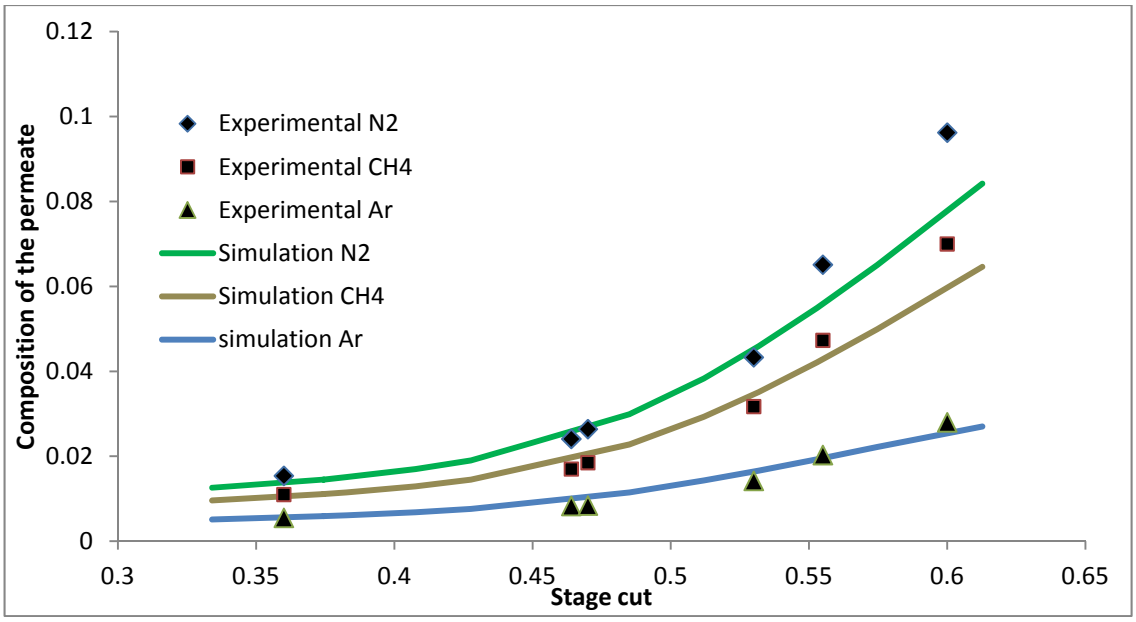

Figure 3-10 Simulation results of concentration of nitrogen ◆, argon▲ and methane■ in the permeate comparing to the experimental data for co-current mode.

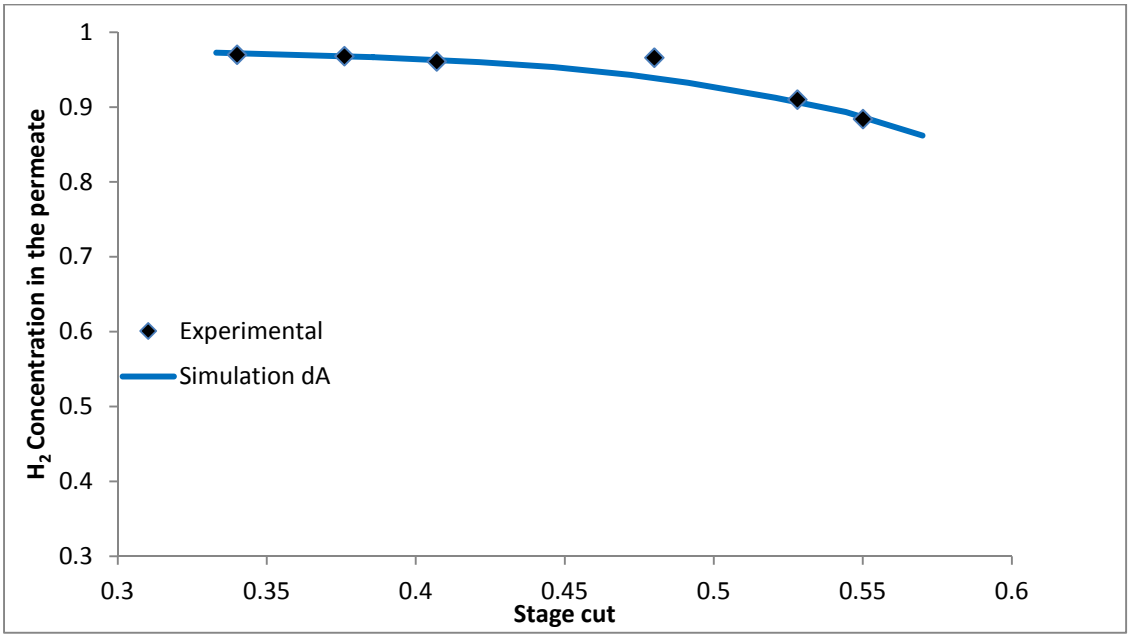

Figure 3-11 Simulation results of concentration of hydrogen in the permeate comparing to the to the experimental data for counter-current mode.

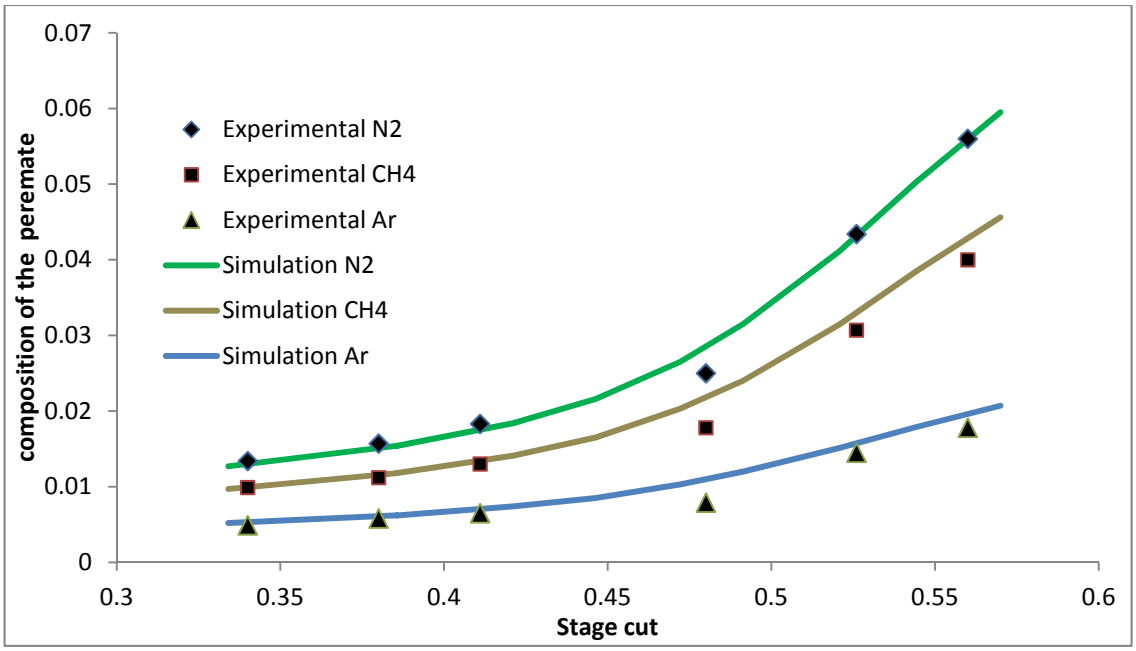

Figure 3-12 Simulation results of concentration of nitrogen ◆, argon ▲ and methane■ in the permeate comparing to the experimental data for counter-current mode.

3.4.2 Template IGCC Separation Unit Design

In this section the outcome of the studies in Chapter 2 and the simulation methods presented in this Chapter are combined for designing a template membrane for the separation relevant to the IGCC process, and thus to demonstrate how the tools developed in this thesis can be used to design and analyze the actual industrial problems.

The design process is started by specifying the inlet and outlet gas specifications. The feed stream is a shifted syngas coming out of a water shift gas reactor, which mainly consists of H_2 and CO_2. The goal here is to separate CO_2 from H_2 since the latter is a valuable feed stock which has various applications. The streams' data were obtained from the conceptual study report of an IGCC plant with partial carbon capture provided by Natural Resources Canada, CANMET Energy Technology Center (CETC) laboratory in Ottawa [16], which is presented in Table 3.3. It is important to note that the presented separation is carried out by an absorption process in the reference conceptual study, so it would not be possible to get the same results using membranes. Here, the separation goal is set to achieve the desired CO_2 concentrations in the sweet syngas stream, which is 2%.

Table 3-5 Feed and permeate streams' compositions in separation step of IGCC process used in simulations [16].

Stream Composition	Shifted Syngas Mol% (dry)	Sweet Syngas Mol% (dry)	CO_2 Product Mol% (dry)
H_2	51.57	85.77	0.87
N_2	5.15	8.58	0.05
CO	1.98	3.25	0.09
CO_2	40.69	1.38	98.98
Ar	0.61	1.02	0.01
Temperature (K)	773	773	773
Pressure (cmHg)	2693	225	2693*
Flow rate (STD m^3/h)	6.60×10^{5}	3.92×10^{5}	2.68×10^{5}
Viscosity (cmHg.s)	2.97×10^{-8}	2.46×10^{-8}	3.53×10^{-8}

* The effect of pressure drop is neglected in the reference study

It should be noted that in reality the total flow rate should be divided into proper number of membrane modules based on the size of the modules and the pressure drop requirements. Since the objective of this is study is to just demonstrate the applicability of the provided methods for designing the membrane systems, and not to design the unit itself, only a small fraction of the inlet gas stream is considered and the system is designed accordingly. This design can then be easily scaled up and updated for the actual process by performing a detailed design, which requires determining the exact number of the membrane modules by taking into account the required recycle rates of streams to achieve the desired separation efficiency. The selected flow rate for performing the study is 36 STD m^3/h (10000 STD cm^3/s) for a single membrane module, and the pressure drop calculations also are carried out accordingly.

For the purpose of these preliminary design calculations the properties of the best out of the four CANMET membranes presented in Chapter 2 is used. The chosen membrane (Membrane 3) has the H_2 permeance of 3.53×10^{-9} (mol/pa.s.m^2) and the ideal selectivity of 56.7 over N_2. The permeances for the other gases that are in the feed stream are evaluated using the concept of the scaling factor introduced in Chapter 2. Considering pore size distribution PSD3, the scaling factor for the selected membrane is 2.05×10^{-3}, and the estimated permeances for the gases comprising the feed stream are listed in Table 3.4.

Table 3-6 Predicting the gas permeances using the scaling factor of Hydrogen for membrane 3.

Gas	Ideal Permeance (mol/pa.sm^2)	Actual Permeance (mol/pa.sm^2)
CO_2	1.39×10^{-8}	2.85×10^{-11}
N_2	2.99×10^{-8}	6.12×10^{-11}
CO	3.02×10^{-8}	6.18×10^{-11}
Ar	3.47×10^{-8}	7.10×10^{-11}

The preliminary design calculations were carried out by assuming a cross-flow configuration. The pressure drop calculations also were carried out and the number of tubes were determined such that the gas flow be laminar and the calculated pressure drop be less than 10% of feed's pressure. The diameter of the tubes was assumed to be 0.7 *cm,* and the required number of tubes turned out to be 121. The results of the simulation are presented in Table 3.5.

Table 3-7 Simulation results for separation of CO_2 from shifted syngas using cross-flow configuration.

Stream Composition	Feed Mol% (dry)	Permeate Mol% (dry)	Retentate Mol% (dry)
H_2	51.57	98.02	24.36
N_2	5.15	0.38	7.94
CO	1.98	0.15	3.05
CO_2	40.69	1.41	63.71
Ar	0.61	0.04	0.94
Pressure (cmHg)	2693	225	2586
Flow rate (STD m^3/h)	36	13.32	22.68

The required membrane area was calculated to be 128,980 m^2, which is unreasonably large. Although the best available membrane was chosen but its very low permeance and insufficient selectivity caused this unusual design. It should be noted that the properties of this membrane are very far from the acceptable range which can be used to design a reasonable membrane module. The results indicate that while the considered properties of the membrane allow for sweetening of the syngas theoretically, but in the actual process much more selective and permeable membranes would be required. Apart from a very large required membrane area to achieve the separation goal, the poor selective properties of the membrane led to high

concentration of H_2 in the retentate stream, which would be undesirable considering that H_2 is a very valuable product in this process. As can be seen from Table 3.3 the amount of H_2 in CO_2 product stream is less than 1% in the original study whereas here it turns out to be more than 24% using membranes. In addition, excessively large membrane area results in a high pressure drop, which is not desired from the operating cost point of view.

It should be noted that the purpose of these calculations was only to demonstrate the application of the proposed methods, and the presented template design is not an acceptable configuration due to the mentioned reasons and cannot be implemented in an industrial unit. It is important to emphasize that the membranes currently synthesized by Natural Resources Canada, CANMET Energy Technology Center (CETC) laboratory in Ottawa are not optimized. Improvements in both permeance and selectivity towards the values reported by some authors in the literature, would greatly improve the economics of the membrane unit in the IGCC plant. Furthermore as in the IGCC process it is required to reduce the CO_2 level in the product stream to blow 2% the possibility of using hybrid membrane and absorption CO_2 removal technologies should be studied as well. The combination of the two technologies will decrease the required membrane area significantly as the membrane area is proportional to the ratio of the CO_2 removed not its amount.

3.5 Conclusions

In this chapter the available methods for simulating membranes were reviewed for binary and multicomponent systems with the objective of providing a tool to be used for simulating the CO_2 separation step in an IGCC process with carbon capture. Essentially, the methods currently used in the open literature for the simulation of membrane modules are based on papers from 1970s and there is very little activity in this field at present. This exercise led to two modifications of the currently used methods to facilitate modeling activities.

To carry out the analysis in cross-flow configuration, it was proposed to divide a membrane into elements of equal differential stage cut, and treat each as a complete mixing configuration. The assumption of complete mixing model in a differential element of the membrane module is commonly used, but the proposed approach simplifies the analysis

compared to the case when the membrane is divided into equal differential areas. Compared to the case when the membrane is divided into elements of equal decrease in the mole fraction of the more permeable component, the proposed approached offers a better stability of the resulting system of equations and a more accurate prediction of the required membrane area in the case of demanding separations in which the mole fraction of the more permeable component in the retentate is to be very small. The new approach does not involve solving any differential equations, nor does not require introducing dimensionless variable.

For multicomponent systems with plug flow at feed and permeate side, i.e., for co- and counter-current configurations a simple yet robust method was proposed, which is based on differential area. Unlike other approaches based on a differential membrane area, which requires solving implicit set of equations in each element, by assuming a negligible change in feed composition in each element, and calculating the actual change in feed by assuming so-called "zero stage cut" conditions. As a result the governing rate equations become linear equations that can be readily solved numerically. Furthermore, in the proposed method incorporation of the effects of the pressure drop does not require an iterative procedure; the calculations of the pressure drop in the differential element are coupled with the calculation of the changes in feed and permeate compositions. Although the proposed approach was developed for co- and counter-current configurations, it can also be easily applied to cross-flow configuration in which feed is in plug flow over the membrane surface while the permeate is pulled out perpendicularly from the membrane surface.

It was discussed that solving rating problems for counter current flow requires a trial and error solution which is started by estimating the composition of the retentate. In this work an additional step was added to the solution in order to make the it converge faster by providing reasonable retentate compositions. This was done by generating a retentate composition table by solving the problem for the cross-flow mode in a few steps by increasing the membrane area gradually.

The results of the simulations were validated using experimental data from literature. As it was expected counter current flow demonstrated the best performance followed by cross-flow and co-current flow. The proposed plug flow model which was developed based on the differential membrane area was validated using multicomponent gas separation data from the

literature. The simulated data showed very good adherence with the experimental result, although some minor deviations were observed at very high stage cuts.

As the reviewed studies which presented experimental data did not provide adequate information for pressure drop calculations, the effect of pressure drop was not considered in model validation. However, in order to investigate the effect of pressure drop a case study was carried out and the performance of the membrane was evaluated using different tube diameters with a constant stage cut. The outcome indicates that as the tube diameter decreases the pressure drop increases and the required area for carrying out the separation becomes greater because the driving force is reduced.

Finally one of the proposed models (cross-flow with differential stage cut) was used to design a template membrane separation unit in an IGCC process using actual data. The feed stream was shifted syngas which is mainly consisted of H_2 and CO_2, and the best membrane from Chapter 2 was chosen to be used in separation process. As the permeances of four out of six gases in the mixture were unknown it was decided to use the scaling factor from Chapter 2 to estimate the values using the ideal permeances of the gases with unknown actual permeance.

After determining the permeances the system was simulated and the compositions and flow rates of the permeate and retentate streams were specified. The simulation was done by considering the effect of pressure drop, and the number of module tubes were determined in such a way to ensure laminar flow in the tubes. The separation process was successfully simulated and the required membrane area for reducing the CO_2 in syngas was determined. However, it was observed that the available membrane is not a suitable option to be used in this process as its very poor properties resulted in unreasonably large calculated membrane area, high H_2 waste and high pressure drop. The objective of this section was to demonstrate the application of the proposed methods, and the presented template design is not an acceptable configuration due to the mentioned reasons and cannot be implemented in an industrial unit. It is important to emphasize that the membranes currently synthesized by Natural Resources Canada, CANMET Energy Technology Center (CETC) laboratory in Ottawa are not optimized and should be improved significantly in order to be able to substitute the current separation technologies such as CO_2 absorption. This can only happen by fabricating membranes with higher permeance and ideal selectivity which is currently a topic of an ongoing research at CETC.

For future studies it is proposed to improve the models by considering the variation is permeate pressure throughout the membrane as it would improve the accuracy of the determined driving force and eventually would result in more realistic simulations. Another area of research could be studies to design the CO_2 separation step in the IGCC process with the actual feed flow rate. This would require carrying out detailed studies on the size and configuration of membrane modules to achieve an efficient separation unit considering the overall IGCC process. The results of this study could be very useful for the determination of the best place of the membrane separation unit in the separation step of the IGCC process. Moreover, they would also provide realistic estimates on the foot print and the operating cost o the IGCC process.

Nomenclature

A_m: Membrane area (cm^2)

d: Diameter (cm)

L: Flow rate (STD cm^3/s)

l: Tube length (cm)

n: Molar flow rate (mol/s)

N: Tube numbers

p: Pressure ($cmHg$)

P_M: Permeability ($Barrer$)

r: Ration of feed pressure to permeate pressure

R: Gas constant $J/mol.K$

t: Membrane thickness cm

T: Temperature (K)

v: Velocity (cm/s)

V: Permeate flow rate (cm^3/s)

x: Feed side mole fraction

y: Permeate side mole fraction

y': Local permeate side mole fraction

dz: length of the element

Greek letters

α^*: Ideal selectivity

α: Actual selectivity

θ: Stage cut

μ: Viscosity (cmHg.s)

ρ: Density

Subscripts

av: Average

f: Feed

h: High pressure side

l: Low pressure side

lm: Logarithmic mean

o: Retentate

p: Permeate

s: Standard

References

[1] Rautenbach, R. and Dahm, W. The Separation of Multicomponent Mixtures by Gas Permeation, Institut fir Verfahrenstechnik der Rhein-Westph. Techn Hochschule Aachen, l'urmstrasse 46, D-5100 Aachen (F.R.G.)

[2] Geankoplis, C. 2003. Transport Processes and Separation Process Principles. 4th ed. Prentice Hall.

[3] Lee, D. Zhang, L. Oyama, T. Niu, S. Saraf, R. Synthesis,characterization and gas permeation properties of ahydrogen permeable silica membrane supported on porous alumina,J.Membr.Sci.231 (2004)117.

[4] Weller, S. Steiner, A. Separation of Gases by Fractional Permeation through Membranes, Journal of Applied Physics 21, (1950), 279-283.

[5] Shindo, Y. Hakuta, T. Yoshitome H. Calculation Methods for Multicomponent Gas Separation by Permeation, Separation Science Technology, 20(1985), 445-459.

[6] Blaisdell T. C. Kammermeyer, K. Counter current and co-current gas separation, Chemical Engineering Science,28, (1973), 1249-1255.

[7] Haraya, K. Obata, K. Hakuta, T. Yoshitome, H. Performance of Gas Separator with High-Flux Polyimide Hollow Fiber Membrane, Separation Science and Technology, 23, (1988), 305-319.

[8] Lee,K. and Hwang, S. Separation of propylene and propane by polyimide hollow-fiber membrane module, Journal of Membrane Science, 73 (1992) 37-45.

[9] Walawender, W. Stern, S. Analysis of Membrane Separation Parameters. II. Counter current and Co-current Flow in a Single Permeation Stage, Separation Science, 7:5, (1972) 553 584.

[10] Pan, C.Y. Gas Separation by Permeators with High- Flux Asymmetric Membranes, AIChE Journal 29, (1983), 545.

[11] Pan, C.Y. Habgood, H.W. Gas Separation by Permeation Part II: Effect of Permeate Pressure Drop and Choice of Permeate Pressure, The Canadian Journal of Chemical Engineering, 56, (1978), 210.

[12] Pan, C.Y. Gas Separation by High-Flux, Asymmetric Hollow-Fiber Membrane, AIChE Journal 32, (1986), 2020-2027.

[13] Li, K. Acharya, D. R. Hughes, R. Mathematical Modelling of Multicomponent Membrane Permeators, Journal of Membrane Science, 52 (1990) 205-219.

[14] Pettersen, T. Lien, K. A New Robust Model for Gas Separating Membrane Modules Based on Analogy with Counter current Heat Exchangers. Computers chem. eng. 18, (1997), 427-439.

[15] Coker, D. Freeman, D. Modeling Multicomponent Gas Separation Using Hollow-Fiber Membrane Contactors, AIChE Journal, 44, (1998), 1289-1302.

[16] Lamprecht, D. (2010), Advanced gasification technology study, Canadian Clean Power Coalition.

CHAPTER 4

Conclusions, Recommendations and Contributions

4.1 Conclusions and Recommendations

The current chapter provides concluding remarks on the first and second parts of this research, and also reports the contributions steaming from this work to the field of membrane science. Finally, the future directions to extend the current project are proposed.

4.1.1 Characterization of Silica Membranes

One of two main objectives of the current thesis was to derive the properties of the amorphous silica membrane, such as permeability and ideal selectivity, from first principles. Such fundamentally-derived properties are to serve as a bench mark when evaluating experimentally determined properties of amorphous silica membranes. Moreover, ultimately they are to be used as a tool for the optimization of the fabrication protocol of amorphous silica membranes.

This part of the study started with reviewing the mass transfer mechanisms in hydrogen selective silica membranes. Knudsen diffusion, surface diffusion and activated diffusion were

identified as the main transfer mechanisms that might occur simultaneously, with the respective contributions depending on the membrane pore size distribution and the temperature of the process. The permeability in Knudsen diffusion can be determined theoretically provided that the properties of the silica network such as porosity and tortuosity are known. For surface diffusion, in addition to the silica network properties, estimating the permeability coefficient also requires adsorption isotherms of every gas from the feed mixture on amorphous microporous silica. In the smallest pores that are comparable to the kinetic diameter of the permeating species, the activated Knudsen diffusion becomes dominant mechanism, which is also the most favorable transfer mechanism to provide high hydrogen selectivities over other gases. These high selectivities arise from presence of an energy barrier for diffusion, which increases with the molecules size of the penetrant. Determination of this energy barrier in the activated Knudsen diffusion, along with the silica network properties, allows prediction of the theoretical permeabilities in this transfer mechanism.

Activation energy in this work was quantified by integrating the interactions between the gas molecules and the membrane at the pore entrance based on the concept of suction energy. Furthermore, if the gas kinetic energy is greater than the suction energy, then Knudsen diffusion is dominant in small pores in which surface diffusion would occur if the suction energy was greater than the gas kinetic energy. In the latter case, gas molecules would not have enough energy to escape the surface potential of the membrane pores. The iso-concentration point (temperature), which for a given pore size strongly depends on the kinetic diameter and the molecular weight of the permeating species, allows a qualitative assessment of the contributions of surface diffusion. More specifically, at the temperature corresponding to the iso-concentration point, the contributions of Knudsen and surface diffusion are the same. However, as the temperature increases above the iso-concentration point, the contribution of surface diffusion to the total gas transfer across the membrane rapidly diminishes.

In next step a hypothetical ideal structure for silica membranes was considered by assuming the values for the membrane thickness (20 nm), porosity (25%) and tortuosity (1.0), as well as a probability factor (1/3). It was then assumed that the temperature is sufficiently high to neglect the effects of surface diffusion so that only the activated and non-activated Knudsen diffusion were possible. With these assumptions, the permeances of He, H_2 and N_2 and the

corresponding ideal selectivities were determined for different pore sizes from a range that would be expected in amorphous silica membranes. As the pore size changes the contributions of the activated and non-activated Knudsen diffusion change accordingly. In reality, the actual microporous silica membranes cannot have a uniform pore size, but rather there is a pore size distribution which may vary considerably depending on the membrane preparation protocol. However, the pore size distribution in the actual amorphous silica membranes is not available, since there are no analytical tools capable of assessing the pore sizes in the range of Angstroms.

Assuming a Gaussian distribution of pore sizes, that result in different, gradually changing the average pore size, the permeances of He, H_2 and N_2 and the corresponding ideal selectivities of the hypothetical silica membranes were determined. The theoretical permeances were then compared with the experimental data for four amorphous silica membranes, kindly provided by Natural Resources Canada, CANMET Energy Technology Center (CETC) laboratory in Ottawa. The experimental data showed as much as one order of magnitude variations in both permeances and the corresponding ideal selectivities. However, the ideal selectivities of the actual membranes were comparable to theoretically predicted values for the assumed pore size distributions. On the other hand, the experimental permeances were two orders of magnitude smaller than the theoretical values. The difference between the experimental the theoretical permeabilities was not surprising considering that the hypothetical silica membranes had the minimum tortuosity (equal to unity, corresponding to straight cylindrical pores), the maximum possible value of the probability parameter, a relatively large porosity, and a very small thickness.

In the next step, rather than imposing a pore size distribution to the hypothetical silica membrane, the experimentally observed ideal selectivities for He/H_2, He/N_2, and H_2/N_2 were used to determine the pore size distribution of the hypothetical silica membrane that would yield the ideal selectivities of the actual membrane. It was observed that different definitions of the objective function led to different pore size distributions of the hypothetical membrane. In other words, the generated pore size distribution depended on the definition of the objective function for a given set of the experimentally obtained ideal selectivities. This indicates ambiguity of such determined pore size distribution. On the other hand, it was speculated that increasing the number experimental permeances for a given membrane would diminish the dependence of the

obtained pore size on the definition of the objective function. For example, having the data for 4 rather than 3 different gases would allow defining the objective function, regardless of its type, in terms of 6 rather than 3 ideal selectivities. Consequently, it is recommended to verify this hypothesis by increasing the number of single gas permeation tests of new amorphous silica membrane. The model developed in this thesis could easily be extended for more than three single gas permeances.

Despite some ambiguity of the model resulting from the selection of the objective function, the estimated pore size distribution along with the assumed transport mechanisms provides a rational explanation of the effect of membrane densification on the properties of actual silica membranes. More specifically, a simultaneous decrease in membrane permeance and selectivity was observed in the CETC laboratory after a certain number of the applied silica layers. In principle, the selectivity should increase or remain constant while permeance should decrease as the number of silica layers increases, i.e., as the membrane becomes denser. On the other hand, if the application of the silica layers decreases the effective pore size of the membrane, then according to the model developed in this thesis, there exist a pore size below which the transport of the smaller molecule transfers from non-activated to the activated Knudsen diffusion. When this happens, the permeance of the smaller, more permeable gas drastically decreases, which would explain the observed simultaneous decrease in membrane permeance and selectivity.

Considering that regardless of the objective function and the resulting pore size distribution, the permeances of the hypothetical membrane matching the experimental ideal selectivities, were much higher than the experimental permeances, the concept of a scaling factor was introduced. The scaling factor, which is simply the ratio of the experimental permeance to the permeance of the hypothetical membrane that matches the experimental selectivities, provides a cumulative correction factor for the assumed morphology of the hypothetical membrane. Using the scaling factor and the pore size distribution based on the experimental permeances of N_2, H_2 and He, the permeances of the other gases that are of interest in the ICGG plant (i.e., CO, CO_2, Ar) were predicted for the best amorphous silica membrane synthesized in the CETC laboratory. In this exercise the pore size distribution resulting from application of a linear objective function was used. Such predicted permeances were used in the second part of this thesis for the preliminary modelling of the separation of gases in the ICGG plant.

The proposed concept of the scaling factor can be easily verified experimentally. It would simply require testing newly synthesized amorphous silica membranes with as many single gases as possible. For example, by testing membrane with four gases, the permeance of any three of them can be used to determine the pore size distribution and the scaling factor. Then the theoretically predicted permeance of the fourth gas could be compared with the experimental data. It is anticipated that increasing the number of single gases used for the determination of the pore size and the scaling factor would improve the prediction of permeances of other gases in a given membrane. In addition, it is recommended to carry out single gas permeation test at least at three temperatures above the iso-concentration point for a given gas. This would allow comparison of theoretically predicted activation energies for diffusion of different species with the experimental values.

4.1.2 Simulating the Separation of Multicomponent Gas Mixtures

The focus in second part of this study was to simulate the separation of the multicomponent mixtures in membranes with different flow configurations, and its objective was to design a template membrane module for separating CO_2 from the shifted syngas in the IGCC process with partial carbon capture. This part started by introducing the available ideal flow patterns in membranes followed by a review of currently available methods for simulation of membrane modules. Essentially, the methods currently used in the open literature for the simulation of membrane modules are based on papers from 1970s and there is very little activity in this field at present. This exercise led to two modifications of the currently used methods to facilitate modeling activities.

To carry out the analysis in cross-flow configuration, it was proposed to divide a membrane into elements of equal differential stage cut, and treat each as a complete mixing configuration. The assumption of complete mixing model in a differential element of the membrane module is commonly used, but the proposed approach simplifies the analysis compared to the case when the membrane is divided into equal differential areas. Compared to the case when the membrane is divided into elements of equal decrease in the mole fraction of the more permeable component, the proposed approached offers a better stability of the resulting system of equations and a more accurate prediction of the required membrane area in the case of

demanding separations in which the mole fraction of the more permeable component in the retentate is to be very small. The new approach does not involve solving any differential equations, nor does not require introducing dimensionless variable.

For simulating multicomponent systems with plug flow at feed and permeate side, i.e., for co- and counter-current configurations a simple yet robust method was proposed, which is based on differential area. By assuming a negligible change in feed composition in each element, and calculating the actual change in feed by assuming so-called "zero stage cut" conditions, the governing rate equations become linear equations that can be readily solved numerically. Furthermore, in the proposed method incorporation of the effects of the pressure drop does not require an iterative procedure; the calculations of the pressure drop in the differential element are coupled with the calculation of the changes in feed and permeate compositions. Although the proposed approach was developed for co- and counter-current configurations, it can also be easily applied to cross-flow configuration in which feed is in plug flow over the membrane surface while the permeate is pulled out perpendicularly from the membrane surface. The validity of the proposed new approaches was validated both qualitatively and quantitatively. For the latter validation, the available literature data was used for comparison of the simulated results. The simulated data showed very good adherence with the experimental result, although some minor deviations were observed at very high stage cuts.

The new approach based on a differential stage cut was applied to simulate a template membrane separation unit in an IGCC process by assuming a cross-flow configuration. The feed stream was shifted syngas, which mainly consists of H_2 and CO_2. In addition, there are four other gases in the feed, i.e., the feed consisted of six gases in total. The membrane used in this separation process was assumed to be the best one out of the four membranes from the CETC laboratory and four other gases. Since experimental permeances of only two (H_2 and N_2) out of six gases present in the feed stream were available. The permeances of the other four gases were estimated using the concept of scaling factor. To initiate the simulation, the separation goal was specified in terms of CO_2 concentration in the product. To include the effect of pressure drop, the number of module tubes was determined in such a way to ensure a laminar flow in the tubes. The separation process was successfully simulated and the required membrane area for reducing the CO_2 concentration in the syngas to the specified level was determined.

The simulation results revealed that the properties of the current membranes from the CETC lab are not yet suitable for this separation process. The calculated membrane area was unrealistically large. Moreover, the recovery of H_2, which is a valuable by-product in the IGCC process, was very low. The main reason of poor performance of the theoretical membrane separation unit was insufficient H_2 permeance of the amorphous silica membrane used in this simulation.

For future studies it is proposed to improve the models by considering the variation is permeate pressure throughout the membrane as it would improve the accuracy of the determined driving force and eventually would result in more realistic simulations. Another area of research could be studies to design the CO_2 separation step in the IGCC process with the actual feed flow rate. This would require carrying out detailed studies on the size and configuration of membrane modules to achieve an efficient separation unit considering the overall IGCC process. The results of this study could be very useful for the determination of the best place of the membrane separation unit in the separation step of the IGCC process. Moreover, they would also provide realistic estimates on the foot print and the operating cost o the IGCC process.

4.2 Contributions

4.2.1 Characterization part

The most significant contribution of the first part of this thesis is the proposed characterization method for the determination of the pore size distribution in amorphous silica membranes based on experimental single gas permeances of different species. The method is not limited to this specific type of membranes; it can be used for any type of membrane with pore sizes in the order of few Angstroms.

The concept of scaling factor along with the proposed method for determination of pore size distribution in molecular sieve membranes can be used for the prediction of gas permeance. This is particularly important when the experimental permeance for a given gas is not available. Simple gases are widely available, but more complex gaseous compounds might not be available commercially nevertheless, they might be a part of a feed mixture for a specific separation process. According to the proposed method for the prediction of gas permeance in a given

membrane for which scaling factor has been determined, it is necessary to know only the molecular weight of the gas and its kinetic diameter.

By reviewing the pore size distribution of the test membranes, using the method developed in this thesis, it was concluded that over-coating the selective silica layer on the support may have negative effect not only on membrane permeance but also on membrane selectivity. The method for the determination of pore size distribution may provide more insight into optimization of membrane synthesis protocols for amorphous silica membranes.

4.2.2 Simulation part

Solving the cross-flow configuration by a differential stage method developed in this thesis offers numerous advantages compared to currently available analytical and numerical methods for the simulation of membrane performance. These include, a reduction of the computational times, in particular when feed stream is a multicomponent mixture, and a better adherence to the assumed complete mixing in each differential element leading to more accurate simulation results.

The proposed method for solving co- and counter-current configurations is another important contribution. It makes the resulting system of rate equations linear, which can be readily solved in design and rating problems. Moreover, this approach allows incorporation of pressure drop analysis without a need for an iterative solution.

In the case of simulations involving counter-current flow configuration, which are inherently iterative problems, it was shown that using the results of cross-flow configuration as a initial guess, greatly facilitates conversion of the actual simulation.

Simulation of a template membrane separation unit in the IGCC process, although very preliminary, clearly indicates insufficient properties, in particular gas permeance, of currently available microporous silica membranes. This represents a starting point to more rigorous simulations and optimization of the IGCC process from the perspective of the membrane unit.

Appendix A: Constrained Linear Optimization

To estimate the pore size distribution it is essential to set up a constrained linear optimization problem. The objective function of the problem can be presented as follows:

$$f(x)=\left|\frac{\sum_{i=1}^{m} x_i \overline{P}_{MA,i}}{\sum_{i=1}^{m} x_i \overline{P}_{MB,i}}-\alpha^*_{A/B}\right|+\left|\frac{\sum_{i=1}^{m} x_i \overline{P}_{MA,i}}{\sum_{i=1}^{m} x_i \overline{P}_{MC,i}}-\alpha^*_{A/C}\right|+\left|\frac{\sum_{i=1}^{m} x_i \overline{P}_{MB,i}}{\sum_{i=1}^{m} x_i \overline{P}_{MC,i}}-\alpha^*_{B/C}\right|+\ldots \quad \text{(A.1)}$$

where *A, B,.. Z* are the test gases set from highest to lowest permeance, *m* is the number of pore size ranges, and $\overline{P}_{Mji}$ is the permeance of gas *j* in the pore size range *i*. It should be noted that the number of terms in right hand side of this equation depends on the number of test gases and it would be equal to $n(n-1)/2$, where *n* is the number of test gases. The constraints of the problem can be defined as follows:

$$\sum_{i=1}^{m} x_i = 1 \quad \text{(A.2)}$$

$$0 < x_i < 1 \quad \text{(A.3)}$$

Several methods and algorithms are available for solving constrained linear optimization problems such as simplex, revised simplex and interior point. The simplex and revised simplex algorithms perform the optimization by moving along the edges of the polytope defined by the constraints, from vertices to vertices with smaller values of the objective function in each step, until the minimum is found [1], and are more suitable for small problems. Interior point algorithms on the other hand iterate from the interior of the polytope of constraints, and get to the solution very quickly, but unlike the other methods do not find the solution exactly.

It should be noted that several application are available for solving optimization problems such as Mathematica and MATLAB. In Mathematica the *minimize* function can be used to solve both linear and nonlinear optimization problems, which employs linear programming, cylindrical

algebraic decomposition, Lagrange multipliers and analytic methods based on the constraints types [1]:

$$\text{Minimize}[\{f, \text{cons}\}, \{x, y, ...\}] \tag{A.4}$$

where f is the objective function, *cons* are the constrains and x and y are the variables. In MATLAB the *Linprog* can be used to solve linear constrained problems using the syntax below:

$$x = \text{linprog}(f,A,b,Aeq,beq) \tag{A.5}$$

where f is the objective function, A and b are the matrix and vector for the inequality constraints respectively, and Aeq and beq are the matrix and vector for equality constraints. *Linprog* function in MATLAB can be used with interior point and simplex algorithms as well. In this work Mathematica's minimize function was used for carrying out the optimization process, as it handled the large amount of objective function's variables without any problem.

References:

[1] Champion, B. Strzebonski, A. Constrained optimization, Wolfram Mathematica Tutorial Collection. 2008 Wolfram Research, Inc.

[2] Vanderbei, R. Linear Programming: Foundations and Extensions. Springer-Verlag, 2001.

Appendix B: Accepted Paper in NTTP Conference

Shortcut Methods for Simulating Separation of Multicomponent Gas Mixtures in Membranes

Sina Deyhim, Boguslaw Kruczek, David McCalden, Mazdak Shokrian

Abstract

In this study shortcut mathematical models are presented for multicomponent systems with cross-flow, co-current and counter current flow configurations. Cross-flow mode is solved numerically in elements defined by differential stage cut and by assuming applicability of complete mixing model in the elements, which makes the model converge in short times. A simple yet robust method is proposed for solving co-current and counter current flow modes, which does not require any trial and error (except for counter current rating problems) or using dimensionless variables, and pressure drop calculations can be incorporated to the model easily. The presented models are applicable for systems with any number of components, including binary systems. The performance of the proposed models is validated by experimental data for co-current and counter current flow configurations with in different stage cuts.

Keywords: multicomponent gas separation, membrane, cross-flow, co-current, counter-current

---

1. Introduction

Gas separation using membranes is a promising alternative to the conventional energy-intensive separation methods such as distillation. Lower capital and operating costs, lower foot print, high turn down ratios and adaptability to variations in feed are some of the characteristics that make membrane technology attractive. Similar to any other processes, mathematical modeling should be carried out for designing these systems, as understanding the effects of different process parameters and flow configurations on performance of the membranes is the determining step in successful integration of these unit operations to the main processes. Several methods are developed for modeling binary systems, which is rarely encountered in actual separation problems, but when it comes to the multicomponent systems there are only a few models available, which either require iterative procedures or using dimensionless variables.

The ideal flow patterns for gas separation in membranes are complete mixing, cross-flow, co-current and counter current flow. In deriving the equations for different models it is assumed that the membrane operates in isothermal condition, the Fick's law is applicable, pressure of the permeate side is constant and the permeabilities are pressure independent. In complete mixing

mode the membrane is treated as a continuous stirred tank, which means the composition is uniform in the both feed and permeate sides along the membrane, and the effect of feed side pressure drop is also neglected in this model. Starting from the Fick's first law and assuming applicability of ideal gas law the rate equation can be written as follows:

$$y_p V_p = \frac{P_{Ma} A}{t}(p_h x_o - p_l y_p) \tag{1}$$

where y_p and x_o are the concentrations of component *a* in permeate and retentate respectively, *t* is the membrane thickness, P_{Ma} is the permeability of the component *a*, and p_h and p_l are the pressures at high and low pressures sides, respectively. The same equation can be written for species *b*, and by dividing them, the following equation can be obtained, which can be used to calculate y_p for a binary system as shown by Geankoplis (2003):

$$\frac{y_p}{1-y_p} = \frac{\alpha^*[x_o - (p_l / p_h)y_p]}{(1-x_o) - (p_l / p_h)(1-y_p)} \tag{2}$$

For multicomponent systems it is required to use a trial and error procedure to find the composition of the permeate by guessing the concentration of one of the components in the permeate. Complete mixing model is straight forward, but it does not consider the actual driving force along the membrane to determine the permeation rates so it lacks accuracy, and the effect of pressure drop cannot be incorporated into it as well. The cross-flow, co-current and counter current modes represent the actual operating conditions of the membranes more closely as the driving force in those models are not approximated as it is done in the complete mixing mode.

2. Modeling

2.1 Cross-flow mode

The cross-flow model assumes no mixing in the permeate side nor on the high pressure side, and local permeation is just a function of local driving force. The high pressure stream is in a plug flow, but the permeate is pulled into vacuum and is perpendicular to the surface. The cross-flow mode was first solved by Weller and Stern (1950) analytically for binary systems without considering the effect of pressure by introducing a set of dimensionless parameters. Shindo et al. (1985) solved this flow pattern by integrating the governing differential equation over differential membrane area.

In this work cross-flow system is solved by dividing the membrane into differential elements and using the complete mixing model's equations in each element. By choosing the elements small enough, the error due to approximating the plug flow by the completed mixing is minimized. Solving the complete mixing mode in multicomponent systems requires a trial and

error procedure, which starts with guessing the concentration of one of the components in the permeate side, and determining the area of the element accordingly. The composition of the permeate is then calculated using the rate equations of other components, and the sum of the fractions of all the components in the permeate side should be equal to unity. In this work a new approach is taken to determine the length of the differential element, which is based on a constant differential stage cut in each element. This makes it possible to control the stage cut in order to minimise the error caused by complete mixing model's equations. The differential stage cut method converges faster as it determines the suitable step size based on the stage cut rather than the membrane area, and the pressure drop calculations can be carried out by an additional iteration in each step after determining the area.

2.2 Co-current and Counter current Modes

In the co-current mode the feed and the permeate are parallel to the membrane's surface, and the local driving force is affected by the concentrations of the diffusant in both feed and permeate side. A few methods are proposed in the literature for solving this model for multicomponent systems. Shindo et al. (1985) proposed a method, which involved integrating the governing differential equation over differential membrane area using dimensionless variables by ignoring the effect of the pressure drop. Pan (1986) proposed a model for co-current and counter-current modes by assuming applicability of cross-flow driving force due to asymmetric structure of the membrane, and neglecting back diffusion from bulk due to presence of the porous support. Their proposed approach required a trial and error shooting method to obtain the solution in case of considering the effect of the pressure drop.

In this work a shortcut method is proposed, which is based on the assumption of a constant concentration of the feed and permeate in each differential element. In this method the composition of the permeate and its flow rate can be determined by solving the rate equations simultaneously in each element. For each differential element, Eq. (1) can be rearranged to the following form:

$$y_i = \frac{p_h x_i}{p_l + Vt/(dAP_{Ma})} \qquad (i = 1,..,n) \tag{3}$$

$$\sum_{i=1}^{n} y_i = 1 \tag{4}$$

where n is the number of components. By solving the above system of equation in each element it is possible to determine the local composition and flow rate of permeate, and by integrating it over the entire module the overall compositions and flow rates can be determined for the permeate and retentate streams. It should be noted that the composition of the feed entering the next step can simply be calculated by setting up the component mass balance for each gas.

The counter-current flow configuration can be solved similarly to co-current flow configuration, but in this flow pattern the calculations should start from the retentate side and continue backward to the membrane's inlet. Solving the counter-current flow requires a trial an error procedure as the composition and flow rate of the retentate are unknown and must be guessed. According to Kowali et al. (1992), the performance of the counter-current flow configuration is similar to the cross-flow configuration so that the results of the latter can be used as a good starting point for solving the counter-current flow configuration.

3. Results

The proposed method was validated using the experimental results provided by Pan (1986) for co-current and counter-current flow modes for a mixture of H_2, N_2, Ar and CH_4, and the simulations results are presented in Figs. 1-4 (Fig. 3-9 to 3-12 in Chapter 3).

As can be seen the presented method demonstrates satisfactory performance over a wide range of stage cuts, with some deviations in higher stage cuts, which is normally seen in all of the available models. The proposed approach is a simple yet robust method for solving plug flow problems as the calculations are straight forward, and the pressure drop calculations can easily be incorporated to the solution without the need for further iterations for the co-current flow.

Acknowledgment

The authors would like to thank Natural Resources Canada for providing the financial support for this work.

References

Geankoplis, C. (2003), "Transport Processes and Separation Process Principles. 4th edition" Prentice Hall.

Kowali, A.S. Vemury, S. Krovvidi, K.R. Khan, A.A. (1992), Models and Analyses of Membrane Gas Permeators. Journal of Membrane Science, 73, 1-23.

Pan, C.Y. (1986), Gas Separation by High-Flux, Asymmetric Hollow-Fiber Membrane, AIChE Journal 32, 2020-2027.

Shindo, Y. Hakuta, T. Yoshitome H. (1985), Calculation Methods for Multi-component Gas Separation by Permeation, Separation Science Technology, 20, 445-459.

Weller, S. Steiner, A., (1950), Separation of Gases by Fractional Permeation through Membranes, Journal of Applied Physics 21, 279-283.